AD-A274 808

# THE MICROSTRUCTURAL RESPONSE OF GRANULAR SOIL UNDER UNIAXIAL STRAIN

S **DTIC**
ELECTE
DEC 27 1993
A

John J. Gill

October 1993

**Final Report**

## PHILLIPS LABORATORY
Advanced Weapons and Survivability Directorate
AIR FORCE MATERIEL COMMAND
KIRTLAND AIR FORCE BASE, NM 87117-5776

93 12 23 066

93-31221

This final report was prepared by the Phillips Laboratory, Kirtland Air Force Base, New Mexico, under Job Order 2302Y209. The Laboratory Project Officer-in-Charge was Aaron Perea (WSSD).

When Government drawings, specifications, or other data are used for any purpose other than in connection with a definitely Government-related procurement, the United States Government incurs no responsibility or any obligation whatsoever. The fact that the Government may have formulated or in any way supplied the said drawings, specifications, or other data, is not to be regarded by implication, or otherwise in any manner construed, as licensing the holder, or any other person or corporation; or as conveying any rights or permission to manufacture, use, or sell any patented invention that may in any way be related thereto.

This report has been authored by an employee of the United States Government. Accordingly, the United States Government retains a nonexclusive, royalty-free license to publish or reproduce the material contained herein, or allow others to do so, for the United States Government purposes.

This report has been reviewed by the Public Affairs Office and is releasable to the National Technical Information Service (NTIS). At NTIS, it will be available to the general public, including foreign nationals.

If your address has changed, if you wish to be removed from the mailing list, or if your organization no longer employs the addressee, please notify PL/WSSD, 3550 Aberdeen Ave SE, Kirtland AFB, NM 87117-5776, to help us maintain a current mailing list.

This technical report has been reviewed and is approved for publication.


AARON PEREA
Project Officer


FOR THE COMMANDER


BRENDAN B. GODFREY, ST
Acting Director, Advanced Weapons
and Survivability Directorate


DO NOT RETURN COPIES OF THIS REPORT UNLESS CONTRACTUAL OBLIGATIONS OR NOTICE ON A SPECIFIC DOCUMENT REQUIRES THAT IT BE RETURNED.

# REPORT DOCUMENTATION PAGE

Public reporting burden for this collection of information is estimated to average 1 hour per response, including the time for reviewing instructions, searching existing data sources, gathering and maintaining the data needed, and completing and reviewing the collection of information. Send comments regarding this burden estimate or any other aspect of this collection of information, including suggestions for reducing this burden to Washington Headquarters Services, Directorate for Information Operations and Reports, 1215 Jefferson Davis Highway, Suite 1204, Arlington, VA 22202-4302, and to the Office of Management and Budget, Paperwork Reduction Project (0704-0188), Washington, DC 20503.

| 1. AGENCY USE ONLY (Leave blank) | 2. REPORT DATE October 1993 | 3. REPORT TYPE AND DATES COVERED Final, Sep 90 - Nov 92 |
|---|---|---|

**4. TITLE AND SUBTITLE**
THE MICROSTRUCTURAL RESPONSE OF GRANULAR
SOIL UNDER UNIAXIAL STRAIN

**6. AUTHOR(S)**

John J. Gill

**5. FUNDING NUMBERS**

PE: 61102F
PR: 2302
TA: Y2
WU: 09

**7. PERFORMING ORGANIZATION NAME(S) AND ADDRESS(ES)**

Phillips Laboratory
3550 Aberdeen Avenue, SE
Kirtland AFB, NM  87117-5776

**8. PERFORMING ORGANIZATION REPORT NUMBER**

PL-TR--92-1064

**9. SPONSORING / MONITORING AGENCY NAME(S) AND ADDRESS(ES)**

**10. SPONSORING / MONITORING AGENCY REPORT NUMBER**

**11. SUPPLEMENTARY NOTES**
This work was funded by AFOSR.

**12a. DISTRIBUTION / AVAILABILITY STATEMENT**

Approved for public release; distribution is unlimited.

**12b. DISTRIBUTION CODE**

**13. ABSTRACT (Maximum 200 words)**

Soil mechanical behavior is described and phenomenological (macroscopic) and microstructural (particulate) theories, developed to predict the constitutive response of granular media, are discussed. Special emphasis is given to the concept of fabric in granular media and how the concept relates to observed mechanical behavior. This report describes an experimental effort to quantify changes which occur in a cuboid specimen of granular silica material under uniaxial strains of up to 10 percent. The material tested was a poorly graded ottowa sand with specimens consisting of either 0.5- or 0.75-mm-diam. granules. The displacement fields perpendicular to the loading axis are generally not directly proportional to applied macroscopic strain as typically predicted by a local theory. Rather, the three "zones" existing in a specimen under uniaxial strain are (1) a zone in which relatively high local displacements (and strain) occur (near the loading cap), (2) a zone behind this "front" wherein the grains move directly in relation to the advance of the loading cap, and (3) a zone which has not yet responded to the advancing cap. Sidewall friction, although not negligible, appears not to play an overriding role in the grain micromotions.

**14. SUBJECT TERMS**
uniaxial strain, soil behavior, microstructure, granular silica material, macroscopic strain, sidewall friction, granular materials

**15. NUMBER OF PAGES**
114

**16. PRICE CODE**

| 17. SECURITY CLASSIFICATION OF REPORT Unclassified | 18. SECURITY CLASSIFICATION OF THIS PAGE Unclassified | 19. SECURITY CLASSIFICATION OF ABSTRACT Unclassified | 20. LIMITATION OF ABSTRACT SAR |
|---|---|---|---|

CONTENTS

CONTENTS (Continued)

| Accesion For | | |
|---|---|---|
| NTIS CRA&I | ☑ | |
| DTIC TAB | ☐ | |
| Unannounced | ☐ | |
| Justification | | |
| By | | |
| Distribution / | | |
| Availability Codes | | |
| Dist | Avail and / or Special | |
| A-1 | | |

DTIC QUALITY INSPECTED 5

# FIGURES

FIGURES (Continued)

FIGURES (Concluded)

# 1.0 INTRODUCTION

## 1.1 GENERAL

Two broad classes of continuum theories appear to exist with regard to the modeling of the loading response of granular materials. These are the phenomenological (macroscopic) and microstructural (particulate) theories. The phenomenological theories attempt to devise constitutive relationships based on analysis of the experimentally determined stress-strain response of granular materials. The microstructural theories are founded upon the premise that actual measurement, geometric modeling, or statistical modeling of the granule contacts or granular motions will provide insight into more accurate modeling of the material response. The microstructural theory can be directly linked to the continuum theory if one maintains that the specimen boundary distances (or loaded volume) are large in comparison to the size of the granules or the distance between them. This stipulation permits one to transform the body of discrete particles into a statistically equivalent macroscopic specimen which is then suitable for mathematical analysis.

Several distinct types of models exist within the two broad classifications described. The dominant modeling techniques used in the two classes will be presented to describe each approach as it has progressed to its current state of achievement. This will permit an objective assessment of the advantages and limitations of each modeling technique and provide an understanding of the contribution of this research effort. Macroscopic continuum theory will be presented first in deference to the historical contributions made by previous researchers. Microstructural theory will follow because of the relatively recent interest in this area of research. Prior to discussion of these classes, a brief qualitative summary of the loading response of soil will be given.

## 1.2 SOIL MECHANICAL BEHAVIOR

Some of the earliest models developed to predict the loading response of soils were predicated on linear elasticity (Hooke's law) and nonlinear elasticity. This was principally

due to a lack of general understanding of soil mechanical response but also due to the inability of performing the large number of numerical calculations associated with more advanced models. This limitation precluded accurate modeling of soil loading response, even at relatively low stress levels, because soils have been shown to undergo plastic strains at very low levels of total macroscopic strain ($\varepsilon \approx 10^{-4}$). The criticality of modeling soil plastic response has been given considerable emphasis in recent models and some (Ref. 1) have entirely eliminated the region of elastic deformation. In light of these developments, it is necessary to be familiar with the essential features of the mechanical response of soils subjected to hydrostatic and/or deviatoric stress states. Furthermore, the existence of plastic strain at such low levels of total stress or strain requires one to be familiar with the fundamental equations of a generic work-hardening elastic-plastic (or elastic-vicroplastic) constitutive model. Because such models require the use of a flow rule, the ramifications of using an associated or nonassociated flow rule for modeling the response of granular materials will also be discussed.

More than most other engineering materials, the constitutive response of soils subjected to external loading is greatly affected by such factors as physical structure, void ratio, degree of void saturation, drainage conditions, current stress state, loading history, and loading rate (Ref. 2). Consider the example of soil subject to a hydrostatic stress state (Fig. 1). The pressure-volume relation is nonlinear. The soil undergoes permanent volume change as shown by the load-unload cycle of deformation. In this example, the permanent volumetric strain is dependent on the initial state of compaction of the material, the degree of void saturation, and drainage conditions. Regarding the initial state of compaction, a dense soil will exhibit relatively little volumetric strain. On the contrary, a highly flocculated soil can render extreme volumetric strains. In addition, soil typically exhibits a small amount of permanent volumetric strain during the unload-reload cycle.

The shearing stress-strain response of soils is much more complex than that of simple hydrostatic response. Figure 2 shows typical qualitative responses of sheared soils. This figure indicates the influence of confining pressure (hydrostatic stress, $\sigma_c$) on the shear strength of the soil. Generally, increased confining pressure results in increased shear strength.

2
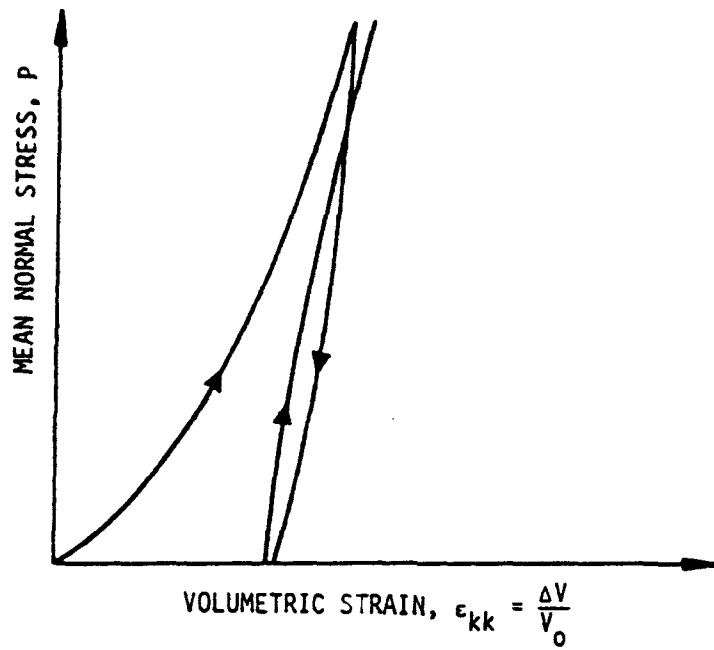
Figure 1. Typical behavior of soil under isotropic loading conditions (from Ref. 3).
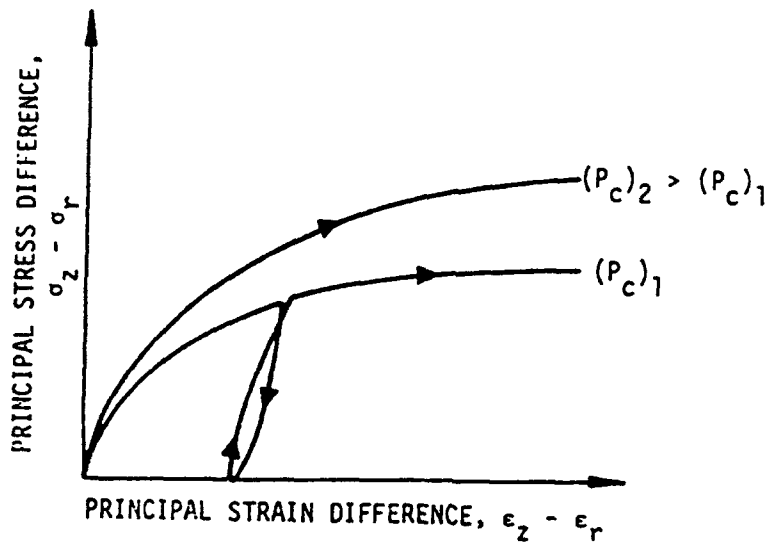


Figure 2. Typical triaxial stress-strain curves for soil (from Ref. 3).

3

Soils typically exhibit volumetric changes when subject to a shearing (deviatoric) state of stress or deformation (Fig. 3a). The volume change can be either contractive or dilative depending on the initial state of compaction. A loose sand or normally consolidated clay will usually contract under shear whereas a dense sand or overconsolidated clay will tend to dilate. Figure 3b shows the responses of strain softening and strain hardening which can be associated with dilative materials. A strain softening (dilative) material shows a relatively well-defined peak stress at relatively low strain. Continued increase in applied strain results in a decrease in the strength of the material. This is a brittle-type failure. Alternatively, a strain hardening (contractive) material will undergo an increase in stress (strength) with strain until some peak stress (strength) is achieved. Figure 3c provides the same information as Figure 3b, but the response is expressed in terms of void ratio.

The stress-strain response for soils has been shown to be dependent on the applied confining stress. Likewise, there is a dependence on time rate of loading. However, the dependence is not so clear cut and varies with respect to the frictional and cohesive properties of the material. To clarify this point, the limiting cases of purely frictional and purely cohesive materials will be presented. Generally, the shear strength of frictional materials is primarily dependent on the confining pressure and relatively independent of the strain (or shearing) rate. Alternatively, the shear strength of a cohesive material is primarily dependent on strain rate and much less so on confining pressure. The shear strength of mixed soils (those having both frictional and cohesive attributes) depends on both the confining pressure and shear rate. The effect of shear rate on mobilized soil strength is shown qualitatively in Figure 4, which depicts the results of four axisymmetric triaxial tests. In this test series, four similar specimens have been isotropically consolidated to the same confining pressure. One of the specimens is then sheared by static load application and the other three are sheared at different rates. The key feature apparent in this figure is the direct relationship which exists between shear rate and material strength. The strength of the material increases as the shear rate increases. The strength, therefore, is defined by an envelope known as the "dynamic failure envelope." This soil attribute permits a specimen to exhibit strain hardening under one loading condition and strain softening under another. Figure 5 shows the results of axisymmetric triaxial tests being conducted on two similar specimens.

4

(a)

(b)

(c)

SHEAR STRAIN
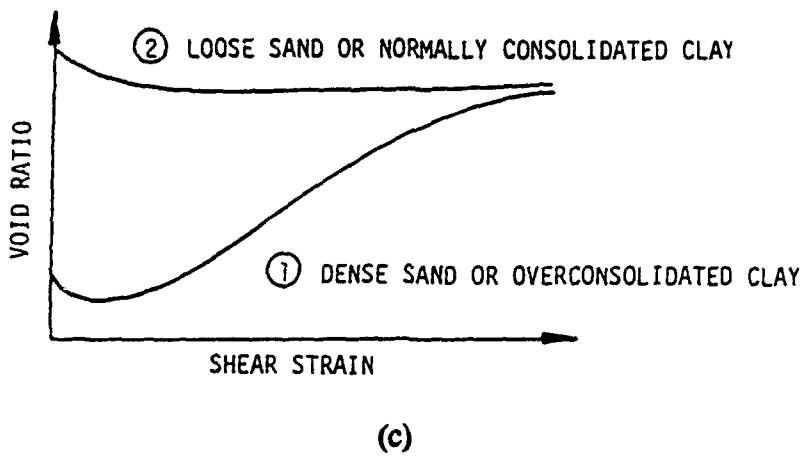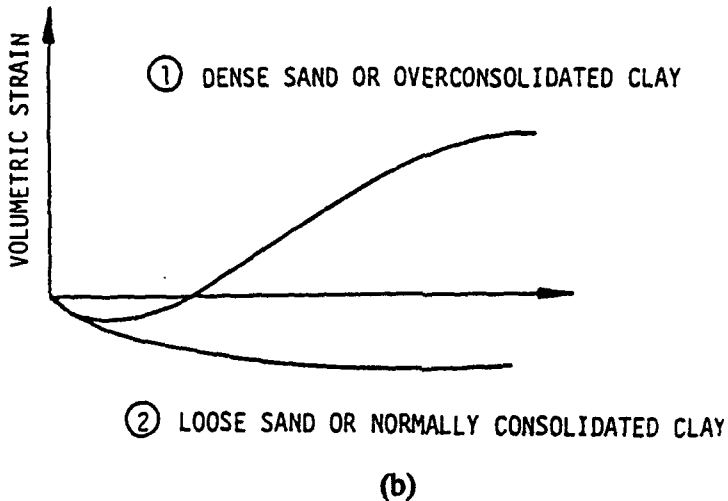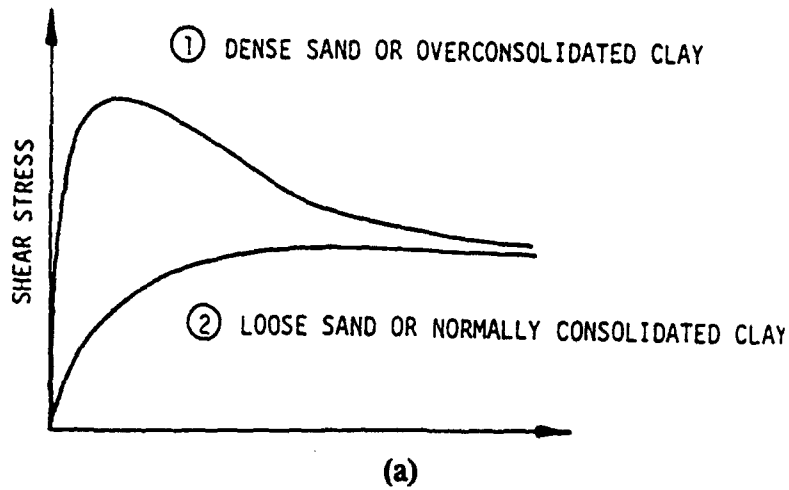
Figure 3. Typical behavior of soils tested under drained triaxial test conditions (from Ref. 3).

5
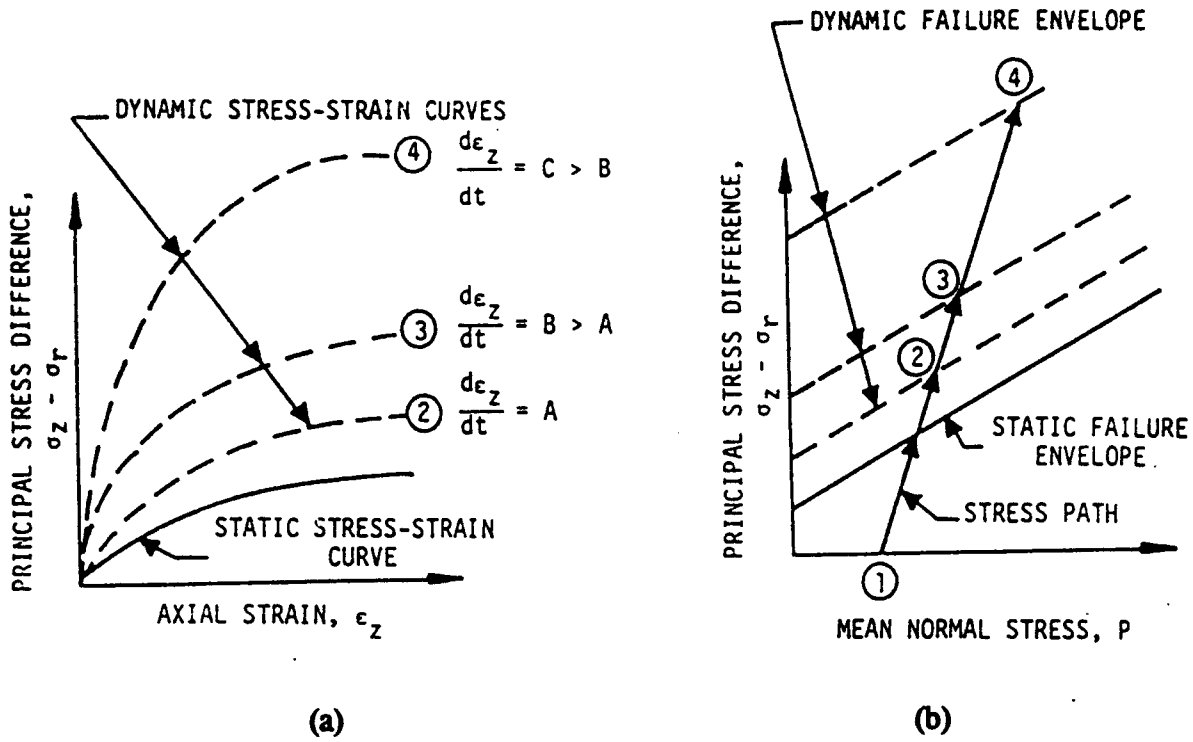
Figure 4. Typical stress-strain curves for different strain rates
from an axisymmetric triaxial test (from Ref. 3).
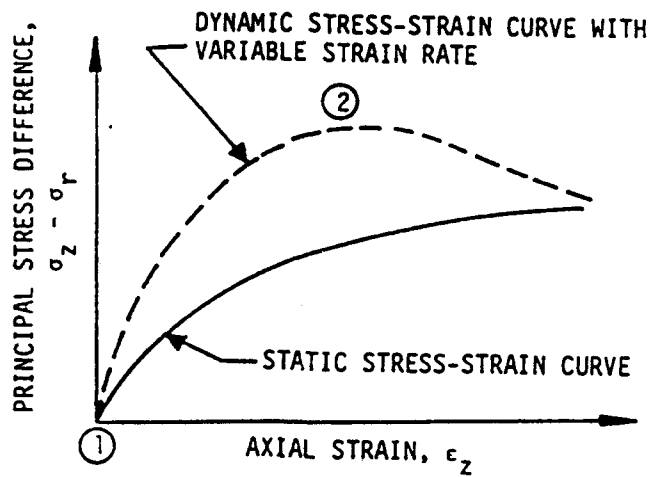


Figure 5. Dynamic stress-strain curve for a variable strain
rate from an axisymmetric triaxial test (from Ref. 3).

The bottom curve shows the results of a test in which the specimen was statically loaded. The upper curve shows the results of a test in which the specimen was rapidly sheared to some peak stress and then slowly sheared to some ultimate (lower) shear stress. The differing responses are induced solely by varying the shear rate during dynamic loading.

All of the information presented thus far reflects tests conducted on specimens in which the pore fluid (if any) has been able to drain during testing. Tests conducted on saturated soils under undrained conditions provide results which differ considerably from the results of similar tests on drained specimens. The limiting cases in undrained tests are those conducted either on saturated overconsolidated clays or very dense sands and tests on saturated normally consolidated clays or very loose sands. Figure 6 shows the qualitative results of tests conducted on "limiting case" specimens (designated 2-3 for a very loose sand or normally consolidated clay and 2-5 for a very dense sand or overconsolidated clay) in undrained shear conditions. The specimen designated 2-4 has material properties somewhere between these limiting cases. Each of the specimens was isotropically consolidated to the same confining stress and then sheared (undrained) at the same constant rate. The radial stress, $\sigma_r$, remained constant throughout the test. Furthermore, each specimen was subjected to a loading regime which followed the same total stress path. Each specimen experienced a different effective stress path.

Effective stress in a fully saturated soil element is defined as the total stress minus the pore pressure.

$$\sigma' = \sigma - U \text{ or } \sigma = \sigma' + U \tag{1}$$

where $\sigma'$ equals effective stress, $\sigma$ equals total stress, and U equals pore pressure. Comparing Figures 6a and 6b, one can see that the effective stress is the only portion of the total stress which affects soil shear strength. Increasing the effective stress causes soil particles to shift into a denser packing, whereas equal increases in the total stress and pore pressure leave the effective stress unchanged. In the latter case, there is little or no effect on the particle packing (Refs. 2, 4, and 5).
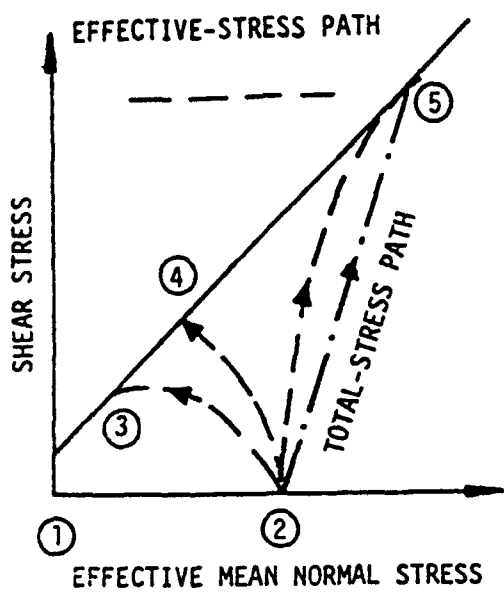
(a)
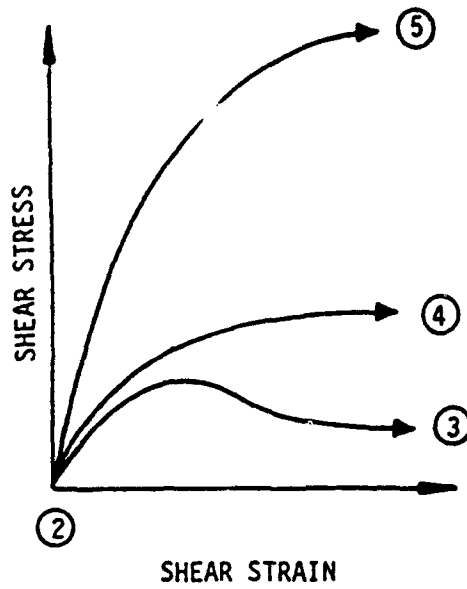
(b)
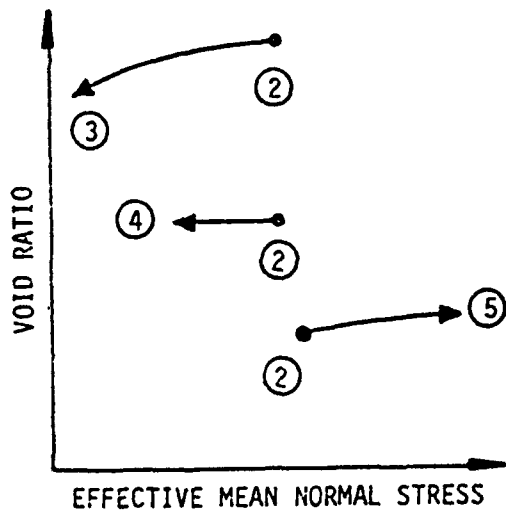
(c)
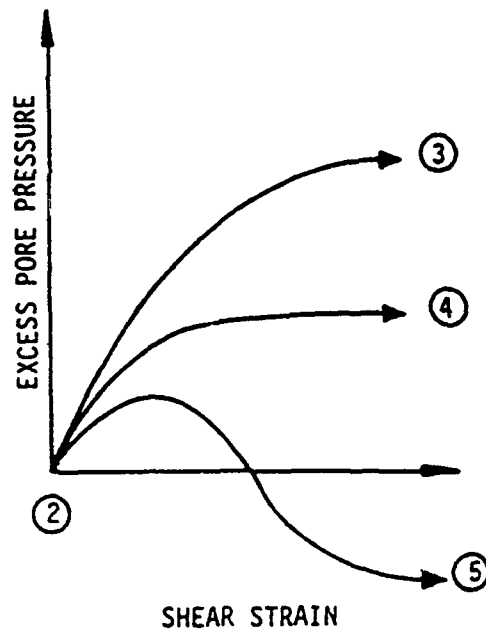
(d)

Figure 6. Typical behavior of saturated soil tested under undrained triaxial test conditions (from Ref. 3).

Previous qualitative results have been predicated on the results of tests conducted on isotropic soils. Aniso.·opy, however, mu : be considered as it is a common soil property. Figure 7 shows qualitative results associated with the conduct of hydrostatic loading tests in an isotropic specimen and an anisotropic specimen. The isotropic specimen exhibits equal strains in the vertical and horizontal directions (i.e., $\varepsilon_z = \varepsilon_r$). The anisotropic specimen exhibits different strains in the vertical and horizontal directions.

The specialized case of uniaxial strain ($\varepsilon_r$ is constrained to be 0) must be considered because many typical loading regimes involve the application of uniaxial stress or strain. Figure 8 shows the qualitative results of the conduct of a uniaxial strain test on a drained specimen with typical behavior (Fig. 8a) and the associated stress path (Fig. 8b). Figure 8a depicts the typical relatively high initial loading modulus due to natural cementation, but the material subsequently densifies and the response approaches that observed under drained hydrostatic loading. Upon unloading, the material exhibits a relatively stiff response due to interparticle locking; however, this response gradually decreases as unloading proceeds. Figure 8b indicates the presence of locked-in horizontal stresses after the specimen has been unloaded.

## 1.3 PHENOMENOLOGICAL (MACROSCOPIC) CONTINUUM THEORY

Accurate prediction of the soil loading response requires two principal ingredients. One must have a model that exhibits the major features of the material response under three-dime. ·onal loading as well as quantitative determinations of the material parameters which characterize the model. It is critically important to view the chosen model and determine the required material parameters as codependent aspects of the problem definition. This will preclude the use of an overly complex model or determination of parameters which have no direct influence on the accuracy of the prediction. It is implied that only those testing devices which subject a specimen to arbitrary three-dimensional loadings (Ref. 6) are suitable for obtaining data for use in constitutive modeling. This is mainly due to the relative ease of making specialized predictions (uniaxial strain, plane strain, etc.) from a
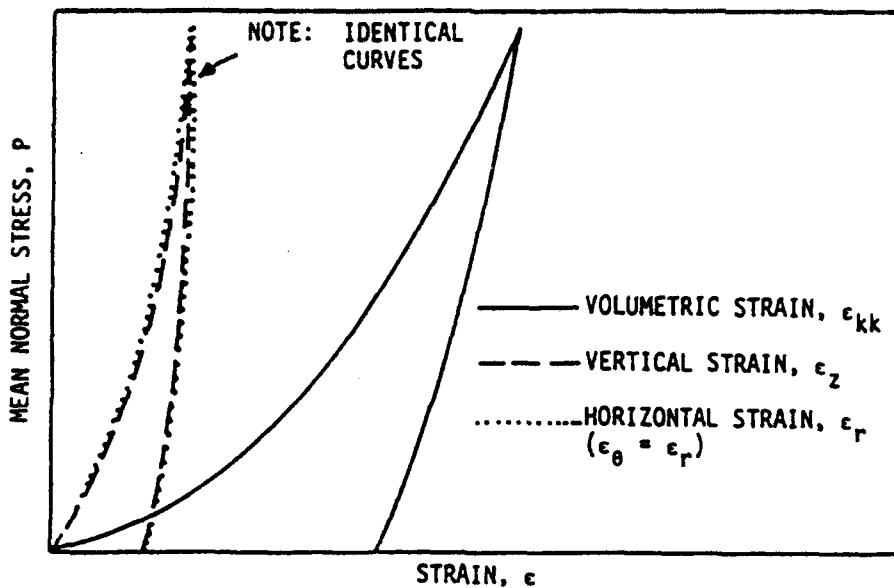
(a) Isotropic soil.
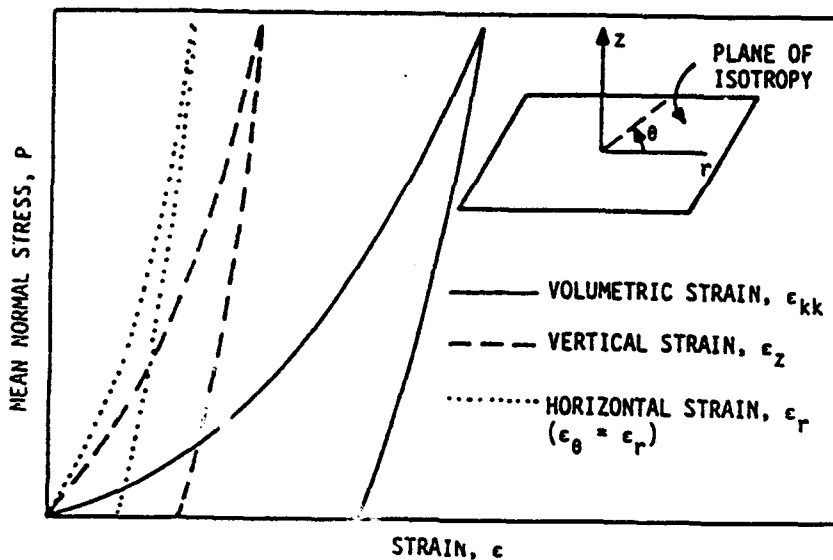


(b) Transverse-isotropic soil.

Figure 7.  Typical behavior of soil under hydrostatic loading
and unloading (from Ref. 3).

10
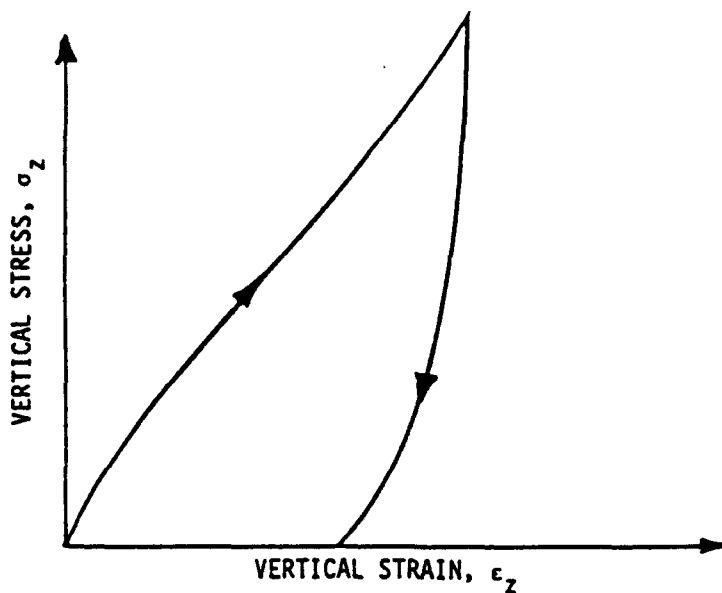
(a) General behavior.
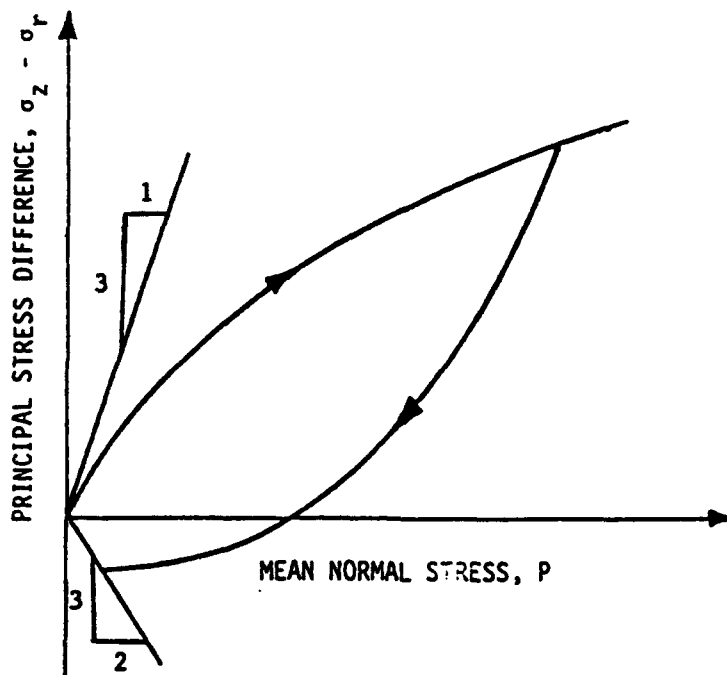


(b) Stress path.

Figure 8.  Typical soil response under uniaxial strain
(from Ref. 3).

11

generalized model rather than vice versa (Ref. 7). The following macroscopic continuum theories, therefore, are presented as being representative of the basic categories (deformation theory, incremental plasticity, and the Endochronic Theory [Ref. 8]) currently used in modeling. Advantages and disadvantages of each will be discussed.

### 1.3.1 Deformation Theory

Deformation theory implies the existence of a relatively simple relationship between stress and strain tensors. The deformation theory equations usually appear as follows:

$$s_{ij} = 2G(\sigma_{mn}, \varepsilon_{pq})e_{ij} \tag{2}$$

$$\sigma_{kk} = 3K(\sigma_{mn}, \varepsilon_{pq})\varepsilon_{kk} \tag{3}$$

where $s_{ij}$ and $e_{ij}$ are the stress and strain deviation tensors, respectively. The elastic shear modulus is G and K is the elastic bulk modulus. Nonlinear behavior can be modeled by the introduction of either stress or strain-dependent moduli. Components of the stress and strain tensors are $\sigma_{mn}$ and $\varepsilon_{pq}$, respectively.

The Duncan and Chang model (1970, Ref. 9) is an example of a model which uses deformation theory. This model is based on the observation that the stress-strain curves of soils tested in a triaxial chamber under a variety of constant confining stresses resemble a hyperbola (Fig. 8). This model replicates only the axial stress-strain behavior of a material and assumes a constant Poisson ratio ($\mu$). Improvements to the model in 1974 (Ref. 10) permit the modeling of nonlinear volumetric strains. Additionally, the model has been refined to incorporate behavior observed upon unloading of the specimen. Unloading and reloading behavior is assumed to be elastic with the value of Young's modulus, depending upon confining pressure. The advantages of this model lie in its simplicity. The model parameters are easily evaluated from standard laboratory tests and generally have a physical significance to the researcher. However, if the modeled loading path deviates significantly

PL-TR--92-1064

from triaxial compression, the predicted strains may not be accurate. Since the model is based on a generalization of Hooke's law for isotropic behavior, it cannot model anisotropic responses. Shear dilatant and postpeak strain softening cannot be modeled, either. Lastly, the model can only predict prepeak response.

## 1.3.2 Incremental Plasticity

A considerable number of plasticity-based models has been developed over the past 30 yr. Common variations include perfect (ideal) plasticity, hypoelasticity, and viscoplasticity. The most promising models appear to be based on the incremental theory of plasticity or viscoplasticity in which the total strain increment is expressed as the sum of the elastic and plastic strain increments.

$$de_{ij} = de^e_{ij} + de^p_{ij}$$ (4)

In most models, each of these increments is rate independent (Ref. 11). Regardless of the variation being considered, the basic equation of all incremental plasticity models is as follows:

$$de_{ij} = \frac{dJ_1}{9K} \delta_{ij} + \frac{ds_{ij}}{2g} d\lambda \frac{\partial f}{\partial \sigma_{ij}}$$ (5)

where $J_1$ is the first invariant of the stress tensor, K is the elastic bulk modulus, $s_{ij}$ is the stress deviation tensor, G is the elastic shear modulus, $d\lambda$ is coefficient of proportionality, and f is the yield function. One must consider the ramifications of having a flow rule in Equation 5. It is the flow rule which provides for the calculation of the plastic strain increment ($de^p_{ij}$) and specifies whether flow is associated or nonassociated. The plastic strain increment is determined as follows:

$$de^p_{ij} = d\lambda \frac{\partial f}{\partial \sigma_{ij}}$$ (6)

13

where g represents the plastic potential function. This function may or may not coincide with the yield function (f) at which plastic strains develop (Fig. 9). In the case of associated flow, the plastic strain increments are normal to the yield surface (i.e., f = g). Furthermore, Drucker's postulate for stability (1950, Ref. 12) applies. However, soil response is typically unstable as the soil approaches yield conditions due to strain softening behavior. Thus, the use of an associated flow rule precludes the accurate modeling of some mechanical behavior in certain soils. Furthermore, usage of the associated flow rule for soils which exhibit strain softening results in excessively large volumetric strain predictions when compared to experimental results. This is because accurate modeling of soils which are expected to undergo strain softening appears to require the use of a nonassociated flow rule (Refs. 13-15).

Proper modeling of soils which are expected to strain harden dictates the inclusion of a strain hardening law. The strain hardening law defines modifications to the yield surface during the course of plastic flow. Two general types of hardening laws (isotropic and kinematic) are suggested. Isotropic hardening laws dictate that the yield surface(s) isotropically expand or contract about the hydrostatic axis in principal stress space (Fig. 10). This type of law was proposed for models developed to predict soil response to monotonic loading. Kinematic hardening laws were developed to predict the response of soils subjected to cyclic loading. These hardening laws dictate that the yield surface(s) translate in stress space, sometimes changing shape or size during plastic flow (Fig. 11). These stress-strain history-induced modifications determine the constitutive response during load reversals. Models with kinematic strain hardening usually agree more closely with experimental results than models using isotropic strain hardening (Ref. 11).

The "cap model" proposed by DiMaggio and Sandler (Ref. 16) and improved by Baladi and Rohani (Ref. 3) will now be presented as an example of incremental plasticity. This model is based on a classical incremental elastoplastic strain-hardening theory. It includes a stationary ultimate strength (failure surface) which serves as the bounding yield surface and a strain-hardening moving cap situated between the ultimate strength surface and the hydrostatic stress axis (Fig. 10). Stress states on one instantaneous surface, therefore, are

14
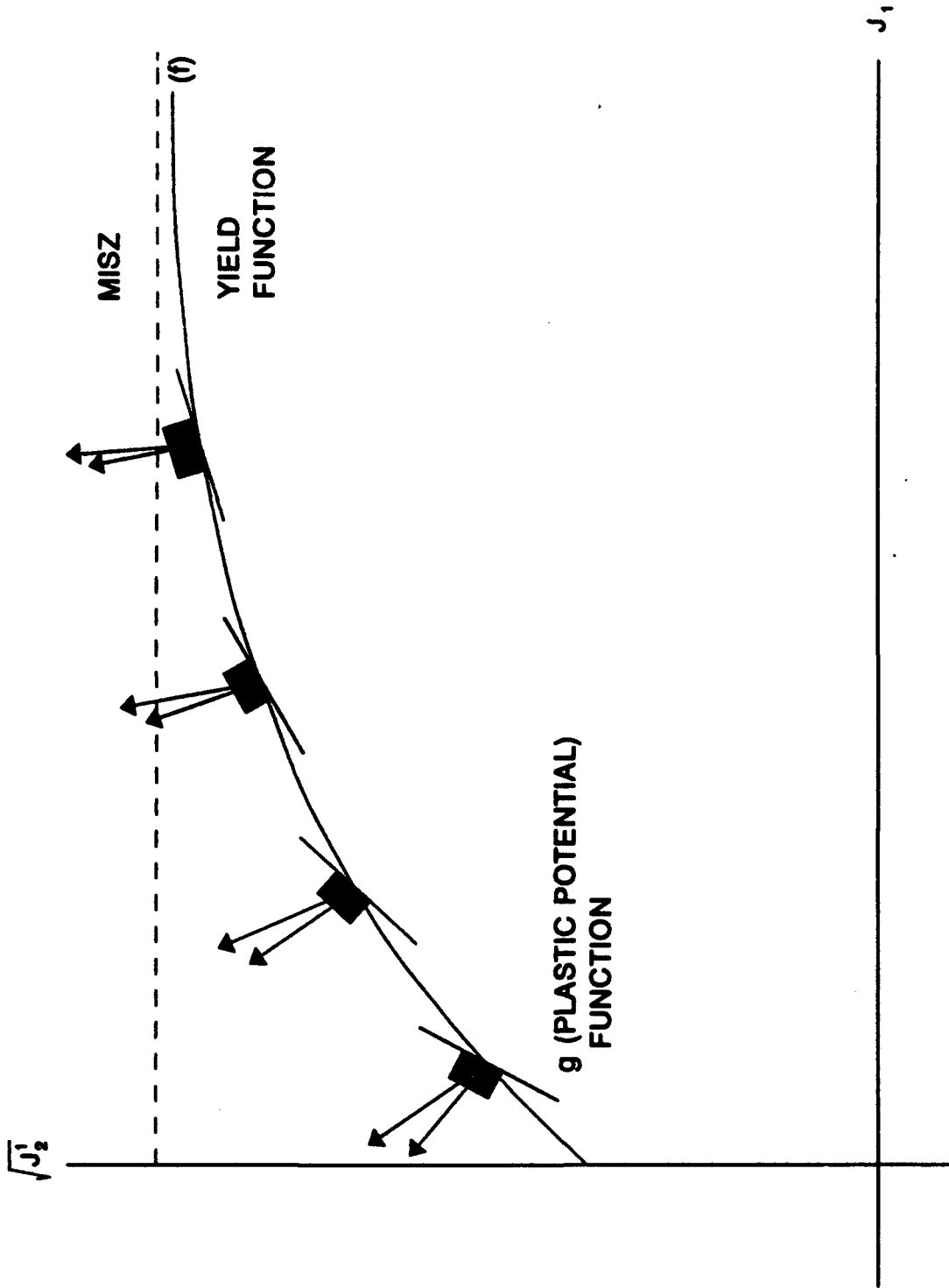
Figure 9. The plastic potential function (g) approaches the yield function (f) as mac·oscopic strain increases.
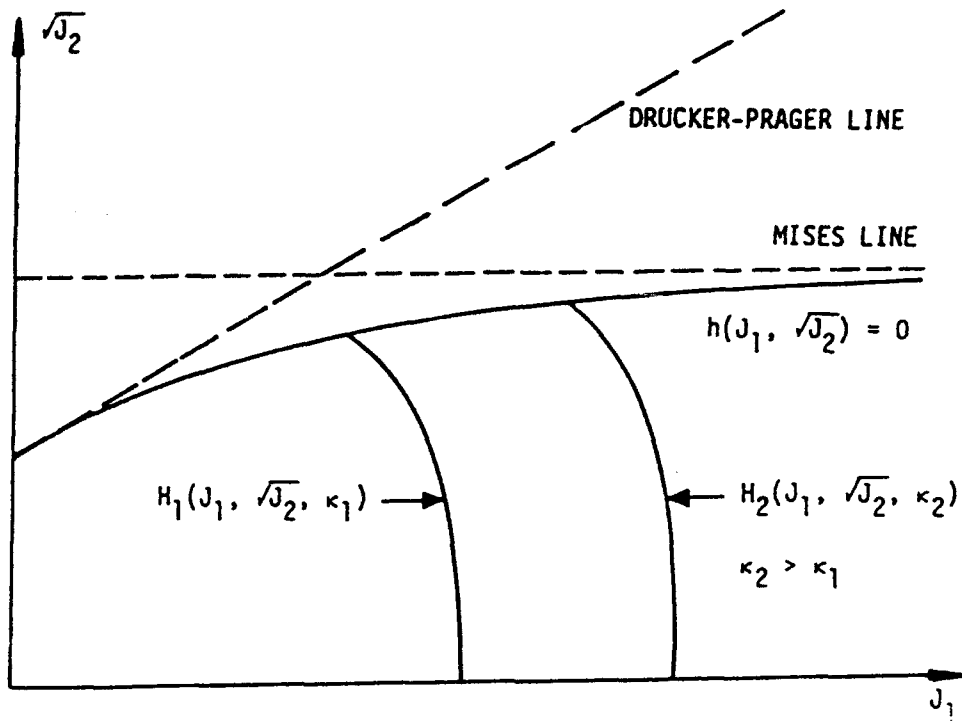
Figure 10. Loading function for the cap model (from Ref. 3).
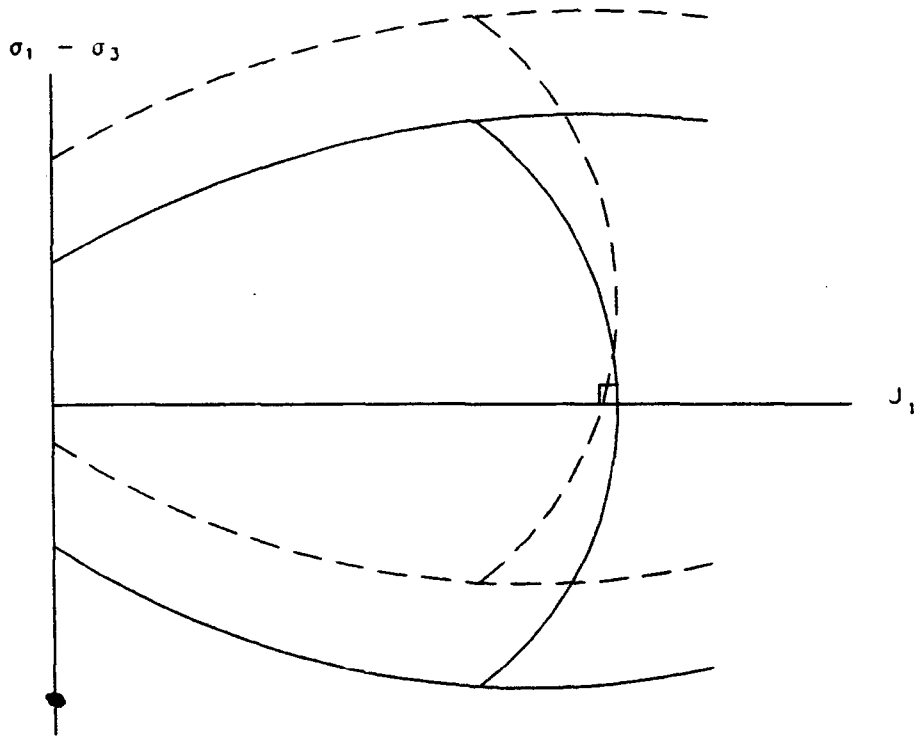


Figure 11. Yield surfaces translate in stress space and
change shape during plastic flow.

cha...cterized by a common single value of a strain parameter such as volumetric plastic strain. This parameter is also used as the state parameter in the hardening rule. Thus, this hardening parameter is the characteristic which determines the movement of the cap surface according to a semiempirically developed hardening rule (Ref. 7). In an attempt to improve the model's ability to account for path-dependent effects and other features of anisotropic hardening plasticity, Reference 3 proposed a means of changing the ratio between the major and minor ellipse axes. At the same time, Sandler and Baron (Ref. 17) introduced kinematic hardening to enable the prediction of hysteresis during repeated loading and unloading. Thus, the plasticity model has been refined to include many realistic aspects of soil behavior; e.g., dilatancy, hysteresis, and densification under isotropic loading. However, as previously mentioned, volumetric strain controls the strain-hardening and volume change characteristics as opposed to void ratio terms. Typically, the void ratio terms are the state variables in critical state models developed expressly for soils. Although the relationship between volumetric strain and changes in the void ratio is direct, the use of the volumetric strain as a state variable instead of void ratio makes determination of the model parameters through laboratory testing more abstract.

As mentioned earlier, the cap model has limitations in the accurate modeling of cyclic loading and the prediction of stress and strain in anisotropic soils. This limitation applies to other models also (Ref. 3), and it is apparent that predictions made using the cap model are most accurate when based on isotropic soils and monotonic loading conditions. Several models have since been proposed which utilize a combination of isotropic and kinematic hardening laws.

## 1.3.3 The Endochronic Theory

The material responses demonstrate the existence of rate effects which are necessarily time dependent. Models which predict the influence of rate effects on material response usually invoke an experimentally determined empirical factor to adjust the response accordingly. A distinctly different approach which considers time to be an intrinsic material property is the Endochronic Theory (Valanis and Read, Ref. 8). This theory is founded on the concept of

intrinsic time. According to Valanis, time is a commonly used measure of change. Using the example of a pendulum,

> "...A change in the position of a pendulum from one extreme to the other measures half a period. If the period of oscillation is one second, then half a second is the measure of change in the above positions. In an ideal pendulum, the period is invariant; i.e., the temporal distance between two events (in this case, the two extreme positions) is always constant. If no one marks off on the real line points corresponding to the ends of half period (or periods), these points are all equidistant. A continuous time scale is now created by assuming that the density of events between any two points is, in fact, constant. As it happens, the motion of the pendulum relative to its own time scale satisfies Newton's second law of motion. Consider now another system which is not cognizant of a Newtonian time scale. A metal whose stress response is strain rate insensitive is such a system. The internal changes that determine the stress state begin at the onset of deformation and end when deformation stops. No further internal changes will take place unless the state of deformation changes. This is another instance in which time is a measure of change. In this case, however, if there is no internal change, there is no time change. Since the stress is, inevitably, determined by the history of internal change, it is obvious that this history cannot be defined with respect to the Newtonian time scale but by one that is determined by the internal material changes brought about by the deformation. Such a time scale is obviously intrinsic to the material at hand. Thus, the Endochronic theory advocates that stress is a function of the history of plastic strain expressed in terms of 'intrinsic time' with this time being the length of the plastic strain path in plastic strain space."

This theory is considered to be applicable in the study of plasticity in granular media because sands are considered to be strain-rate insensitive.

## 1.3.4 Local and Nonlocal Theory Formulations

Two general approaches exist when modeling the global response of granular media, the local and the nonlocal theories. A local theory is predicated on the understanding that the stress in a neighborhood is a function of the history of strain in the neighborhood. A uniform surface traction will result in a linear deformation gradient within the specimen and, thus, a uniform strain gradient. Other solutions cannot exist without a loss of well posedness

18

as will be explained shortly. However, certain phenomena which cannot be explained using a local theory (e.g., shear banding and nonlinear deformation gradients) have been observed experimentally. These phenomena are termed localizations. It is well accepted that these phenomena can only be modeled by the use of a nonlocal theory which can accommodate nonlinear deformation gradients. Brief descriptions of the local and nonlocal theories are presented next.

One must make an informed choice when selecting the partial differential equation to model materials which demonstrate nonlinear gradients. Consider the partial differential equations which define the wave propagation equation and the diffusion equation. These partial differential equations are hyperbolic and parabolic, respectively. Equation 7 is the wave propagation equation (hyperbolic) and Equation 8 is the diffusion equation (parabolic).

$$\frac{\partial^2 u}{\partial x^2} + \frac{\partial^2 u}{\partial y^2} + \frac{\partial^2 u}{\partial z^2} = C^2 \frac{\partial^2 u}{\partial t^2} \tag{7}$$

$$\frac{\partial^2 T}{\partial x^2} + \frac{\partial^2 T}{\partial y^2} + \frac{\partial^2 T}{\partial z^2} = b \frac{\partial^2 T}{\partial t} \tag{8}$$

If one expresses the Laplacian ($\nabla^2$) in a standard form, the equations appear in a more recognizable format.

$$\nabla^2 u = c^2 \frac{\partial^2 u}{\partial t} \tag{9}$$

$$\nabla^2 T = b \frac{\partial^2 T}{\partial t} \tag{10}$$

The Laplacian equals the following:

$$\frac{\partial^2}{\partial x^2} + \frac{\partial^2}{\partial y^2} + \frac{\partial^2}{\partial z^2} \qquad (11)$$

Thus, the wave equation is characterized by the wave propagation speed (c) and the diffusion equation by the diffusivity constant (b). Both of these equations are open-ended in that any positive values of c and b are acceptable for use in the equations. If the right-hand side of either equals a constant, the equations reduce to elliptical equations like:

$$\nabla^2 u = CONSTANT \ or \ \nabla^2 T = CONSTANT \qquad (12)$$

The elliptical form is used to obtain closed-form solutions for conditions of static equilibrium. It is the elliptical form of these partial differential equations that is typically used to satisfy equilibrium conditions in the formulation of nonlocal constitutive models. The formulation is necessarily open-ended and equilibrium cannot be satisfied when one uses the higher order partial differential equations (either parabolic or hyperbolic) in an attempt to model the aforementioned localizations. Attempts to use the higher order partial differential equations to model the nonlinearities associated with localization result in a formulation which is mesh-dependent. Well posedness is lost.

Nonlocal theories are being investigated in an attempt to model localizations. On the evidence of some recent literature (Refs. 18 and 19), it appears that nonlocal theories have the potential of explaining the onset of localization. The results, however, are not quite definitive yet. There is currently no robust theory which will predict the onset of shear banding without the insertion of, for example, a weakened element within a finite element model or some other user-input catalyst.

A qualitative explanation of local theory is provided next using the example of uniaxial loading. Refer to Figure 12. A uniform load is applied at the top of the specimen and
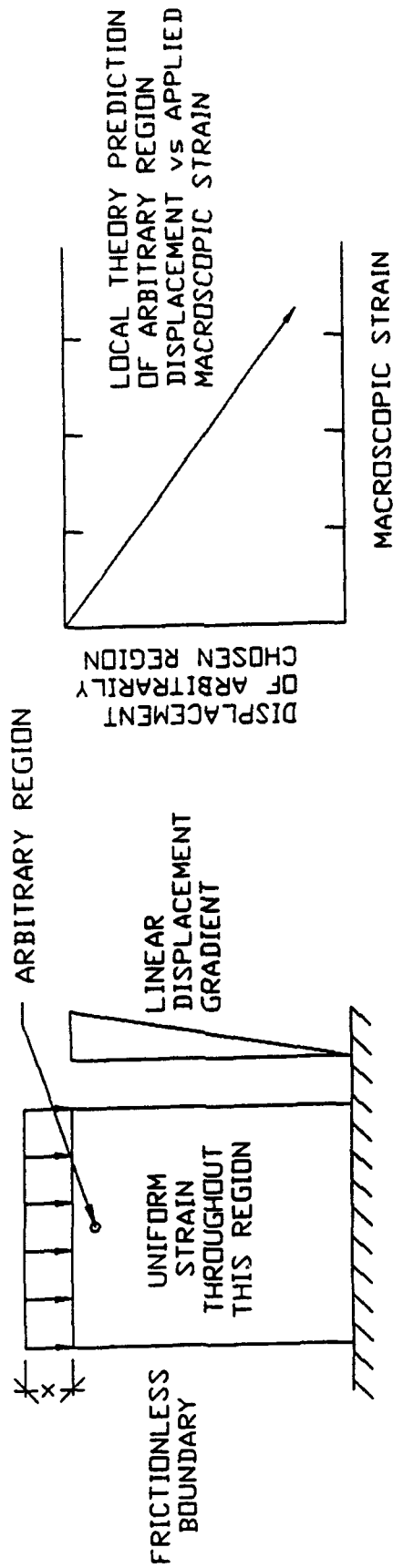
Figure 12. Linear displacement gradient and uniform strain prediction of local theory formulations.

some vertical displacement (x) results. The resulting displacement (U) within the specimen is then a linear function of x. They are directly related by the following:

$$U = \mu(x) \tag{13}$$

$$\varepsilon_x = \frac{\partial \mu}{\partial x} = a(constant) \tag{14}$$

And thus,

$$\mu = ax \tag{15}$$

Strain ($\varepsilon_x$) at any point in the specimen is the partial derivative of U with respect to x and is constant throughout. Thus, the local theory will predict a linear relationship between displacement of the specimen surface and resulting displacement at some point within the specimen and constant strain throughout. Furthermore, unloading will result in a line which retraces the loading path back towards the origin. This relationship will be true whether one is modeling an elastic, plastic, elastic-viscoplastic material, etc. A key element of this discussion is the assumption of no friction at the specimen container sidewall. However, friction is ever present in the systems (soil, structure, soil-structure) which these models are developed for, and to some extent present in the laboratory devices used to determine material parameters. Therefore, one cannot neglect its influence. Figure 13 shows the same uniaxial test chamber of Figure 12, but the effects of sidewall friction have been inferred.

Qualitatively, this influence results in a drag force being exerted on the specimen as it moves downward in response to loading cap displacement. The magnitude of the drag force is a function of the friction coefficient at the interface as well as the lateral force exerted by the specimen on the container wall. The significance of this influence is shown in the extreme case of the development of a shear band in granular soils. The width of the band is typically 6-10 grain diameters. Within the band, grains displace, rotate, and fracture,
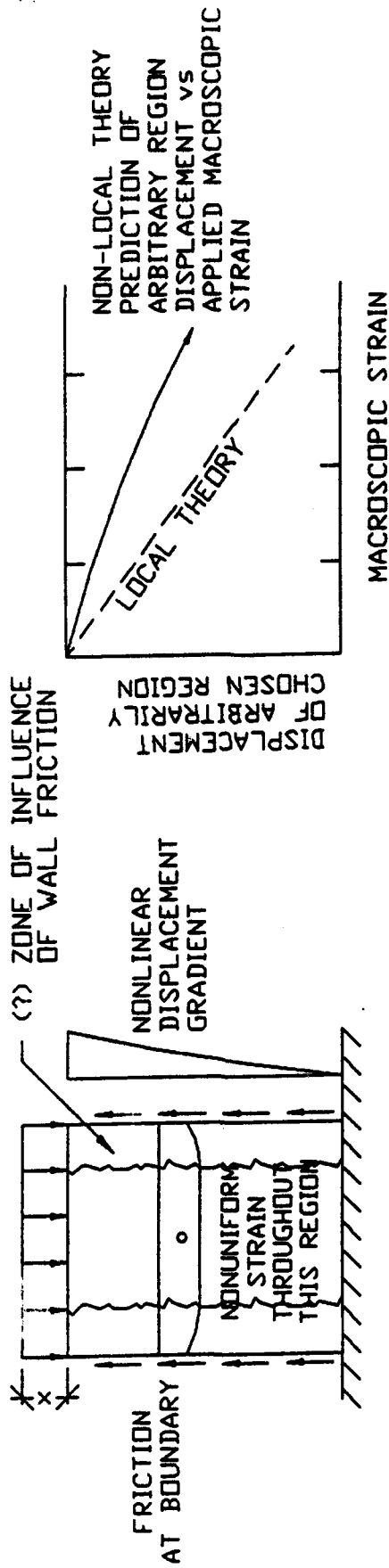
Figure 13. Nonlinear displacement gradient and strain prediction of nonlocal theory formulations.

resulting in energy dissipation. In the extreme, if one considers the sidewall interface as the middle of a shear band, the influence of the wall may only extend into the specimen for a distance of three to five grain diameters. As the localized disturbance associated with the formation of a shear band is not observed at the sidewall while the specimen is under uniaxial strain, the influence of sidewall friction is thought to be small. One must then consider how the presence of the wall alters the fabric of the soil near the interface and whether this influence may alter the perceived micromotions. As discussed in Section 6.0, direct comparison of the average grain displacements on the face of the specimen with those of grains within the specimen provides an indication of the influence sidewall friction has on the observed micromotions.

### 1.3.5  Summary of Phenomenological Theory

The loading response of granular material has been shown to be dependent on such aspects as stress state, loading rate, initial macroscopic conditions, loading path, degree of saturation, and drainage conditions, among others. Attempts to develop a model accurately accounting for all of these variables have frustrated due to a lack of understanding of how each of these aspects individually influence the material response and how they interact with one another as the original structure of soil changes during loading. Therefore, a wide range of innovative models has been proposed to model specific aspects of the response or predict behavior resulting from a specified loading regime. These models are based on the principles of elasticity, plasticity, elastic viscoplasticity, etc. The variety is increased by the need to invoke either an associated flow rule or a nonassociated flow rule and the existence of localizations. However, all of these models can be collectively grouped under the heading of phenomenological models. Such models attempt to predict the stress-strain response of soils following the determination of material parameters which are subsequently used to characterize the model. These models frequently incorporate experimentally determined empirical factors as a basis for predicting material response. At this writing, experiments are underway at the U.S. Army Corps of Engineers Waterways Experiment Station, Vicksburg, Mississippi, to develop a constitutive law based on triaxial laboratory experiments conducted expressly with the intention of investigating hardening rules, changes in the shape of the yield surface, normality, etc. This effort involves the conduct of

experiments on many laboratory specimens to better define a single yield surface. The results, though, will be applicable only to soils which will be subjected to monotonic loading. Thus, the resulting model may not accurately predict soil response during cyclic loading due to the effects associated with prestraining. The resulting model will be developed based on phenomenological results and not micromechanical considerations. The microstructural attributes of the material being tested are not considered in the formulation of the model.

In summary, some local theory phenomenological models have proven extremely successful in predicting soil response to specific loading regimes. Certain aspects of soil behavior such as shear banding and nonlinear deformation gradients (called localizations), however, cannot yet be accurately modeled using such techniques. Nonlocal theories have been recently developed to accommodate the development of localizations and some show reasonable promise. An alternative approach to modeling the continuum response of soils is the micromechanical or microstructural approach. These models attempt to replicate the stress-strain response of soils using theories founded on microstructural aspects of soil specimens. For granular soils, such aspects include grain geometry, fabric, intergranular contact forces, etc. Basic considerations of such theories will be presented in Subsection 1.4.

## 1.4 MICROSTRUCTURAL (PARTICULATE) CONTINUUM THEORY

Microstructure-based continuum theory is predicated on the understanding that the constitutive response of a granular material is influenced by microstructural properties (fabric, interparticle contact laws, granule composition, and cementation, etc.) as well as macroscopic properties such as void ratio, unit weight, degree of saturation, etc. Such an approach to modeling typically requires that simplifying assumptions be made regarding the geometry of the granular media. The media is usually represented by an assemblage of equal-sized disks (spheres) or mixtures of two or three different sizes. Furthermore, the material should be statistically isotropic with regard to contact orientation. These assumptions are made to simplify the computational demands of the respective models. Recent advances include the incorporation of elliptical (2D) disks or ovoid (3D) shapes (volumes) in discrete element formulations. Chang, Misra, and Sundaram (Ref. 20) have

investigated the influence of microstructural aspects on the modeling of granular media under low amplitude oscillations (<0.01% strain). Cundall and Strack (Refs. 21 and 24), Petrakis and Dobry (Ref. 11), and Trent (Refs. 23-25), among others, have investigated the evolution of microstructure in two and three dimensions during arbitrary loading of computer-generated granular media through the use of discrete element computer programs.

The following discussion presents basic microstructural considerations when one contemplates modeling the elastic response of granular media (wherein no plastic strain is considered to occur) and modeling the plastic response wherein the full array of microstructural effects (grain displacement, rotation, fracture, and disintegration) are known to occur.

## 1.4.1 Elastic Response of Granular Media

A "stiffness tensor" is commonly used to relate stress and strain in the generalized Hooke's law for elastic deformation. This tensor is strongly dependent on the packing structure of crystalline and granular materials having a high degree of symmetry. Examples of symmetric structures for which stress and strain appear to be dependent upon the stiffness tensor are the simple cubic, face-centered cubic, and close-packed hexagonal structures. Since these packings are not assumed to rearrange themselves under elastic deformation, the material response is considered to be related to the stiffness tensor of the symmetric structure. The same relationship between stiffness tensor and material response is also thought to exist for random packings of grains found in sands. Chang and Misra (Ref. 26) conclude that for soils, the regularity associated with symmetric structure does not exist and "...it is easier to derive the stress-strain relationship based on a microstructural continuum approach." Therefore, derived stiffness tensors appear suitable only for cases where very small changes in the packing structure are expected during loading. To accurately model deformations beyond the elastic limit of the material, it is necessary to understand the evolution of the stiffness tensor as loading progresses. Discrete element techniques are appropriate alternatives for modeling this evolution. Basic components of discrete element formulations with special emphasis on the modeling of frictional materials are presented next.

## 1.4.2 Plastic Response of Granular Media

Discrete element techniques are not widely accepted as being suitable for the modeling of interaction between discrete bodies. Originally developed for the study of rock block movements, this technique has been refined to permit the study of interaction between 100s (and even 1000s) of arbitrary shapes (volumes) under a wide variety of static and dynamic loading configurations. The technique is particularly well suited for the study of frictional materials.

The principal difference between discrete element modeling and classical continuum modeling is that the discrete element method considers the specimen to be made of 10s, 100s, or 1000s of individual grains which interact with one another during loading. This interaction allows for highly nonlocalized response in some portions of the specimen. As mentioned earlier, classical (local) continuum models are typically based on the assumption that uniform macroscopic loading/deformation of a specimen results in a linear deformation gradient and, thus, a uniform strain gradient within the specimen. Other solutions cannot exist without loss of the well posedness of the boundary value problem. Thus, discrete element models have been developed in part to account for the possibility that uniform surface loadings may result in nonuniform interior deformation and strain gradient fields. Two such models, TRUBAL and CONBAL, will be presented.

1.4.2.1 TRUBAL. Discrete (distinct) element programs have been used to exercise constitutive models which are based on the microstructural changes observed in granular media under arbitrary loading. The first widely accepted program of this type was BALL (Cundall and Strack, Refs. 27 and 28). The program was intended to account for the changes in fabric which occur in granular media under deformation. BALL is used for modeling two-dimensional grain structures; the program TRUBAL is used for modeling in three dimensions. Many improvements have been made to the basic program as well as the constitutive model within it. Such improvements include the capability of modeling the response of assemblages of different size grains and modeling the response of lightly cemented grains. Improving the technique caused modification of the contact laws which dictate the force-displacement relationship between individual grains. Variations of these

27

improved models have been created to focus on specific aspects of granular media response as well as produce output in a tailored format. This subsection will focus on the development of the original concept of the BALL program and its implementation. Limitations in this modeling technique will also be discussed.

The BALL program uses an explicit time-marching scheme to track the motion of individual particles, with the motion of each being governed by conservation of momentum. Figure 14 shows two particles, x and y, which are in contact at point C. Two unit vectors ($e_i$ and $t_i$) are defined as pointing from the center of disk x to the center of disk y and rotated 90-degrees clockwise, respectively. The relative velocities, $X_i$, of the points on overlapping surfaces are shown to be functions of the absolute rotations and velocities of each particle. The normal and shear components of these velocities may then be calculated as the projections of $X_i$ in the appropriate directions, e.g., $e_i$ and $t_i$, respectively. The velocities are assumed constant over a time step. Thus, the incremental displacements are obtained by time integration. The normal and shear stiffnesses ($k_n$ and $k_s$) are then used to obtain incremental forces. These are then added to the previous values to obtain total normal and shear forces with the constraint that the shear force is limited to a fraction of the normal force, $\tan\phi_u$, plus a constant cohesion. This sequence of calculations is performed for each contact prior to the application of the motion equations for any particle. Since all forces are known at every contact point, the moment and force totals on each particle may then be used to calculate translational and rotational accelerations through a difference approximation to Newton's second law. The moments and forces are assumed to be constant from time $t^{n-1/2}$ to $t^{n+1/2}$ so the velocities, centered at time $t^{n+1/2}$, are obtained by integrating the accelerations over $\Delta t$ and incrementing the previous values. A second integration yields the new position and rotation, centered at $t^{n+1}$. The time step is taken to be small enough that particles are unaffected by motions more than one diameter away. The new total velocities will then be used to calculate accelerations at time $t^{n+1}$ after the force-displacement relations have again been applied to the contacts. As interparticle overlaps change, contacts are deleted and new ones added. For additional detail, see Cundall and Strack (Refs. 27 and 28).

$$e_i = \frac{y_i - x_i}{D} = (\cos\alpha, \sin\alpha)$$

$$t_i = (\sin\alpha, -\cos\alpha)$$

| Particle Center | Translational Velocity | Rotation Rate |
|---|---|---|
| $(x_1, x_2)$ | $\dot{x}_i$ | $\dot{\theta}_x$ |
| $(y_1, y_2)$ | $\dot{y}_i$ | $\dot{\theta}_y$ |

### FORCE-DISPLACEMENT LAW

**For all contacts**

1. Relative Velocities: $\dot{X}_i = (\dot{x}_i - \dot{y}_i) - (\dot{\theta}_x R_x + \dot{\theta}_y R_y) t_i$
   $\dot{n} = \dot{X}_i e_i, \qquad \dot{s} = \dot{X}_i t_i$

2. Relative Displacements: $\qquad \Delta n = \dot{n}\, \Delta t, \qquad \Delta s = \dot{s}\, \Delta t$

3. Contact Force Increments: $\quad \Delta F_n = k_n \Delta n, \qquad \Delta F_s = k_s \Delta s$

4. Total Forces: $\quad F_n = F_n^{n-1} + \Delta F_n, \qquad F_s = F_s^{n-1} + \Delta F_s$

5. Check for Slip: $\quad F_s = \min\left(F_s, \; F_n \tan\phi_\mu + c\right)$

6. Calculate Moment: $\quad M_x = \Sigma F_x R_x, \qquad M_y = \Sigma F_y R_y$

### EQUATIONS OF MOTION

**For all particles**

1. Assume Force & Moment Constant over $\Delta t$: $(t^{n-1/2} \text{ to } t^{n+1/2})$

2. Acceleration: $\quad \ddot{x}_i^{\,n} = \frac{\Sigma F_i}{m}, \qquad \ddot{\theta}^{\,n} = \frac{\Sigma M}{I}$

3. Velocity: $\quad \dot{x}_i^{\,n+1/2} = \dot{x}_i^{\,n-1/2} + (\ddot{x}_i^{\,n})\Delta t$
   $\dot{\theta}^{\,n+1/2} = \dot{\theta}^{\,n-1/2} + (\ddot{\theta}^{\,n})\Delta t$

4. Assume velocities constant over $\Delta t$: $(t^n \text{ to } t^{n+1})$

5. Displacements: $\quad x_i^{\,n+1} = x_i^{\,n} + (\dot{x}^{\,n+1/2})\Delta t$

6. Rotation: $\quad \theta^{n+1} = \theta^n + (\dot{\theta}^{\,n+1/2})\Delta t$

INCREMENT TIME

Figure 14. Calculational sequence for distinct element code (from Ref. 27).

1.4.2.2 **CONBAL**. Because of shortcomings in the early version of the discrete element program TRUBAL, particularly with respect to the interparticle contact laws, Petrakis and Dobry (Ref. 11) refined the code by introducing Hertz-Mindlin contact laws (Refs. 29-31). This research was proposed to develop a constitutive model for granular soils expressed in traditional continuum mechanics terms but grounded on the particulate micromechanical behavior of the material. The primarily analytical effort involved refinement of the laws modeling the response between two elastic spheres, using the new laws to study the response of regular and random arrays of spheres. The refined contact laws were incorporated in a discrete element program. Analytical predictions using the program were compared with test results on glass beads subjected to axial-torsional tests in a hollow cylindrical loading device. The experiments and numerical simulations confirmed that the yield surface(s) of the granular material compress(es) along the loading axis as loading progresses but not in other directions.

As mentioned previously, this effort required generalization of the contact laws for interaction between two rough spheres. Although Hertz, Mindlin, and Deresiewicz (Refs. 29-33) had solved this problem for a limited number of cases, incorporation of the law into a discrete element program required laws to be developed for arbitrary loading and the utilization of an incremental elastic-plastic model.

The question of contact law between two particles is most critical in modeling the deformation of noncemented granular materials. This is because the macroscopic response is considered to be a function of the elasticity of the particles and the geometry of the contacts as well as the coefficient of friction at the contact. Particle elasticity and contact geometry appear to be the most important at low levels of strain with particle shape, contact geometry, and friction becoming the controlling factors as interparticle shearing increases. Reference 29 demonstrates that the normal force deformation behavior at a contact is nonlinear elastic if fracture is not permitted. Various solutions have since been proposed for contact between unequal diameter spheres with arbitrary combinations of normal and shear forces being applied. Typically, these solutions dictate an infinite shear stress at the edge of the contact area and permanent slip is induced. This aspect of the model introduces the need to consider energy dissipation and represents the key advance in Seridi and Dobry's

solution (Ref. 34) vice the early models of Mindlin (Refs. 30 and 31). Figure 15 shows the nonlinear force-deformation curve associated with the application of a monotonically increasing tangential force to two spheres in contact under a constant normal force. Reference 34 has solved this problem with the constitutive law founded on the incremental theory of plasticity. The model assumes kinematic hardening and relies on the existence of an infinite number of yield surfaces. These are features which have been shown to provide the most accurate predictions in earlier phenomenological models. The constitutive relation (implemented in the program CONTACT) has been shown to provide accurate reproductions of the analytical solutions obtained by Mindlin and Deresiewicz (Ref. 31). The constitutive law has since been incorporated in the discrete element program TRUBAL resulting in the program CONBAL.

Although the aforementioned modifications in the discrete element program BALL have resulted in improved predictive capabilities, it appears that a wider variety of micro-structural effects must be incorporated before one can predict responses in a complex loading environment. As a minimum, localized displacement of particles, the development of clusters, individual particle fracture and disintegration, and particle rotation must be explored and incorporated. If moist or saturated soils are to be modeled, then one must also consider effective stress, hydrostatic pressure, dynamically included pore pressure, and fluid flow within the voids. Many attempts have been made to quantify changes in these microstructural parameters on specimens which have been subjected to some prespecified macroscopic strain or stress level. Some of these efforts have even provided such information as the soil (soil simulant) was deforming. However, limitations in experimental techniques and computational abilities have precluded the development of a unified theory which links microstructural effects to the continuum response of frictional materials.

### 1.4.3 Summary of Microstructural Theory

Several computer-based techniques have been used to aid in the investigation of microstructural effects and their influence on the continuum response of granular media. The principal technique involves using the discrete element codes BALL and TRUBAL (or their derivatives) to conduct parametric studies on macroscopically similar specimens.
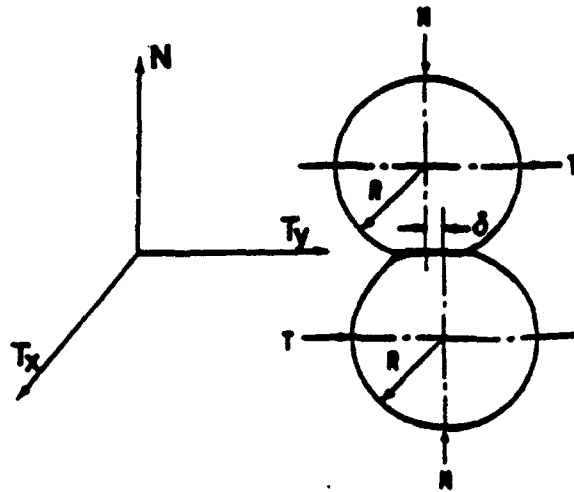
Elastic spheres under normal and tangential loads.
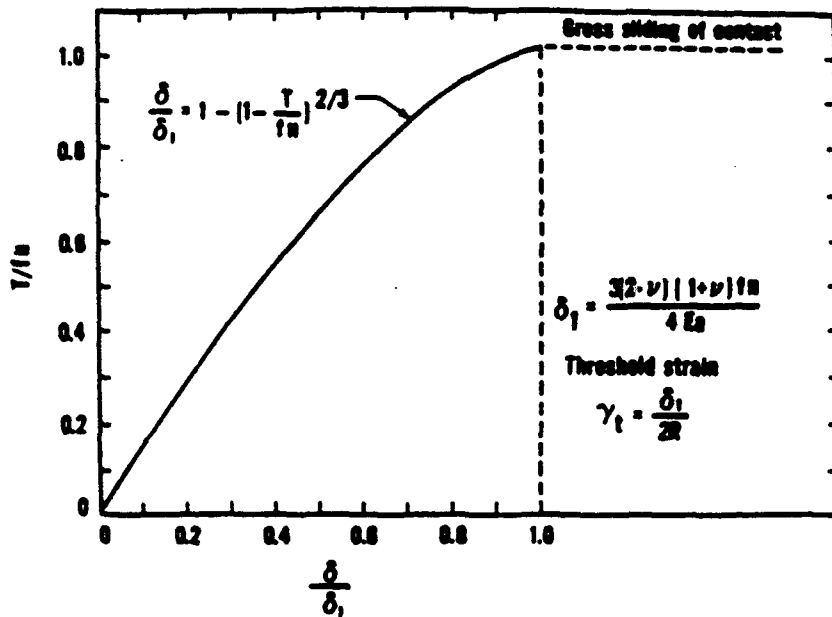


Figure 15.  Nonlinear force-deformation curve for elastic spheres under normal (N) and tangential (T) loads (constant N, T increasing) (from Ref. 34).

Similarly, numerical studies are conducted on "specimens" which have been changed subtly or subjected to various stress paths prior to testing. The purpose of such testing is to identify and quantify the influence of some specified microstructural effect. A perceived limitation is the inability to model other than disks (in 2D) and spheres (in 3D). Thus, the influence of particle shape could not be investigated using the early codes. Recent advances in the discrete element technique involve the incorporation of particle bonding and the ability to model elliptically shaped particles. These codes provide the stress-strain response of the assemblage as well as the response to elastic wave passage; however, only a limited capability exists to highlight and visualize specific microstructural events which may control the macroscopic response. As the codes are refined to include irregularly shaped particles and particle fracture, the ability to isolate and study specific microstructural occurrences may provide insight regarding the formation of localizations which control the overall response.

## 1.5 PURPOSE

The purpose of this research was to investigate the evolution of microstructural effects in granular material under uniaxial strain of up to 10.0 percent. The relative influence of several microstructural effects (such as grain displacement, rotation, fracture, and disintegration) on strength mobilization was studied. These microstructural effects were investigated to quantify the influence of each on the constitutive response of granular material and to develop methods of incorporating such effects into a microstructure-based constitutive model. Special attention was paid to those microstructural effects which easily lend themselves to incorporation in a discrete element computer code.

## 1.6 OBJECTIVES AND SCOPE

The principal objective was to investigate the evolution of fabric, the preferred orientation of individual grains as well as their packing arrangement, in granular media under uniaxial strain. T¹ purpose was also to investigate the evolution of damage in granular media under uniaxial strain to better understand how these microstructural effects contribute to the

constitutive response of the material. A related goal was to quantify microstructural effects which occur on the surface of a granular specimen as well as internal effects. Such information is required to discern how the existence of a specimen boundary might influence the manifestation of microstructural effects. Furthermore, this effort was intended to identify the microstructural effects which most directly influence the macroscopic response of granular media. Lastly, a goal was to identify methods of refining studies of the evolution of fabric in granular media under loading.

Cuboid specimens of poorly graded, well-rounded silica grains (nominal diameters of 0.50 and 0.75 mm) were subjected to uniaxial strain in a rigid-walled confinement vessel. Micromotions and the evolution of damage were directly observed through sapphire windows in the sides of the confinement vessel in a series of displacement-controlled tests. Companion displacement-controlled tests were conducted using x rays to study the micromotion of embedded lead particles. Macroscopic vertical strain was limited to 10 percent. Lateral strain was not permitted. Selected specimens were epoxy-impregnated and subsequently sectioned to investigate internal microstructural changes. The microstructural effects observed during loading and following epoxy impregnation were related to the constitutive response of the material and limitations in the current experimental techniques (principally edge effects) are discussed. An integrated experimental/computational microstructure study technique is proposed.

## 2.0 REVIEW OF PREVIOUS RESEARCH

Several distinct approaches have been taken regarding the study of the microstructural response of loaded soils. The most direct, but potentially tedious approach involves quantifying the coordination number (number of contacts per particle), contact orientation, and changes in these attributes following load application. This approach generally involves immersing a specimen in paint or ink and then draining the pore fluid to create rings at particle contacts, the number and orientation of which can subsequently be quantified. Another common method of microstructural investigation involves epoxy impregnation of soil specimens to permit sectioning and direct observation of specimen internal attributes. Yet another approach involves the use of embedded lead particles and x rays to directly view or infer the displacement (strain) which occurs in a specimen during loading. Lastly, a common technique for studying the loading response of soils involves the use of assemblies of photoelastic disks subjected to various loading regimes while being viewed in polarized light. This technique permits the direct determination of the stress distribution among disk assemblies under either static or dynamic loading. The advantages and disadvantages of these approaches will be presented.

The technique of using paint/ink infiltration techniques to identify particle contacts and infer assemblage geometry enjoyed brief popularity in the early stages of microstructural studies. This technique required the creation of an assemblage, of either spherical or slightly irregularly shaped particles, which was subsequently immersed in dilute paint or ink. Drainage of the pore fluid resulted in small rings remaining at the points of contact between adjacent particles. "Dissection" of the specimen permitted the researcher to determine the number of contacts per particle and the general distribution of contacts on the particle surface. The static nature of the data collection technique limited this type of analysis to studies of the packing geometry and provided no information regarding the evolution of this geometry, or "fabric," as the specimen was subjected to stress or strain. Furthermore, the contact geometry associated with each individual particle served as the basis for the development of a geometry which was then attributed to an "average" particle. Subtle changes in particle orientation or contact geometry which might influence the constitutive

response of the assemblage were being lost during data reduction. This technique has also been applied to soil specimens (irregularly shaped particles with a nominal diameter of ~ 1.0 cm); however, the sheer tedium of this method and the limited data available make this an unattractive technique.

Matsuma Oda (Ref. 35) is considered to be the pioneer in the study of soil fabric using the technique of epoxy impregnation and sectioning. These studies helped define the concept of fabric to be discussed in Section 3.0. Oda's technique involved the epoxy impregnation of soil specimens which served to "freeze" the individual particle orientations. Subsequent sectioning of the ecimens (through the use of a diamond saw) permitted the researcher to view particle orientations and infer contacts. This technique was used to study a variety of granular soils with literally thousands of individual particle orientations and contacts being observed/inferred. Although innovative, several shortcomings in this technique became apparent. Polishing the cut surface of the specimens permitted limited observation of the contacts which existed slightly below the exposed surface. This was useful as very few contacts fell exactly on the plane of the exposed section. Out-of-plane contact orientations had to be inferred through manual observation. This aspect of the technique introduced subjectivity. Furthermore, limitations in visualizing the three-dimensional fabric or incorporating such information in a computer code limited presentation of results to a two-dimensional format. Figure 16 shows a rose diagram typically used in the representation of contact orientations. Such diagrams have become useful in the visualization of the force exerted on an "average" particle at a specified orientation. Thus, Oda's work highlighted the need to explore and visualize the three-dimensional nature of the particle contact orientations. However, it was limited by the need to manually interpret particle and contact geometry and an inability to visualize fabric in its true three-dimensional form.

Regarding the use of x-ray techniques, Reference 4 defined the strain field which occurs in cylindrical specimens of dry, dense sand subjected to triaxial compression. The deformation field in laboratory-prepared specimens was quantified by placement of lead beads within the specimen in a vertical plane which was parallel to and passing through the specimen longitudinal axis. X rays taken during loading were used to quantify the deformation and

36
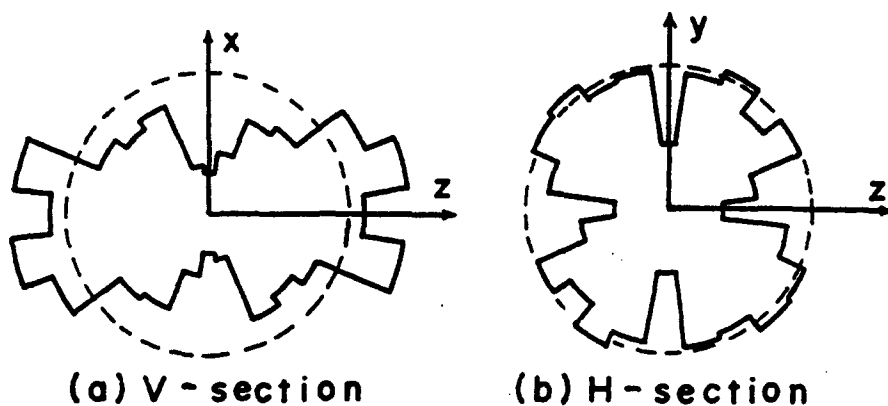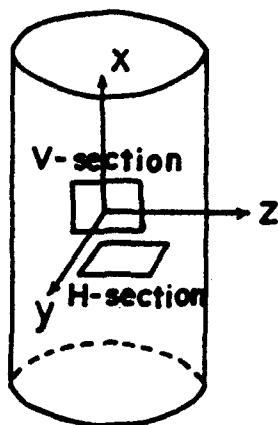
Figure 16. Typical rose diagram for granular material. The V-section
shows that the long axes of particles have assumed a primarily
horizontal orientation (from Ref. 35).

strain fields. Deman (Ref. 4) determined that when deformations are nearly homogeneous, dense, granular soils exhibit little or no strain softening. This determination was made by comparing the response of triaxial specimens with some having either lubricated or nonlubricated end platens (Fig. 17). Triaxial compression tests were performed on flat specimens of dense, dry sand and concluded that only an insignificant amount of strain softening occurred. Vardoulakis (Ref. 18) used x-ray radiographs on sand specimens to study deformation patterns in sand under biaxial compression loading. Macroscopically, the specimen deforms uniformly until failure is reached; however, there is inhomogeneous internal deformation and thin shear zones develop and dilate during loading. The density of these zones is qualitatively different than that of the remaining sand specimen. Chen, Wang, Schreyer, and Rutland (Ref. 36) have used real-time x-ray radiography and image analysis to investigate the growth of small zones of localized, relatively large deformations within uniaxially loaded concrete mortar specimens. Considerable localized damage occurs within specimens (as reflected by macroscopic softening) when as little as 40 percent of the peak load has been applied. This result applies when the ends of the specimen are lubricated at the platen. Chen et al. conclude that the stress-strain relation cannot be directly derived from the force-displacement curve due to the nonhomogeneous material response. This type of research has provided a qualitative glimpse into the distribution of displacement and strain within laboratory-prepared specimens; however, the microstructural events which contribute to the development of the macroscopic response have continued to elude researchers.

Photoelasticity has been used quite effectively in the study of particulate material response to both static and dynamic load application. Regarding static loading, Oda, Kishino, and Nemat-Nasser, among many others, have explored the response of granular materials using two-dimensional assemblages of photoelastic disks. The disks resided in a loading frame which subjected the assemblage to a variety of loading paths while permitting the resulting isochromatic lines to be studied and photographed. These studies have typically involved quasi-static loading rates and circular "particles" of uniform size. Round particles of different diameters, however, have been mixed in the same specimen and ellipsoidal particles have also been studied. Research on such particle assemblages is conducted to

TRIAXIAL COMPRESSION OF DENSE SAND
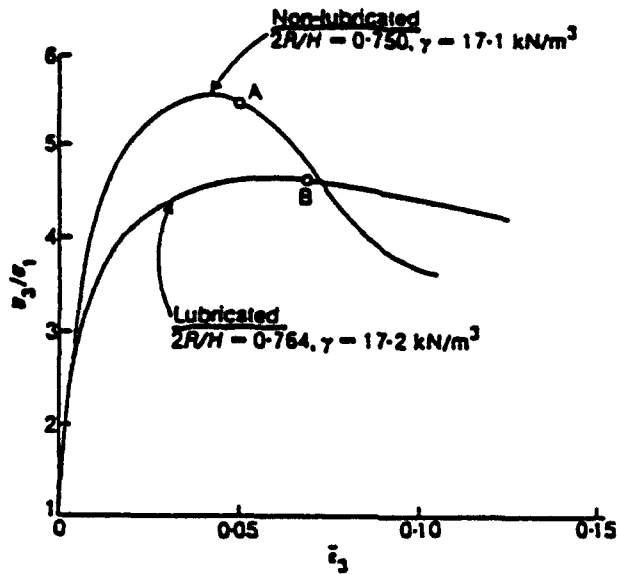
Stress ratio versus axial strain for dense sand -- triaxial compression (after Oeman, 1975)
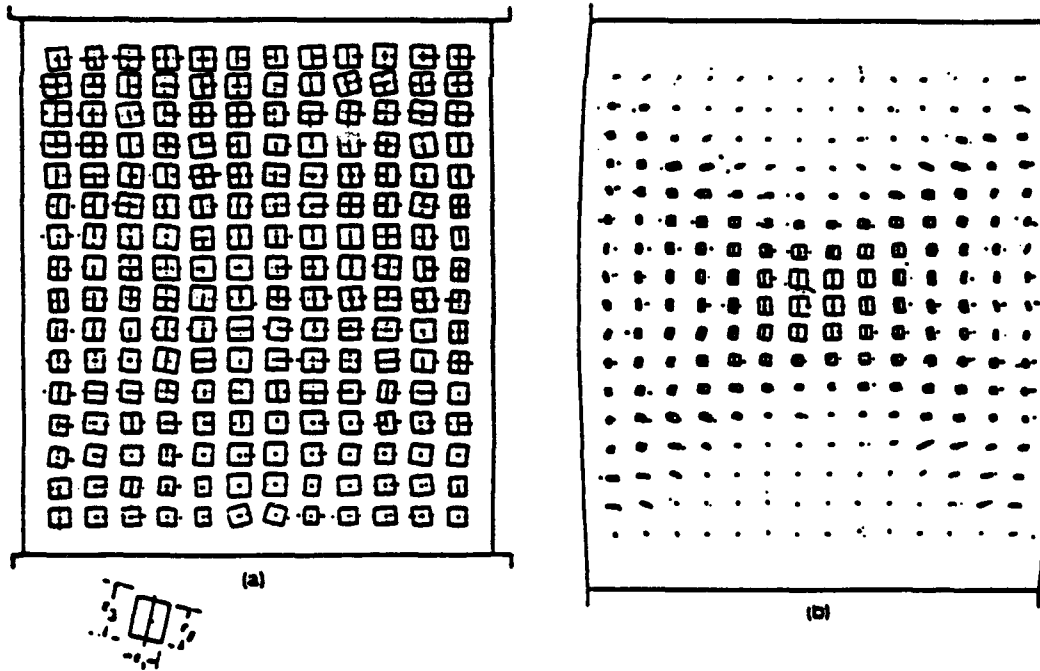
Figure 17. Internal deformation field for dense sand: (a) Lubricated end platens, and (b) Nonlubricated end platens (from Ref. 38).

better understand interparticle force and mobilized angle of friction. Additionally, the technique permits continuous observation of the assemblage response at the "particulate" level. The technique of testing round photoelastic particles lends itself most directly to comparison of experimental results with predictions made using discrete element programs such as TRUBAL and CONBAL. But direct comparison of the results of a photoelastic disk experiment with laboratory soil specimens highlights the relatively stiff response of the photoelastic disk assemblage. The two-dimensional representation of the soil particles does not capture the realities of the three-dimensional soil specimen. Additionally, the experiments conducted using photoelastic disks provide little or no information regarding the failure and postfailure response of the assemblage as the disks are typically not stressed to the point of fracture. This technique is limited by the need to conduct tests using only two-dimensional representations of simple geometric shapes and the inability of testing beyond "failure" of the assemblage.

Photoelasticity has been used for the study of wave propagation in granular media by Shukla and Sadd (Ref. 39). Cinema photography using stroboscopic light permits the recording of shock wave passage through an assemblage of two-dimensional photoelastic disks. As this effort is concerned primarily with quasi-static loading of particles, microstructure study using dynamic photoelastic techniques will not be discussed.

### 3.0 THE CONCEPT OF FABRIC IN GRANULAR MEDIA

There are two basic components of fabric, particle orientation and packing (Fig. 18), in nonspherical particles. These two concepts are used to quantify the spatial arrangement of particles as well as the resulting voids. Within these two categories, there are five commonly accepted elements of fabric. Particle orientation can be quantified using the elements of vector mean direction and vector magnitude. Packing can be quantified using the probability density function of normals at contacts, the mean of the coordination number, and the standard deviation of the coordination number (Ref. 35). These terms will be explained shortly. These elements are useful in exploring some properties of granular materials such as anisotropy and dilatancy during shear. Furthermore, they have been used as the basis for theories regarding the constitutive response of granular media.



**(1) Orientation**  **(2) Packing**
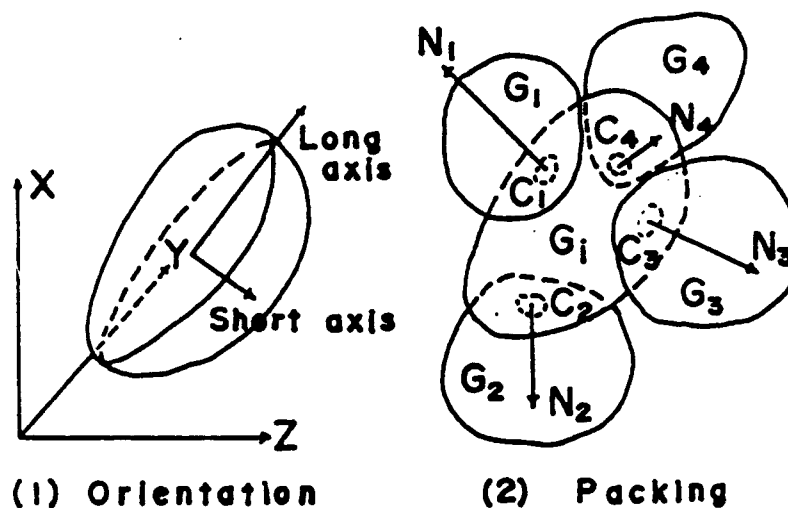
Figure 18. Concept of fabric in granular material (from Ref. 35).

Particle orientation fabric is determined from knowledge of the vector mean direction and magnitude of typical dimensional axes of a suitable number of particles within a given sample. The exact determination of the true long axis of a particle is quite difficult in practice. Therefore, an alternate procedure has been developed which utilizes the

information available from the thin sectioning of epoxy-impregnated granular specimens. Particle cross sections are exposed using this technique and the long axis of each of the exposed cross sections is designated the apparent long axis of the particle. The apparent long axes are then summed with respect to length and orientation and a weighted average of their distribution is used to produce a rose diagram. The principal attributes of this diagram are the vector mean direction ($\theta$) which denotes the preferred direction of the apparent long axes of each of the particles considered and the vector magnitude (VM) which is a measure of parallel alignment. Theta and VM are defined as:

$$\theta = 0.5 \, tan^{-1}\left\{\sum_{i=1}^{n} sin \, 2\theta_i\right\} + \left\{\sum_{i=1}^{n} cos \, 2\theta_i\right\} \tag{16}$$

$$V \cdot M = \left(\sum_{i=1}^{n} sin \, 2\theta_i\right) + \left(\sum_{i=1}^{n} cos \, 2\theta_i\right) \times \frac{100}{n} \, (\%) \tag{17}$$

where n is the number of measurements and $\theta_i$ is the inclination of the apparent long axis with respect to a specified axis. The vector magnitude is expressed as a percentage with 0 percent being a totally random orientation and 100 percent being a totally parallel alignment. Determination of these parameters on three mutually orthogonal planes can be used to define orientation fabric in three dimensions. An obvious limitation of this technique is that the orientation and magnitude of the apparent long axes may be influenced by the orientation of the chosen cutting plane(s). Additionally, the tedious nature of obtaining such information precludes the processing of a large number of samples.

Packing fabric is determined from knowledge of the particle's positions with respect to one another as well as the orientation and distribution of their contacts. Figure 19 shows one method of specifying the orientation of the two contact normals which result when two particles touch. When a substantial number of particles are considered, the coordination number (number of contacts per particle) becomes an important parameter in the determination of packing fabric. The importance of the contact normal orientations and the

mean and standard deviation of the coordination number are considered in the works of Oda, Nemat-Nasser, and Chang (Refs. 10, 20, 26, 35, and 38) among others, and will not be presented here. Only a limited capability exists to relate static load bearing capacity to various fabric attributes and configurations. The microstructural deformations and micromotions of individual particles in granular media under arbitrary macroscopic strain have yet to be incorporated in a microstructure-based model. Thus, there is no data relating the evolution of microstructural effects to the material constitutive response. This research has been conducted to provide such information by the direct observation of granular material under uniaxial strain and also to provide insight into the evolution of fabric under the same.
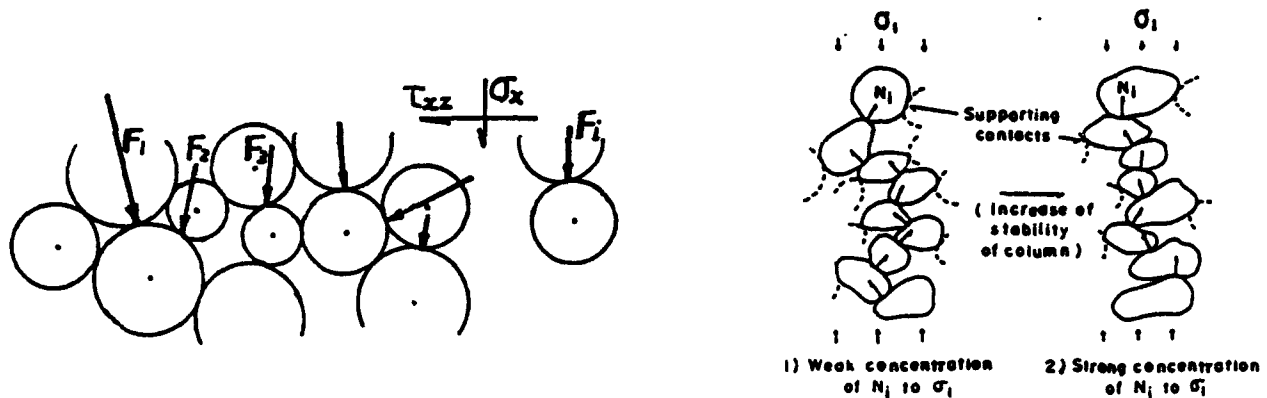


Figure 19. Schematic representations of two-dimensional granular assemblies.

## 4.0 EQUIPMENT DESIGN AND OPERATION

This section describes the equipment and some techniques used to observe the microstructural response of poorly graded sand under uniaxial macroscopic strain. Methods used to quantify the microstructural effects visible on the specimen surface as well as within the specimen are presented.

### 4.1 SPECIMEN CONTAINER

A specimen container (confinement vessel) was designed to prevent lateral expansion of the specimen and permit direct viewing (through sapphire windows fixed in the steel wall) of a soil mass' response to uniaxial strain. The confinement vessel consisted of a base plate, four walls, and a loading cap. The sidewalls extended up beyond the specimen and served as a guide for the cap which was used to displace the top of the specimen. The base plate, walls, and loading cap were made of 4130 heat-treated steel to resist abrasion by the soil grains. Initial testing was conducted in a container which permitted the simultaneous recording of specimen response through three orthogonally placed sapphire windows (Fig. 20). Tests revealed that no appreciable activity occurred at the base of any specimens up through the application of 10 percent macroscopic strain. Subsequently, testing was conducted in specimen containers which permitted simultaneous viewing of the specimen response through windows in three of the sidewalls. The containers were made to house a cuboid specimen with each side being 50 mm in length. The containers were designed to permit viewing at 0.375, 0.50, 0.56, and 0.75 specimen height (h) (Table 1).

Each viewing port was 25 mm in diameter and fitted with a 37.5-mm-diam. 0-deg sapphire window. The windows provided the means of viewing microstructural effects (individual grain displacement, rotation, fracture, and disintegration) during loading. Zero-degree sapphire was required for the windows because this material did not introduce any visual distortion as lateral loading increases on the window during uniaxial compression of the specimen. Fiducial marks were laser-etched on one side of each of the sapphire windows to serve as references against which grain motion could be measured. As the marks create a weakness in the window, they had to be on the inside (compression side) of the
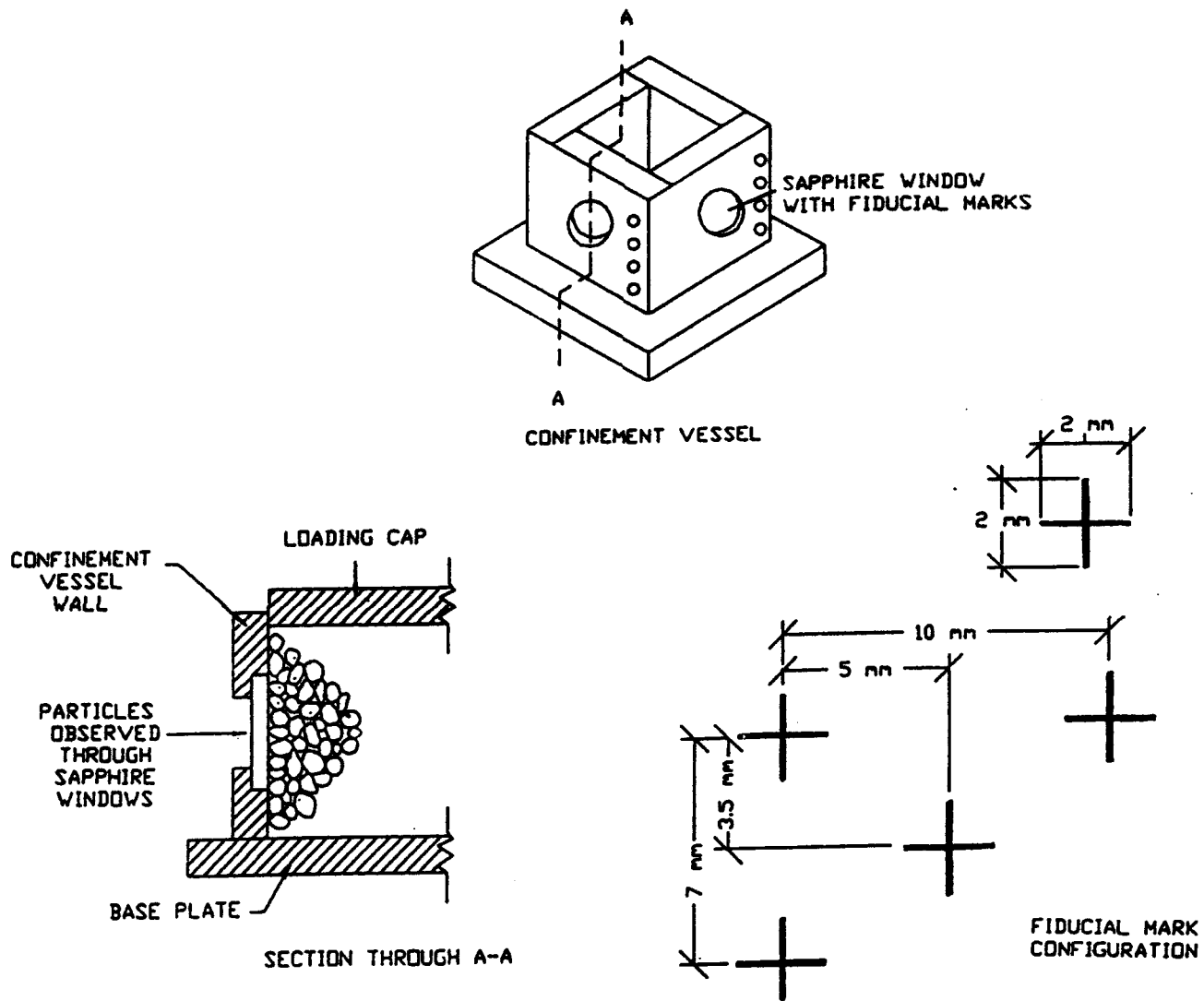
Figure 20. Confinement vessel details.

windows to reduce the potential for window fracture. This was beneficial as it also reduced parallax error during micromotion recording. The fiducial mark geometry is shown in Figure 20. The center cross hair in each window was located at the window center height as listed in Table 1.

Table 1. Height of viewing port centers for the specimen containers window center height (mm).

| h | 0.375 | 0.50 | 0.56 | 0.75 |
|---|-------|------|------|------|
| 50 | 19.0* | 25.0 | 28.0 | 37.5 |

NOTE: *This window was set at 19.0 mm because it was the lowest the window could be set within a confinement vessel wall. The window center height corresponds to 0.375 h.

## 4.2 SPECIMEN LOADING FRAME AND MACROSCOPIC PROPERTY RECORDING

All tests were conducted with the specimen being subjected to a constant macroscopic uniaxial strain rate of 0.5 percent per minute whether loading or unloading. Displacement control of the loading platen was the chosen method of applying strain to the specimen. Thus, for the 50-mm-tall specimen, the loading cap was displaced at 0.25 mm/min (0.0417 mm/s).

Two different loading frames were used for testing. The capacity of each was 100 kip. The maximum force required of the loading frames was ~35 kip (for specimens subjected to ~12.0 percent macroscopic strain). The principal loading frame was located at Los Alamos National Laboratories, Los Alamos, New Mexico, and was used during cinema recording of micromotions. The second frame was located at the University of New Mexico, Albuquerque, New Mexico, and was used when x rays were utilized to determine the internal micromotions during loading. Standard XY-plotters were used to display

measured load versus cap displacement during testing. Additionally, the load versus displacement response was digitally recorded as tests progressed.

## 4.3 MICROSTRUCTURAL RESPONSE RECORDING

The observation and recording of several microstructural effects (individual grain displacement, rotation, fracture, and crushing) were considered critically important during testing. The distinction is now made between the microstructural effects which are visible and can be recorded during testing (called surficial microstructural effects) and the effects which can only be observed posttest through the use of epoxy impregnation and sectioning (called internal microstructural effects). Although these effects are essentially similar on the surface as well as inside the specimen, the techniques needed to observe each are different and, thus, the distinction is made. Grain displacement and rotation on the specimen surface were observed through the mutually exclusive use of cinema or video recording of micromotions during testing. Internal micromotion was observed through the use of x rays as presented in Subsection 4.3.2. Evidence of fracture and crushing (considered as artifacts of the loading process) was observed after testing through the use of epoxy impregnation and sectioning techniques, presented in Subsection 4.3.3. The following subsections present the two techniques explored for the recording of the surficial microstructural response during loading.

### 4.3.1 Surficial Microstructural Response

Surficial micromotions were recorded primarily through the use of either 16- or 35-mm cinema or video techniques. The data regarding grain displacements were obtained solely through analysis of cinema images. Unsuccessful attempts were made to quantify grain rotations from these images. Shortcomings in this technique highlighted the need to develop a more refined system. Subsequently, video recording techniques were explored. No quantitative data were obtained using the video techniques; advantages of and recent advances in both techniques will be presented.

47

4.3.1.1 <u>Data Capture Through Cinema Photography</u>. Cinema images of the grain micromotions were obtained using either a 16-mm system with one image being recorded per frame or a 35-mm system with four images per frame recorded simultaneously. The 16-mm system relied on one lens per camera with one set of lens and camera being required for each sapphire window being viewed. The 35-mm system consisted of a photo-optic cable which permitted the simultaneous recording of up to four images per frame. The advantage of the photo-optic cable system (called the hydra-head) was that the microstructural response could be recorded from several positions on the same specimen with no ambiguity regarding the application of macrostrain at the time the image was obtained. Furthermore, only the hydra-head system was capable of recording images from the bottom of any given specimen. One "channel" of the photo-optic system was usually used to record the force versus deformation history from an XY-plotter. Thus, microstructural response could be more easily correlated with macrostrain-state. Both systems utilized the same 50-mm fixed-focal length lenses with the appropriate extension tubes for the desired degree of image magnification. Although the hydra-head offered the advantage of flexibility with regard to the choice of windows being viewed, as well as the ability to record the response at several locations at once, the images provided by the 16-mm system were far superior. As a result, the hydra-head system was not used following the determination that there was no appreciable microstructural activity to be studied through the sapphire window at the bottom of the specimen. The photo-optic cable had an insufficient number of strands to transmit a picture of quality suitable for the subsequent analysis of micromotion or grain rotation.

The preferred system, whether cinema or video cameras are used, appears to be that which uses one camera per specimen window. This restriction dictates the need to devise a method of equating a given image with loading cap displacement. Towards this end, a frame counter was used for each of the cinema cameras and the appropriate frame number recorded at critical points in the loading sequence, i.e., start of cap displacement, reversal of cap displacement during cyclic loading, and maximum displacement, etc. This system is suitable only if the loading and unloading strain rates are known and constant.

4.3.1.2  <u>Data Capture Through Video Recording</u>.  An alternate technique which relies on video camera imaging was investigated for quantifying the surficial microstructural response.  The feasibility of using such "machine vision" to quantify microstructural effects was demonstrated and a prototype system (hardware and software) is being developed.  Preliminary results are reported to aid the reader in choosing the appropriate technique (either cinematic or video imaging) for subsequent research.

The developmental video system uses three high resolution black and white video cameras, a laser-disc video recorder, and a sequencer to ensure that images are obtained from the appropriate camera at the proper time.  The principal advantage of using the video system is the ability to consistently determine the centroid and orientation of a given grain in each frame.  Grain fracture and disintegration can also be quantified unambiguously by such a system given suitable image analysis software.  Because these microstructural effects are important in the evolution of fabric under loading, they must be quantified in an unbiased and consistent manner.

Several processes must be performed on a single digitized image of the specimen to permit the detection and tracking of individual grains and remnants from image to image.  The images must undergo preconditioning to maximize the contrast between adjacent grains and between grains and voids.  The high-contrast image must then be "labeled" to separate the grains which are being tracked from the remainder of the image.  Subsequently, grain centroids and orientation must be determined to permit comparison between their current location/orientation and that in the previous image.  The results of this process then serve as the basis for analysis which includes determination of average direction and velocity of motion with respect to the fiducial marks, grain rotation, the formation of clusters, grain fragmentation, and the growth of damage.  The individual tasks in this process are detailed next.

Preconditioning is performed to produce the best possible image for labeling.  The three types of preconditioning used are histogram equalization, median filtering, and homomorphic filtering.  Histogram equalization is a commonly used contrast stretching

technique which broadens the grey level distribution of an image so that the image spans the entire grey level range available. This technique does not alter the information in the image. Rather, it matches the image to the range of grey levels best perceived by humans. Histogram equalization can be applied to the image as seen by the video camera before a test is conducted. This aspect ensures that only high contrast images will be provided for analysis. "Hot spots" due to uneven lighting can be minimized by this technique.

The second preconditioning technique, median filtering, is a process used to reduce noise in the image. A median filter is a nonlinear spatial filter which smoothes out random noise but preserves the grain edges.

The last method, homomorphic filtering, is used to improve the evenness of the image. This filtering technique is based on the multiplicative relationship between reflectance and illumination which constitutes an individual pixel's brightness. Brightness equals reflectance times illumination. Because of this relationship, reflectance and illumination cannot be filtered separately using linear filters. Therefore, one must take the logarithm of the image, which converts pixel brightness to the form log (reflectance), plus log (illumination). One can then take a two-dimensional discrete fast fourier transform (2-D FFT) of the image and apply a frequency-domain filter. This suppresses low frequencies which correspond to general illumination. Taking the inverse 2-D FFT and then the antilog of the transform results in a "reflectance-only" image. As reflectance is a material property, the image is necessarily more even.

The labeling process seeks to recognize object classes in the image (grains, remnants, voids, etc.) based on spatial and grey level properties. This process results in similar objects in each class being distinguished by a unique grey level. A threshold is then applied to highlight objects of interest, either grains, remnants, voids, etc.

A morphological filter is applied following preconditioning. This technique selects the objects in the image which most closely conform to the physical features dictated to the filter; i.e., shape and size of the grains, typical area covered by a grain or remnant, etc.

Individual grain and cluster silhouettes have been identified at this point. Following application of the morphological filter, determination of the grain centroids and orientation is a relatively simple process. As indicated earlier, the morphology is dictated to the filter. This technique can easily be adapted to recognize a wide variety of geometric shapes or other microstructural aspects. Thus, this automated process may eventually be used for the microstructural/micromotion analysis of a wide variety of soils such as well-graded soils and/or clayey soils.

Tracking is the process by which the centroids and orientation of selected grains are detected and recorded from image to image. Equally important is the added capability of monitoring the growth of damage within the viewed field through the implementation of an adaptive morphological filter. Such a filter will recognize the existence of remnants, which may have dramatically different geometric properties than the parent grain, and continue to track their micromotions/orientations.

Analysis involves compilation of the information obtained during tracking to highlight a desired feature of the microstructural response. Clustering and damage growth are two important features which are being examined. The consistency and precision associated with the automated processing and analysis of images provide a degree of accuracy which cannot be efficiently attained through manual analysis.

## 4.3.2 Micromotion Recording Using X-Ray Techniques

Several tests were conducted using a 120-keV x-ray device (Ref. 36). These tests involved the placement of 1.3-mm-diam. lead pellets (called particles) within a specimen of 0.50-mm-diam. silica grains in the array shown in Figure 21. The specimen container was configured to have two opposing windows at the same height (0.56 h), thus permitting transmission of the x rays through the specimen. Three tests were conducted with macroscopically similar specimens being subjected to 6.0-percent strain. The test regime (macroscopic strain application and removal of 0.5 percent per minute) was similar to that used during tests

51
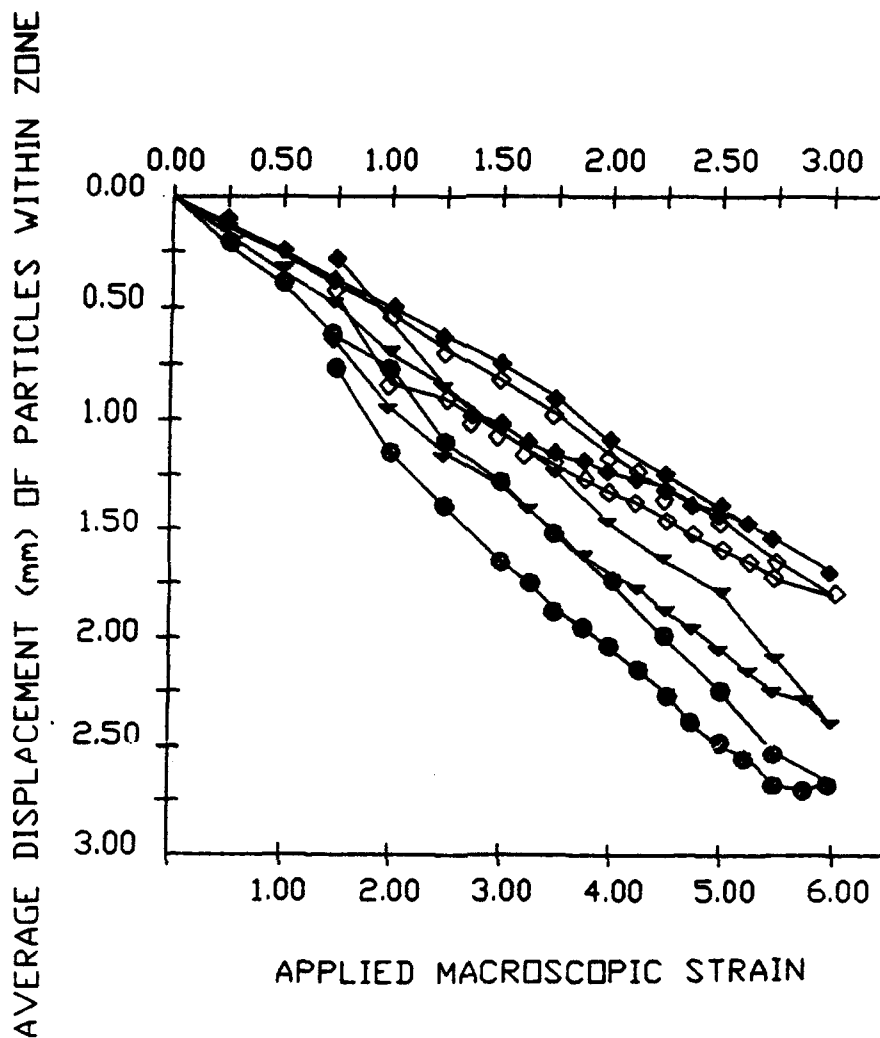
a. Loading cap displacement (mm).
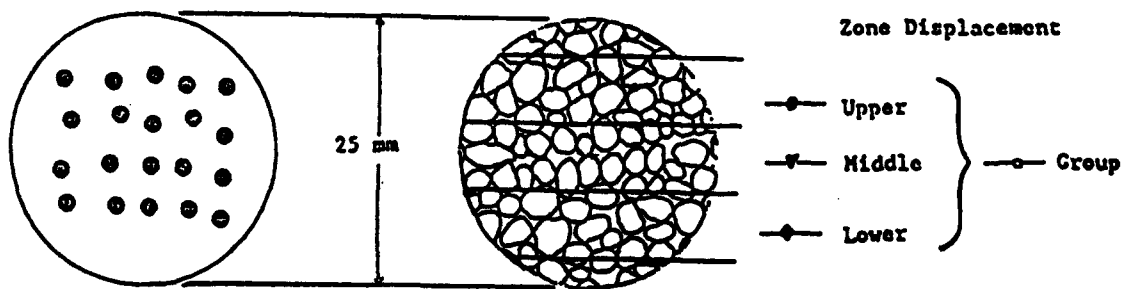


b. Particle arrangement.

c. Zone definition.

Figure 21. Displacement of average particle embedded within upper/
middle/lower zones of viewing window (window at 0.56 h).

52

in which cinema images were obtained. These tests provided qualitative insight into the influence of sidewall friction on the surficial grain motion compared to the motion of particles located in the center of the specimen which are presumably unaffected by sidewall friction. Although the use of x rays cannot yet provide the detailed images of particle motions (displacement and rotation) which are seen in the cinema images, comparison of the "average grain" motion (determined by tracking the motions of 10s of grains within a predetermined zone) provides a means of inferring whether internal micromotions are the same as the surficial micromotions.

### 4.3.3 Internal Microstructural Response

The internal microstructural response is the changes which occur within the specimen as observed at discrete stages during the application of macroscopic uniaxial strain. This response is limited to changes which can be observed in the specimen after it has been loaded to some increment of macroscopic strain (2 percent, 4 percent, 6 percent, etc.) and then unloaded. Micromotions cannot be observed by examining specimens which are not subject to a changing stress (strain) state during observation. Rather, observations are limited to a study of changes in grain orientation, damage levels, and the distribution of damage throughout the specimen. Information regarding these changes in the specimen was obtained using an epoxy impregnation technique with subsequent sectioning to expose the interior of the specimen. These techniques are described next.

4.3.3.1 Epoxy Impregnation, Wafering, and Polishing. Standard petrographic procedures were used for the epoxy impregnation of the tested specimens as well as the subsequent sectioning and polishing of the exposed cut. Buehler, Ltd., Lake Bluff, Illinois, offers a variety of systems which are suitable for this type of microstructural analysis. As relatively large specimens were being examined, refined techniques had to be developed for each phase of the microstructural investigation. With regard to impregnation, a low viscosity resin was used as the epoxy mixture had to flow easily within the voids between the grains. The mixture had to be "worked" into the specimen by subjecting the specimen to a vacuum while it was submerged in an epoxy bath. The vacuum served to draw air out of the voids

in the specimen which were then filled with epoxy mixture when the specimen was again subjected to atmospheric pressure. Several cycles of "vacuuming" were necessary to achieve full impregnation. As the duration and number of vacuum cycles are dependent on the void size and volume, epoxy temperature and viscosity, and specimen size, the impregnation regime is best determined through trial and error. Extra care must be taken to keep the specimen and epoxy at the low end of the working temperature for the chosen epoxy because relatively high temperatures cause the epoxy to cure more rapidly. Rapid curing results in either shrinkage cracks, as a minimum, or the onset of an exothermic reaction within the specimen which causes uncontrolled curing. The specimen is destroyed in either case as the fabric is distorted and previously intact (possibly fractured) grains are broken into many pieces. Damage occurs due to impregnation which might wrongly be attributed to damage which was supposed to have occurred during loading.

The 50-mm-size (cubic) specimen appeared to be the largest specimen which could be sectioned by commercially available diamond saws (assuming the saw is not modified to accommodate larger specimens). Following impregnation, the specimen must undergo additional preparation to remove excess epoxy from the sides and top. This is accomplished by either cutting or grinding and serves to restore the specimen to its nominal dimensions of 50 mm on a side. The specimen can then be halved and subsequently sectioned into slices and smaller pieces as appropriate.

Regardless of the size and orientation of the exposed face, grinding and polishing were necessary to prepare the face for optical analysis. Several commercially available systems are capable of producing a surface suitable for optical analysis, thus techniques for use with a specific system will not be discussed here. The difficulty of obtaining a highly polished surface is closely related to the amount of damage the specimen has undergone. This is mainly because the epoxy may not fully impregnate grains which have fractured but not shattered. These grains tend to break and crumble as polishing progresses. The remnants are subsequently drawn across the face of the specimen and scarring results. Such scarring may interfere with the ability of most off-the-shelf optical analysis systems to discern microstructural effects of interest; e.g., damage and fracture of individual grains. It is often

a trade-off between the amount of information one wishes to obtain from an image and the ability of the optical system to perform the analysis as fine polishing is required to expose some of the more subtle damage occurring in the specimen. More importantly, the visible damage may be more a function of the polishing process than a function of the true damage existing in the specimen. One must also consider the fact that the peak load has been removed and the specimen allowed to relax before impregnation. Approximately 30 percent elastic rebound of the local displacement occurs during load removal. Thus, the grains are collectively under a relatively low stress at the time of grinding and polishing, yet spalling still occurs. This is worth noting because of the expected difficulty in obtaining a well-polished face on a specimen impregnated while still under load. Although such an image is desirable, the amount of spalling and scarring might preclude obtaining a useful image. Techniques have been conceived to impregnate specimens under load; however, they have not been pursued.

4.3.3.2 Optical Analysis. An Olympus CUE system was used for optical analysis purposes. Several capabilities exist within the system to aid in the determination of microstructural changes within the specimen. These algorithms include edge detection, small feature enhancement, various filters for highlighting the boundaries of grains, and the ability to quantify a limited number of geometric aspects of individual grains and their orientation. The suitability of these capabilities and their use in the development of a microstructural-based constitutive will be discussed in Subsection 6.4.

## 5.0 SPECIMEN PREPARATION AND TESTING

### 5.1 PREPARATION

All tests were conducted using specimens manufactured from either 0.50-mm- or 0.75-mm-diam. silica grains ($\gamma = 2.65$). Macroscopically, each specimen had a dry unit weight of 1.7 g/cc. Thus, the void ratio (e) was 0.61 percent and the porosity (n) was 38 percent. A measured weight of grains was uniformly rained into the specimen container and subsequently vibrated until the desired macroscopic properties were obtained. The rigid loading cap (Subsection 4.1) was then placed atop the soil and the assembly placed within the loading frame for testing.

### 5.2 TESTING

All tests were displacement-controlled. The displacement rate equated to a macroscopic loading/unloading rate of 0.5-percent strain per minute. The two types of tests conducted were monotonic loading and unloading as well as cyclic loading with higher macroscopic strain being applied with each cycle. Unloading was typically initiated immediately upon attaining the desired macroscopic strain, but the peak strain (peak displacement of the loading cap) was held constant after some peak macroscopic strain applications to investigate the stress relief properties of the granular material. The test regime is presented in Table 2. The first two digits in the test number designate the grain size (50 = 0.50 mm, 75 = 0.75 mm), the second two designate the peak macroscopic strain, and the character within the parentheses designates whether strain application was monotonic (M) or incremental. If the strain was incrementally applied, the number in the parentheses indicates the size of the increment. Test designations with a suffix of I or II indicate that like tests were performed with sapphire windows at different heights to determine micromotions at various locations on the side of the specimen.

Table 2. Uniaxial strain application test regime.

| Test | Macroscopic Strain Regime | Window Height (h) | Peak Displacement Retained |
|---|---|---|---|
| 50.03 (M) | 0-3-0 | 0.56 | No |
| 50.06 (M) | 0-6-0 | 0.56 | Yes; 6.5 min |
| 50.09 (M) | 0-9-0 | 0.56 | Yes; 7.5 min |
| 50.09 (3) | 0-3-0-6-0-9-0 | 0.56 | Yes; 1.0 min at each peak |
| 75.05 (M) | 0-5-0 | 0.375 0.500 0.750 | Yes; 4.0 min |
| 75.05 (1) | 0-1-0-2-0-3-0-4-0-5-0 | 0.750 | Yes; 4.0 min at 5.0% strain |
| 75.06 (M) | 0-6-0 | 0.56 | No (Interior particle displacement measured using x rays.) |
| 75.10 (M) I | 0-10-0 | 0.375 0.500 | Yes; 5.0 min at 10% strain |
| 75.10 (M) II | 0-10-0 | 0.500 0.750 | Yes; 5.0 min at 10% strain |
| 75.10 (2) I | 0-2-0-4-0-6-0-8-0-10-0 | None | Yes; 4.0 min at 10% strain |
| 75.10 (2) II | 0-2-0-4-0-6-0-8-0-10-0 | | Yes; 4.0 min at 10% strain |

NOTE: Suitable photographic records of grain displacement and fracture were only obtained for 0.75-mm-diam. grains as the 0.50-mm-diam. grains proved too small to be manually (and precisely) distinguishable from frame to frame. Therefore, only the analysis results of the 0.75-mm grain diameter cinema records will be presented. General trends observed in the micromotions of the 0.50-mm-diam. grains are included in the interpretation of the results.

## 6.0 TEST RESULTS AND DISCUSSION

### 6.1 INTRODUCTION

Two approaches were used in evaluating the microstructural effects which were induced and observed during the application of uniaxial strain. The first approach involved recording the micromotions and observation of other microstructural effects which occurred on the specimen surface. Such effects included fracture and disintegration of grains and the formation of damage chains and clusters. The second approach involved epoxy impregnation of unloaded specimens which were then sectioned and polished to reveal changes in the internal microstructure of the specimen. The results and discussion associated with each approach will be presented in separate subsections. Subsection 6.2 presents the test results in macroscopic terms, i.e., uniaxial stress-strain response, pretest and posttest grain size distribution curves, etc. Subsection 6.3 presents the surficial microstructural response and Subsection 6.4 presents the internal microstructural response.

### 6.2 OBSERVATIONS ON THE SPECIMEN MACROSCOPIC RESPONSE

Table 3 summarizes the peak axial stress associated with peak-applied (incremental or final) strain for each test. Figures 22-30 present the stress-strain curves associated with each test and the development of axial stress versus time.

Figures 31-33 show the grain size distribution charts for virgin materials used in the test series as well as for those materials subjected to the same macroscopic strain levels (incremental and peak) as the tested specimens. The first two digits in the grain size distribution curves indicate the maximum macroscopic strain which was applied to the specimen. The character within the parentheses designates whether strain application was M or incrementally applied. If the strain was incrementally applied, the number in the parentheses indicates the size of the increment. For example, a test designated 06(02) indicates that a specimen was subjected to a peak macroscopic strain of 6.0 percent in increments of 2.0 percent. As always, the macrostrain was removed from the specimen before the application of the next strain increment.

Table 3. Summary of axial stress for given incremental or peak strain.[a]

| Test | Incremental or Peak Strain (Percent) | | | | | | | | | |
|------|------|------|------|------|------|------|------|------|------|------|
|  | 1 | 2 | 3 | 4 | 5 | 6 | 7 | 8 | 9 | 10 |
| 50.03(M) |  |  | 19.3 (2.80) |  |  |  |  |  |  |  |
| 50.06(M) |  |  |  |  |  | 37.3 (5.41) |  |  |  |  |
| 50.09(M) |  |  |  |  |  |  |  |  | 47.1 (6.83) |  |
| 50.09(3) |  |  | 24.0 (3.48) |  |  | 41.0 (5.94) |  |  | 49.1 (7.12) |  |
| 75.05(M) |  |  |  |  | 20.1 (2.90) |  |  |  |  |  |
| 75.05(1) | 0.2 (0.03) | 1.1 (0.16) | 3.9 (0.57) | 9.4 (1.36) | 16.1 (2.33) |  |  |  |  |  |
| 75.10(M)I |  |  |  |  |  |  |  |  |  | 46.7 (6.77) |
| 75.10(M)II |  |  |  |  |  |  |  |  |  | 47.3 (6.56) |
| 75.10(2)I |  | 2.4 (0.35) |  | 13.9 (2.01) |  | 25.9 (3.75) |  | 38.8 (5.62) |  | 46.9 (6.80) |
| 75.10(2)II |  | 1.8 (0.26) |  | 8.3 (1.20) |  | 20.5 (2.97) |  | 38.8 (31.1) |  | 45.0 (6.52) |

NOTE: [a]Axial stress is given in units of megapascal and kips per square inch.
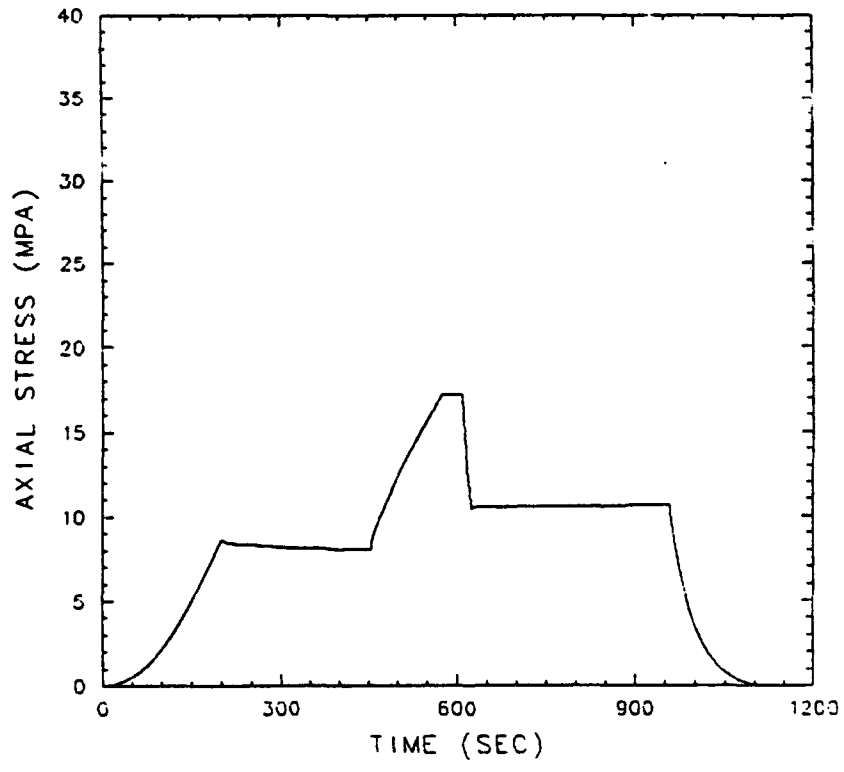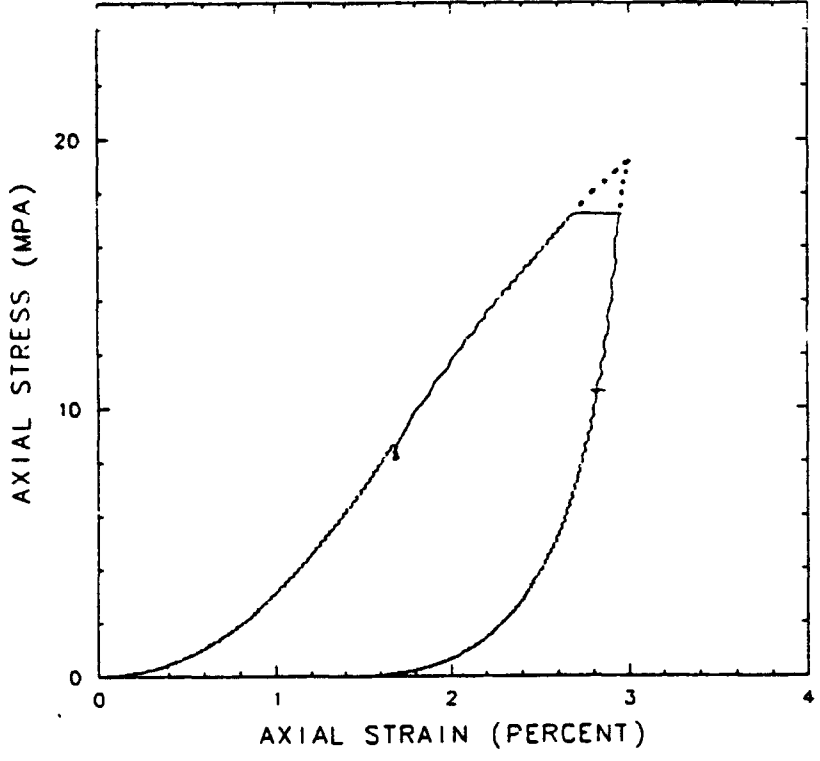
Figure 22.  Stress-strain response and axial stress versus time
response for test 50.03(M).
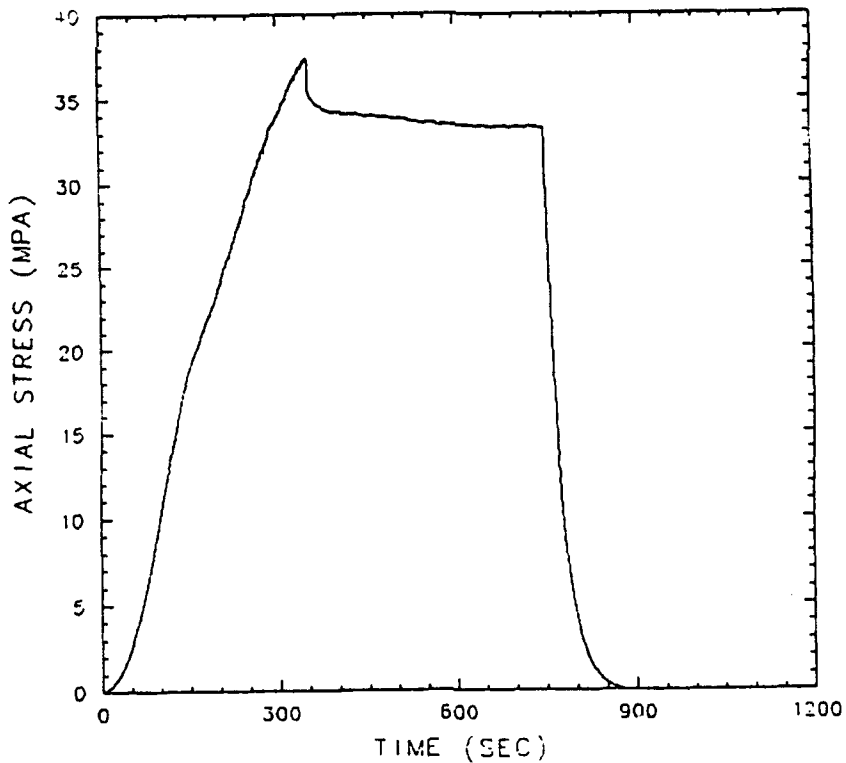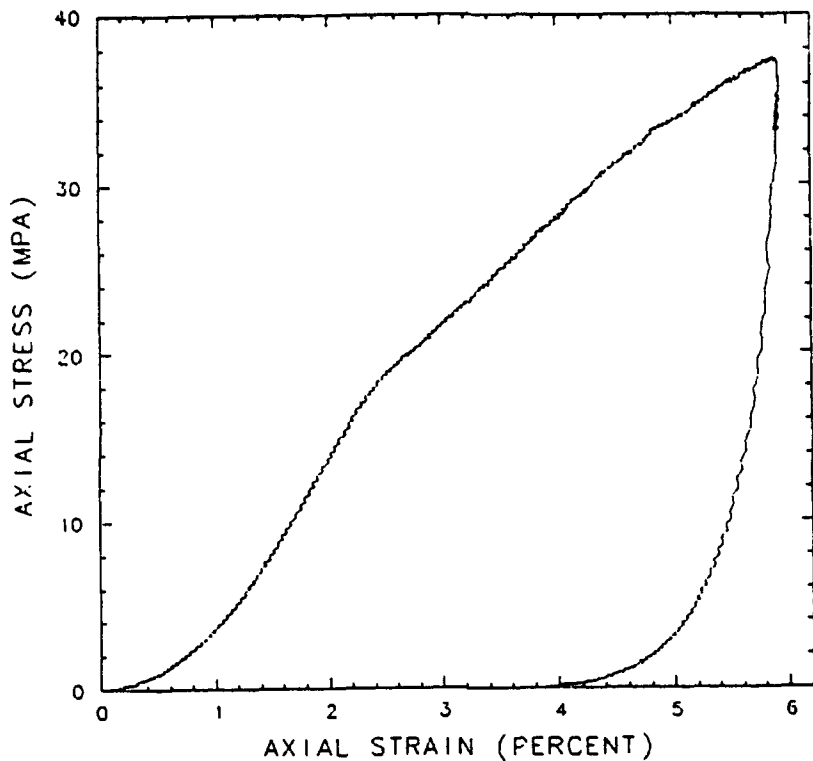
Figure 23. Stress-strain response and axial stress versus time response for test 50.06(M).
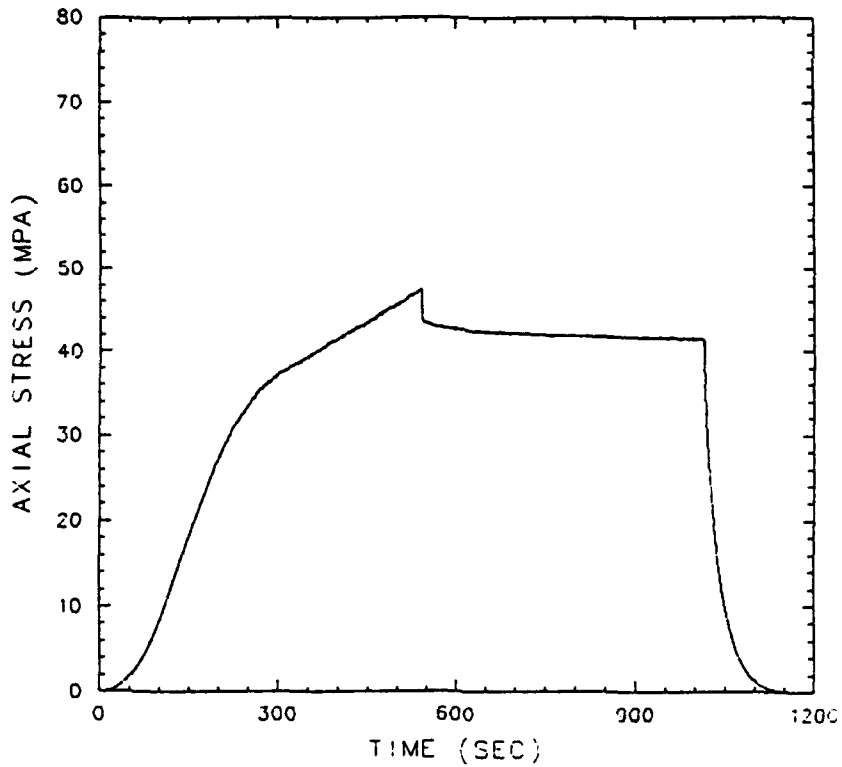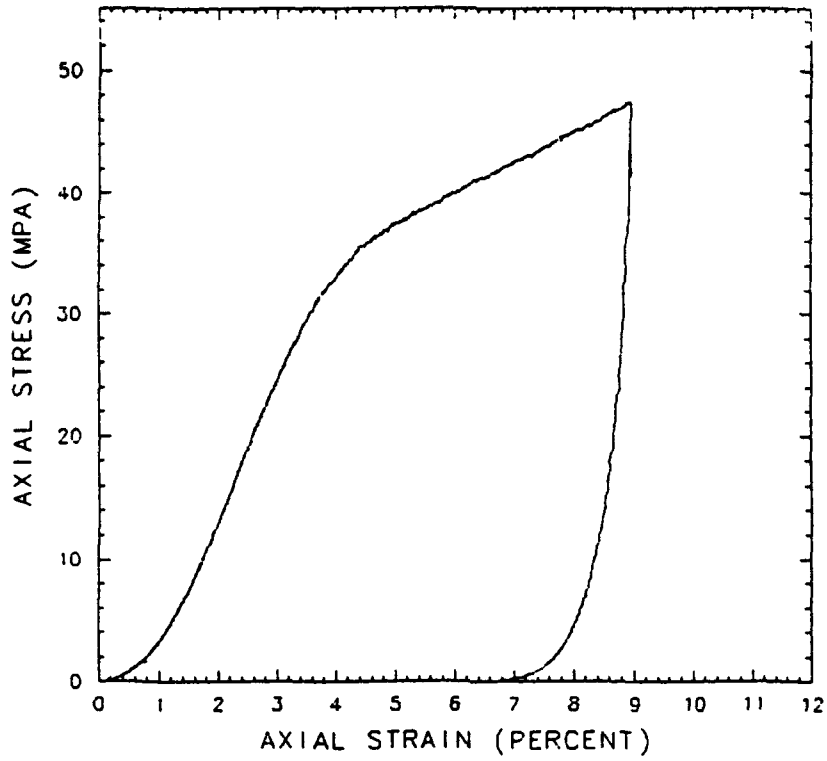
Figure 24. Stress-strain response and axial stress versus time
response for test 50.09(M).

62
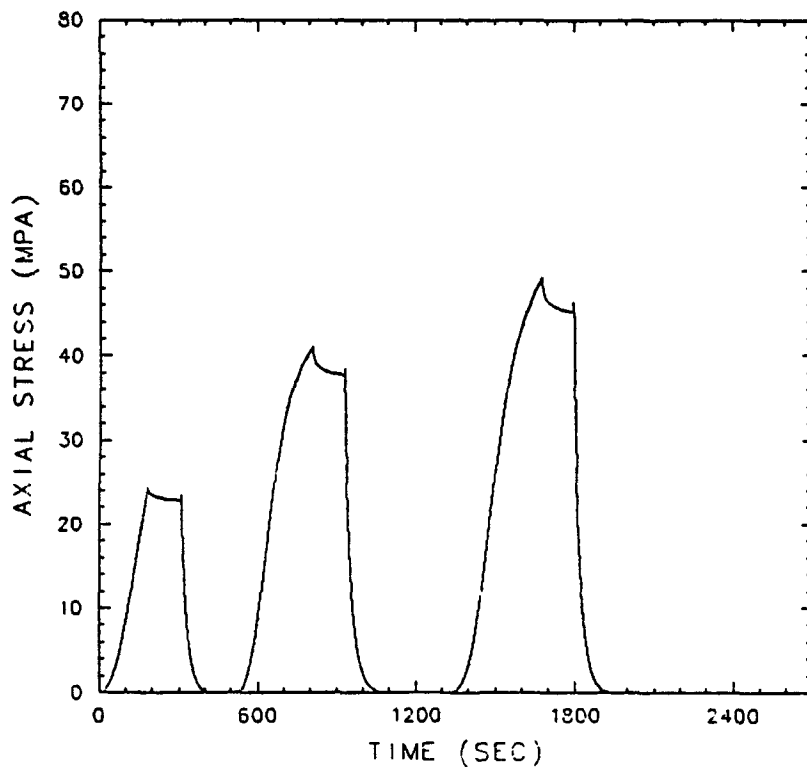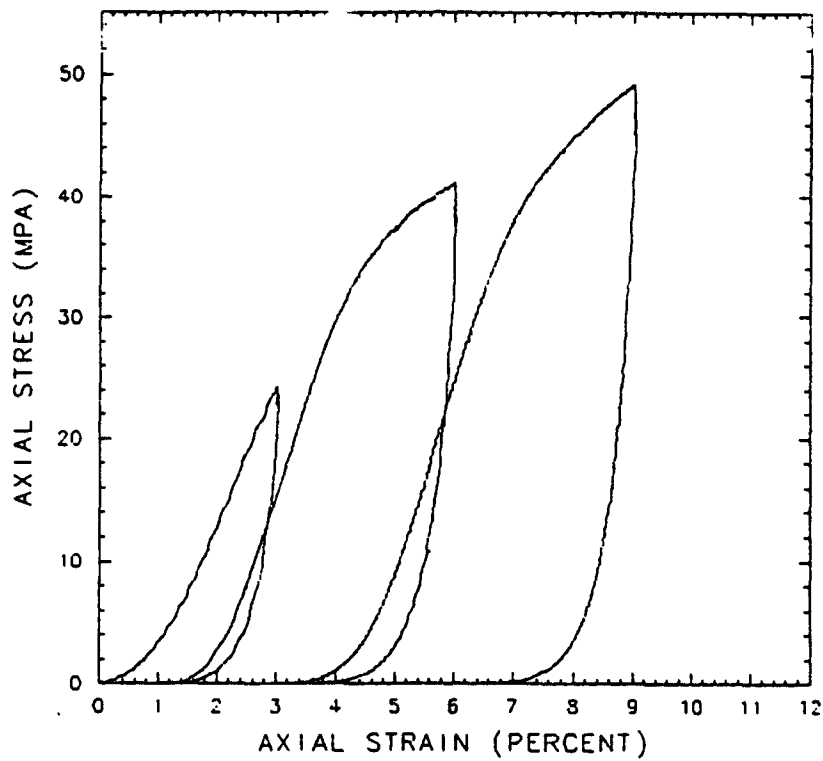
Figure 25.  Stress-strain response and axial stress versus time
response for test 50.09(3).
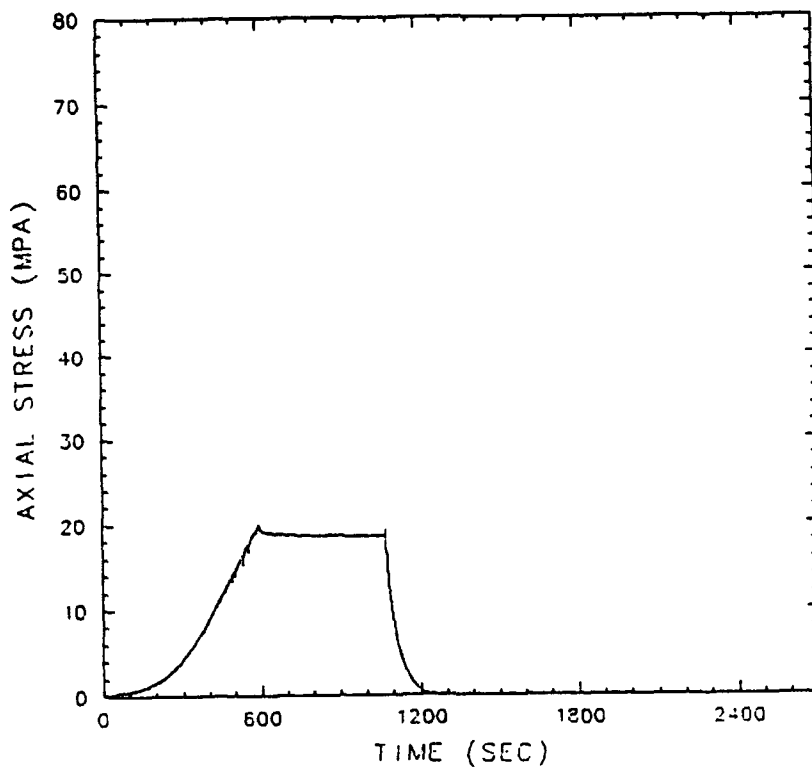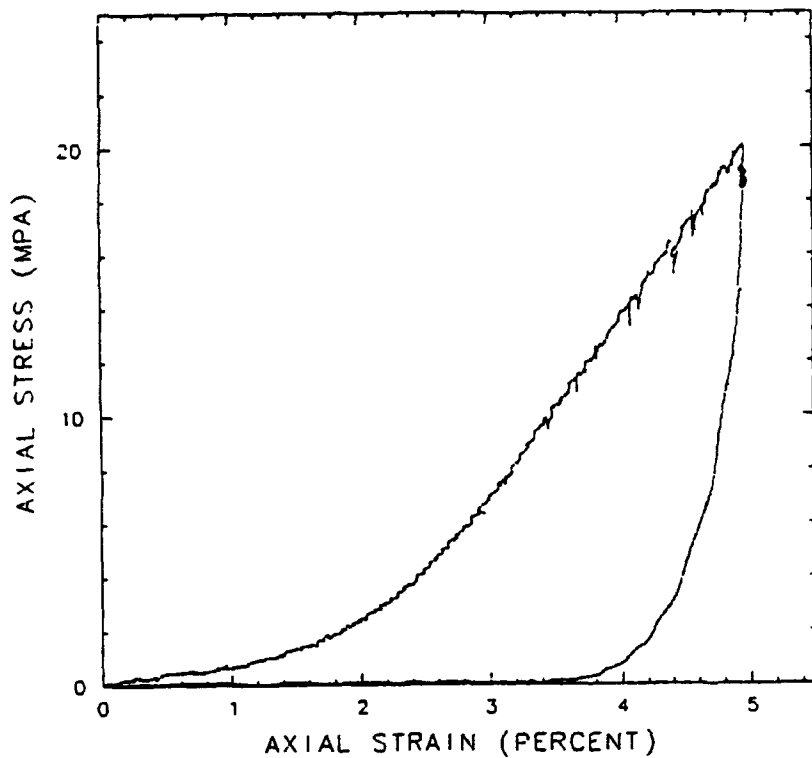
Figure 26. Stress-strain response and axial stress versus time
response for test 75.05(M).
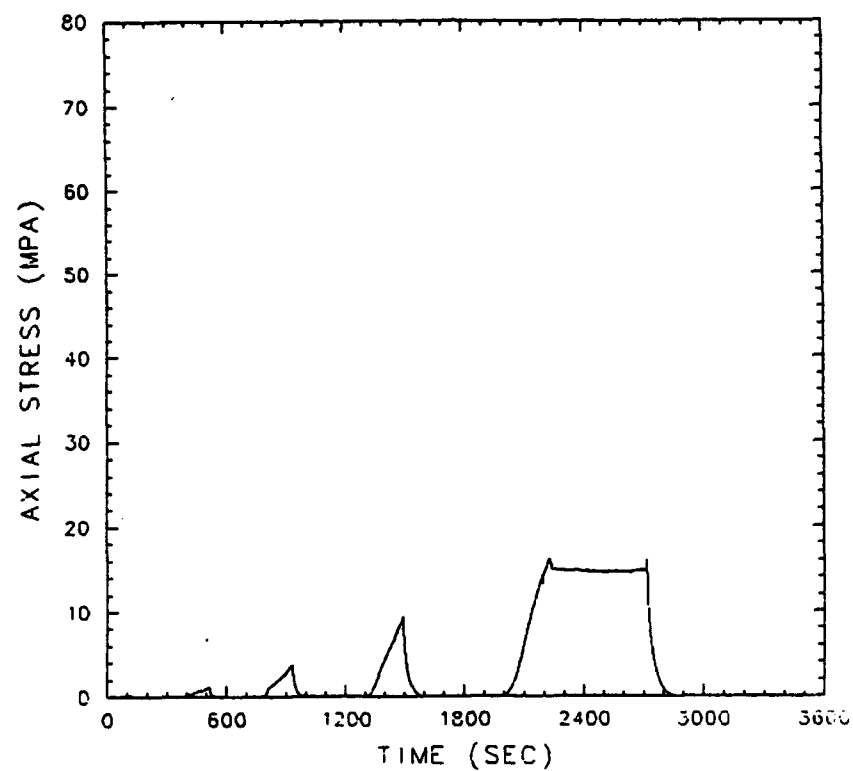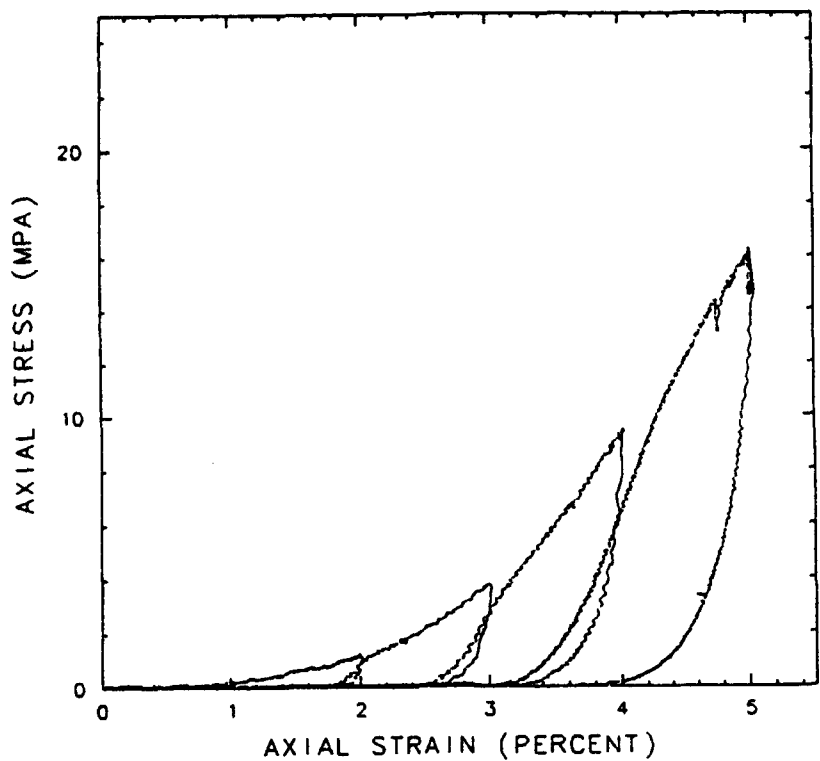
Figure 27. Stress-strain response and axial stress versus time response for test 75.05(1).

65
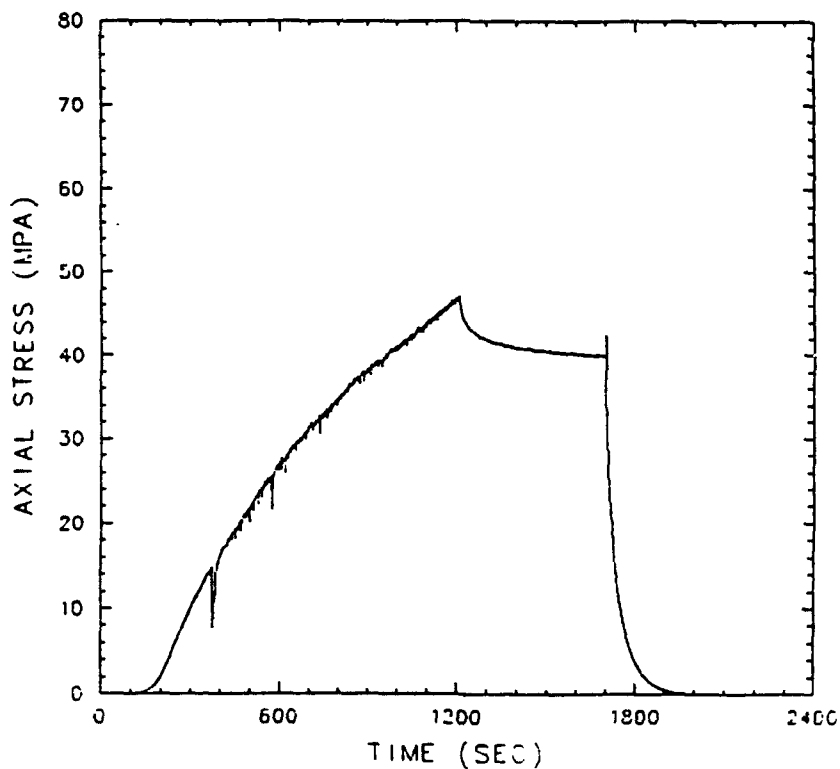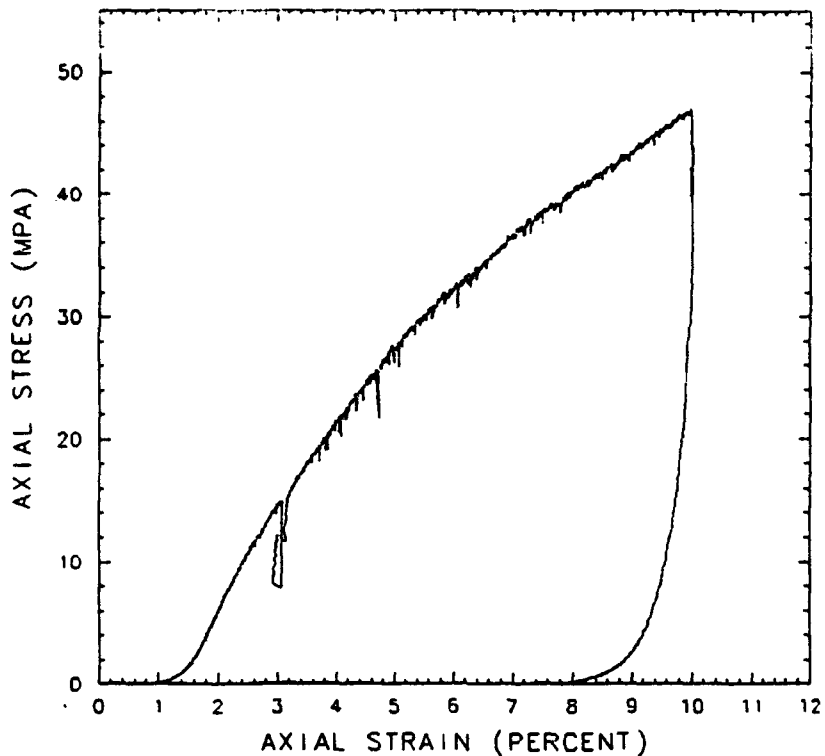
Figure 28.  Stress-strain response and axial stress versus time
response for tests 75.10(M)I and 75.10(M)II.
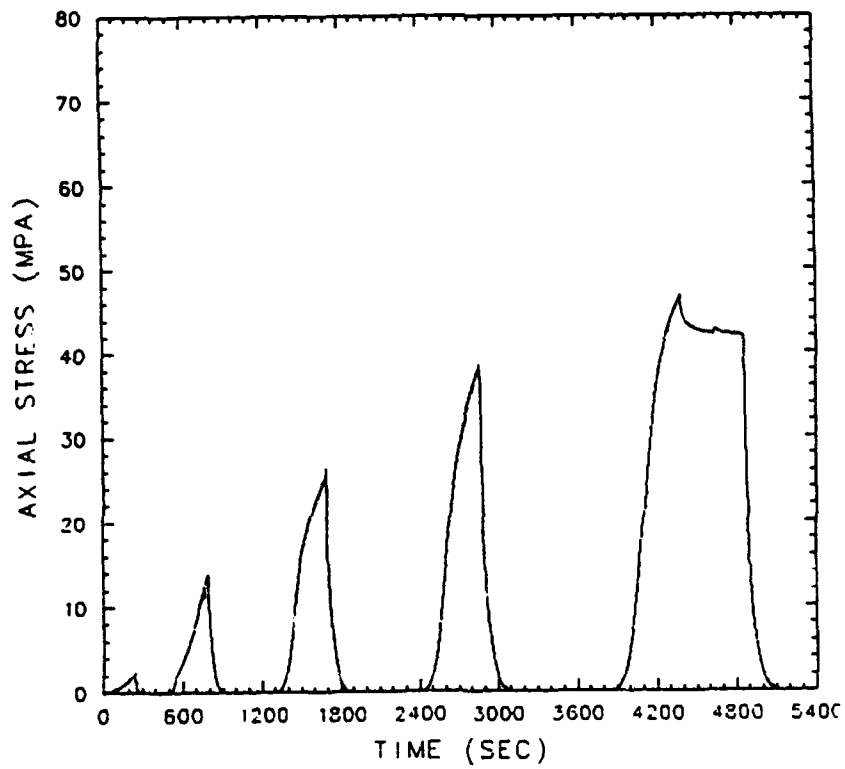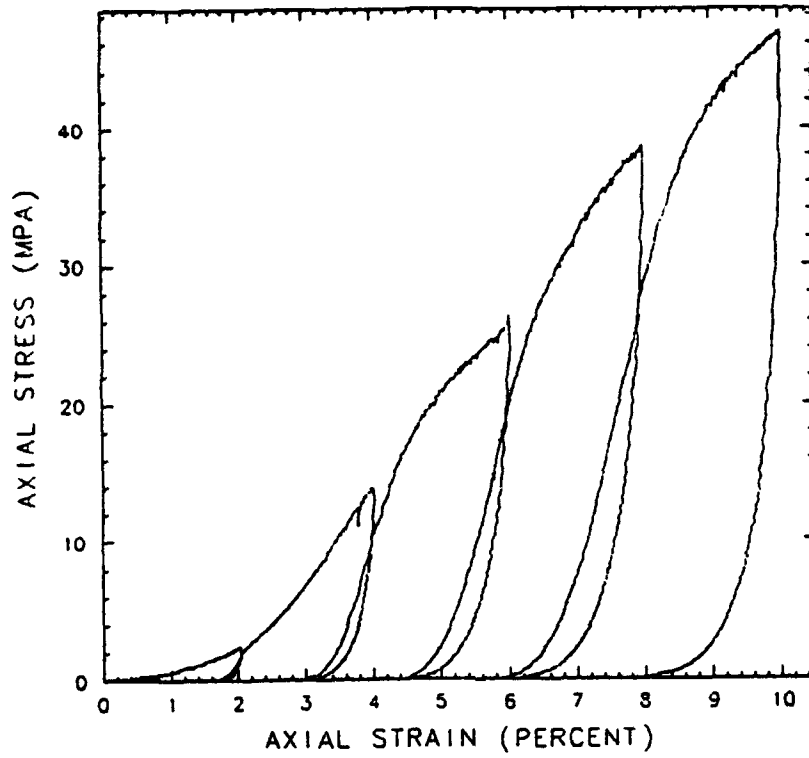
Figure 29. Stress-strain response and axial stress versus time
response for test 75.10(2)I.
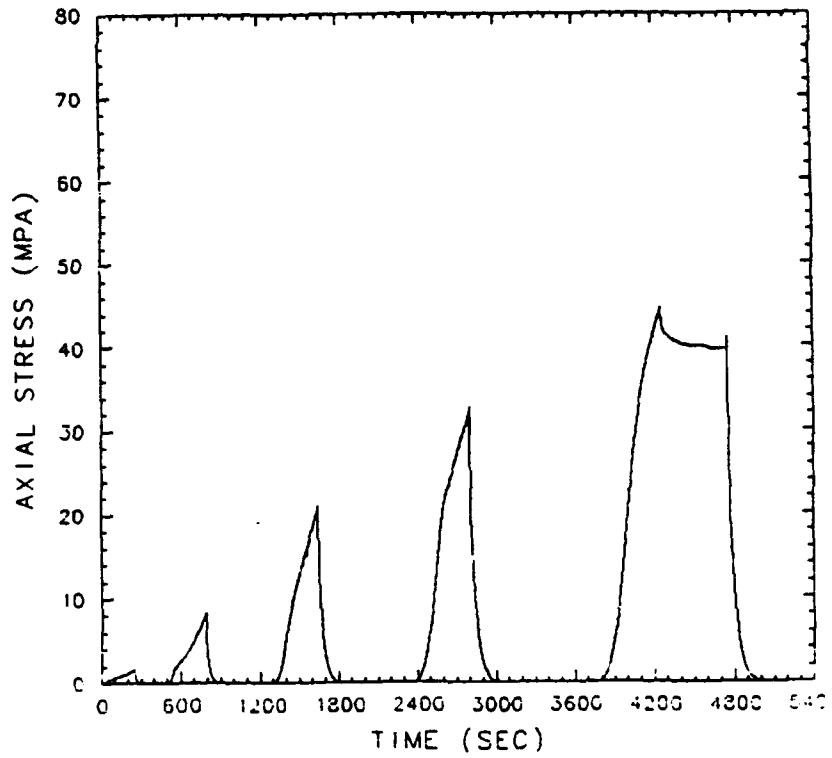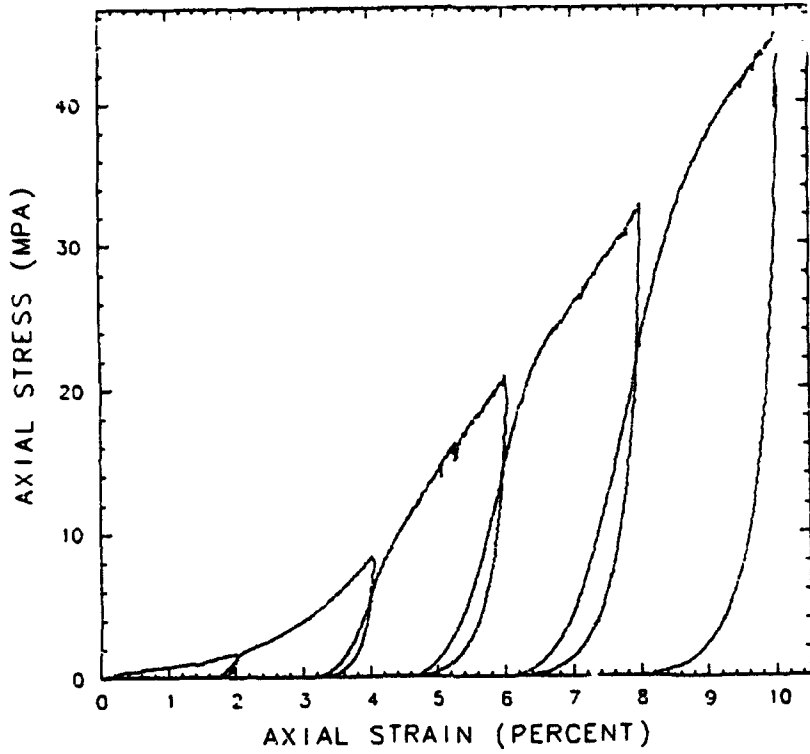
Figure 30. Stress-strain response and axial stress versus time
response for test 75.10(2)II.

Figure 31. Gradiation curves for 0.75-mm-diam. particle specimens (virgin, 04[2] and 10[2]).

Figure 32. Gradiation curves for 0.75-mm-diam. particle specimens (virgin, 03[M], 03[1]).
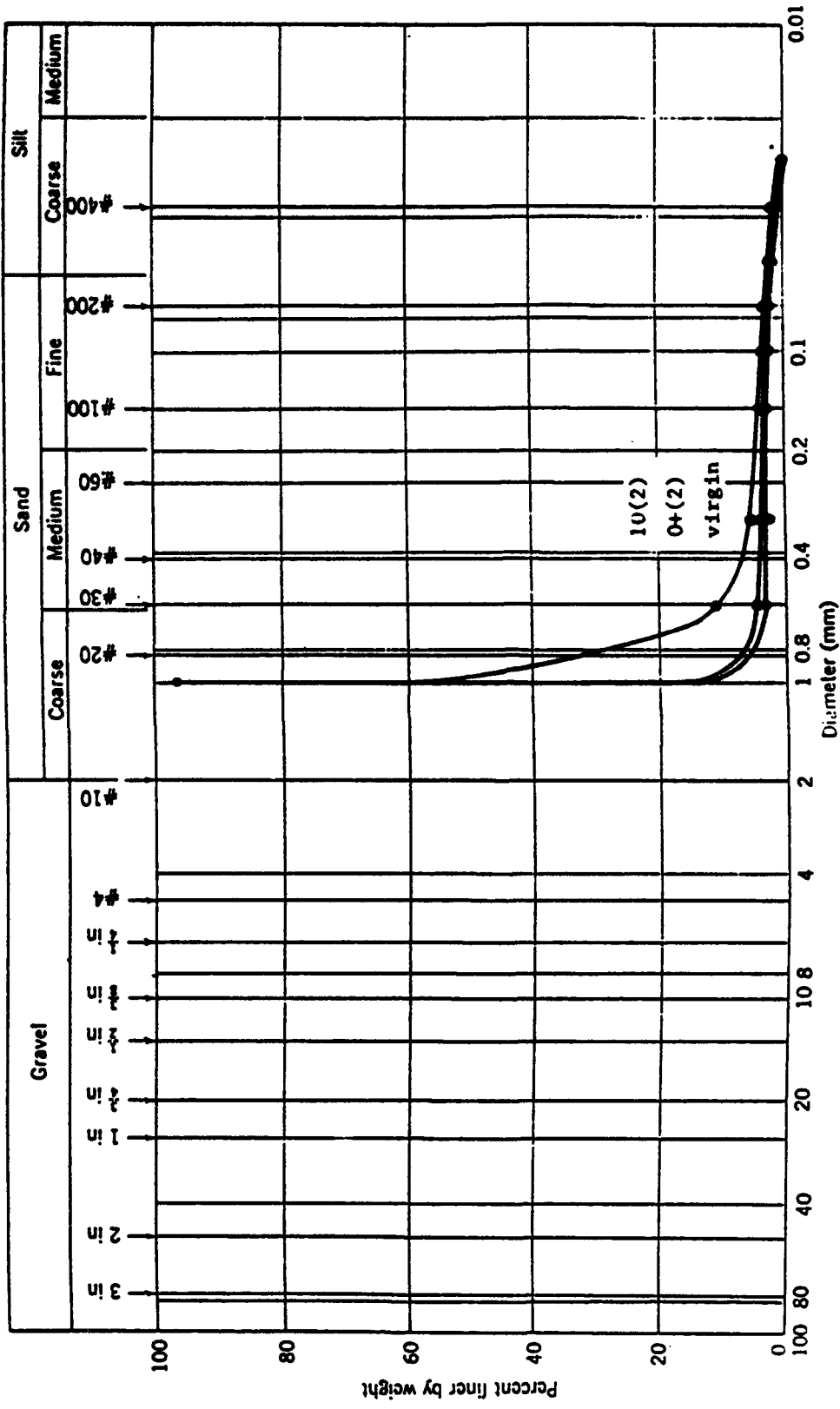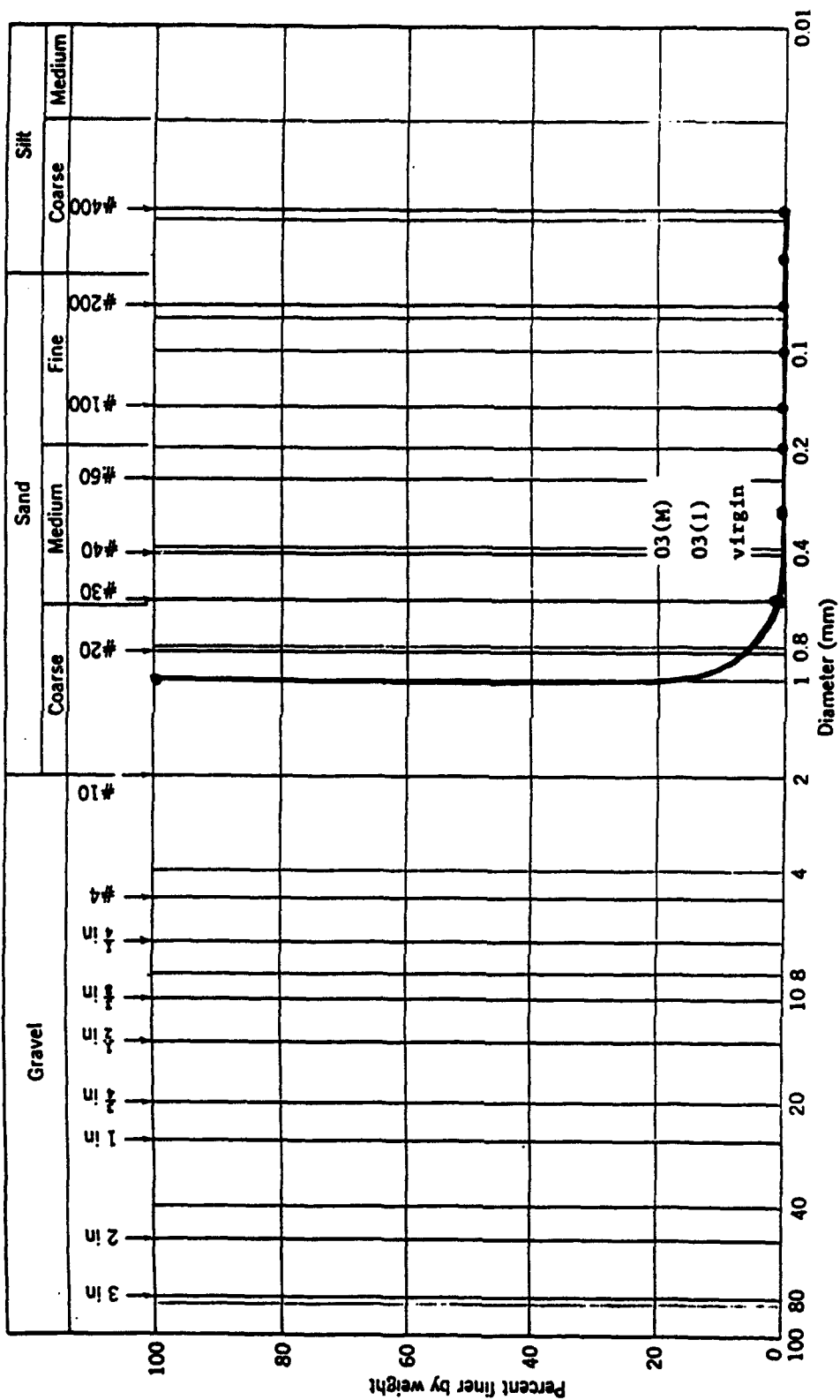
Figure 33. Gradation curves for 0.50-mm-diam. particle specimens (virgin, 03[M], 06[M], 09[M], 09[3]).
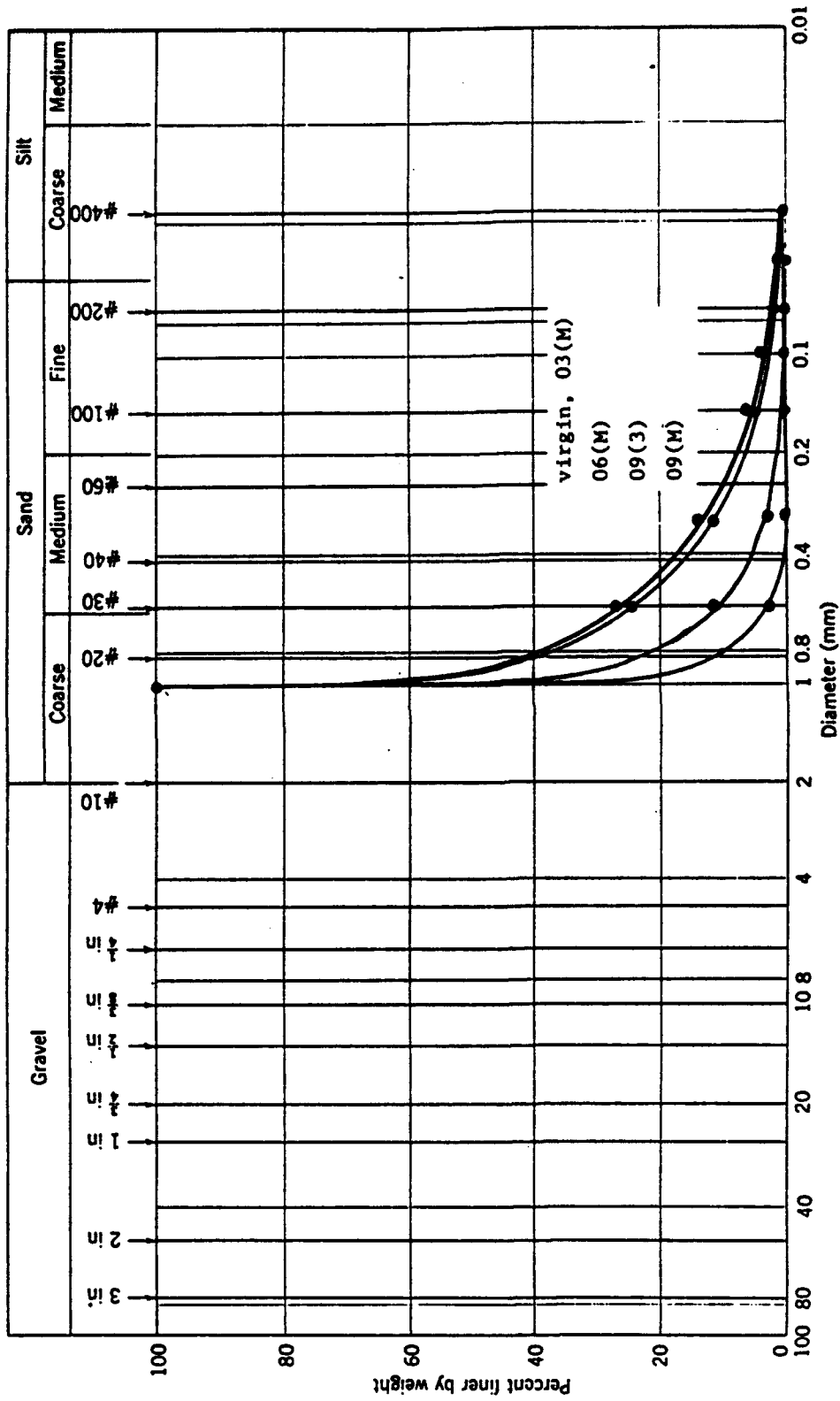
The listed results indicate nothing unusual in the expected response. Generally both types of specimens (50- and 75-mm grains) demonstrated a relatively weak Young's modulus during initial strain application (0 to 1.0 percent macroscopic strain) with the strength of the material increasing as strain was applied. This stiffening occurred from 1.0- to ~3.0-percent macroscopic strain for the 0.50-mm-diam. grain specimens and from 1.0- to ~5.0-percent macroscopic strain for the 0.75-mm-diam. grain specimens. It appeared that after ~5.0 percent macroscopic strain had been applied to a given specimen, a slightly decreased, yet constant, Young's modulus was exhibited.

## 6.3 SURFICIAL MICROSTRUCTURAL RESPONSE

As mentioned previously, the surficial microstructural response considers the micromotions, fracture, and disintegration of individual grains at predetermined locations on the surface of the specimen. The following observations were made from cinema records obtained through the sapphire windows. Two approaches were used in the interpretation of the images. First, the motion of the "average grain" within the viewed neighborhood was considered. Second, the images were viewed with the intent of developing an understanding of the growth of clusters, the motion of such clusters, and the development of damage within the specimen. Each of these responses will be discussed because of the limitation imposed by the presence of the sapphire viewing window. A qualitative description of the grain micromotions and the evolution of damage is given next.

The following observations were made through the window at 0.56 h with specimens entirely made up of either 0.50- or 0.75-mm-diam. grains. It appears that individual grains shift and reorient themselves during the early stage of strain application (<1.0 percent macroscopic strain) and remain intact. As strain application progresses, the stress at grain contacts for the now "locked in" grains increases until the stress level is adequate to fracture and crush individual grains. Such stresses appear to have fully developed by the time the 0.50-mm-diam. grain specimens have been subjected to 3.0-percent macroscopic strain and the 0.75-mm-diam. grain specimens have been subjected to 5.0-percent macroscopic strain. After these levels of macroscopic strain have been attained, fracture and crushing of

72

individual grains are readily apparent. Even though these observations are made from viewing through the window at 0.56 h, the same general observations were made through windows at other heights. It is reasonable to assume, therefore, that each of these responses coexist in the specimen during any stage of load application. Even at low macroscopic strain levels, combinations of these factors may result in highly localized damage. More importantly, it is reasonable to assume that all of these responses are occurring simultaneously in the specimen during loading. These responses continue to occur in specimens held at some peak level of macroscopic strain as the resisting load decreases with time after the peak strain level has been attained. The mechanisms of individual grain displacement, rotation, fracture, and disintegration can thus be considered the principal causes for time-dependent strain (creep) under constant load.

With regard to the motion of the "average grain," the individual vertical and horizontal displacements of selected grains within a given cinema frame (approximately 50 grains per series of frames) were summed with the resulting average motion being assigned to an imaginary average grain. The motions of these average grains are shown in Figures 34-37. Although one would expect the averaged grain motion to appear rather continuous and be a smooth curve, the path is erratic and nonlinear. Furthermore, the path of the average grain does not retrace the path it followed during the loading phase. The wide variation in this response is evident in Figure 36, which shows the average grain rebounding more than expected in one case (viewing window at 0.75 h) and less in another (viewing window at 0.50 h) within the same specimen. In this test, the unloading paths of the average grains veer toward the linear displacement path suggested by a local theory formulation. Two facts are evident. First, although one might expect the loading and unloading paths to be nonlinear and lag behind the predicted linear displacement path due to wall friction, this is not the case. Second, such microstructural responses remain hidden if one considers only the macroscopic material response. Regarding the loading and unloading paths, wall friction is considered to retard the vertical motion of individual and groups of grains. If this influence was considered significant, the motion of all grains adjacent to the walls or windows would lag behind the displacements predicted by assuming a linear displacement
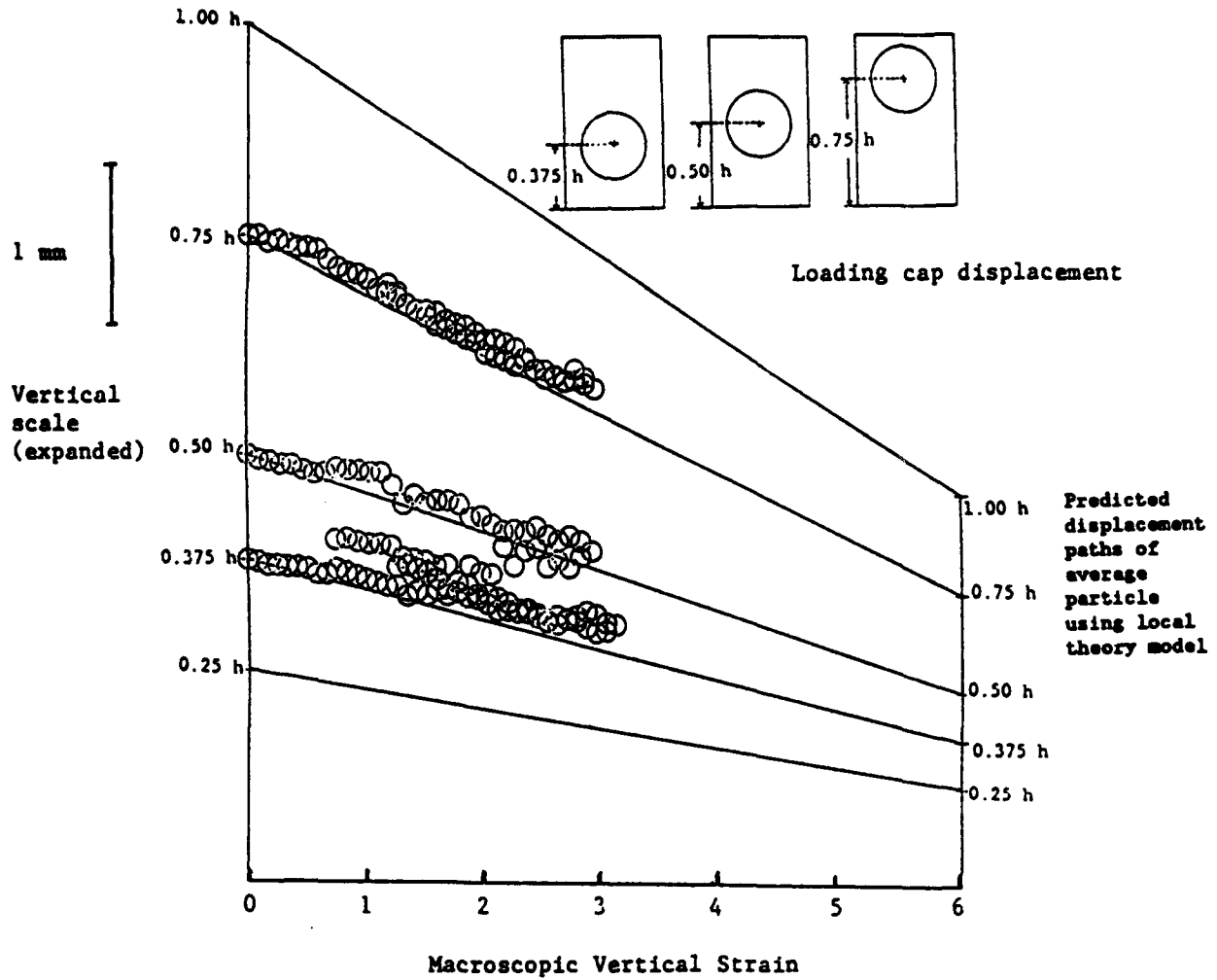
Figure 34. Displacement of average particle for observations made at 0.375, 0.50, and 0.75 h; monotonic loading to 3.0-percent macroscopic strain, monotonic unloading; and 0.75-mm-diam. particles.
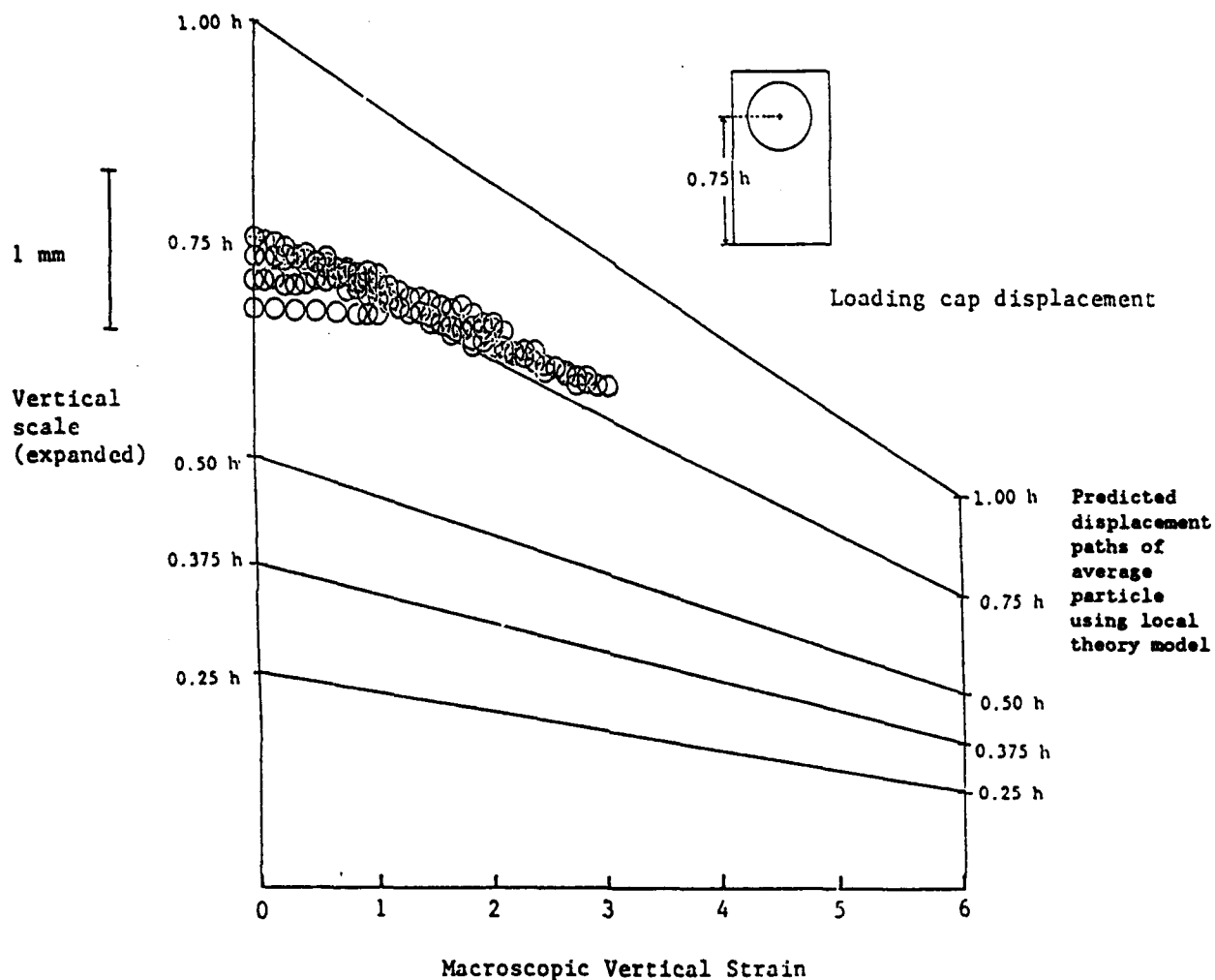
Figure 35. Displacement of average particle for observations made at 0.75 h;
cyclic loading to 1.0-, 2.0-, and 3.0-percent macroscopic strain,
monotonic unloading between cycles; and 0.75-mm-diam. particles.
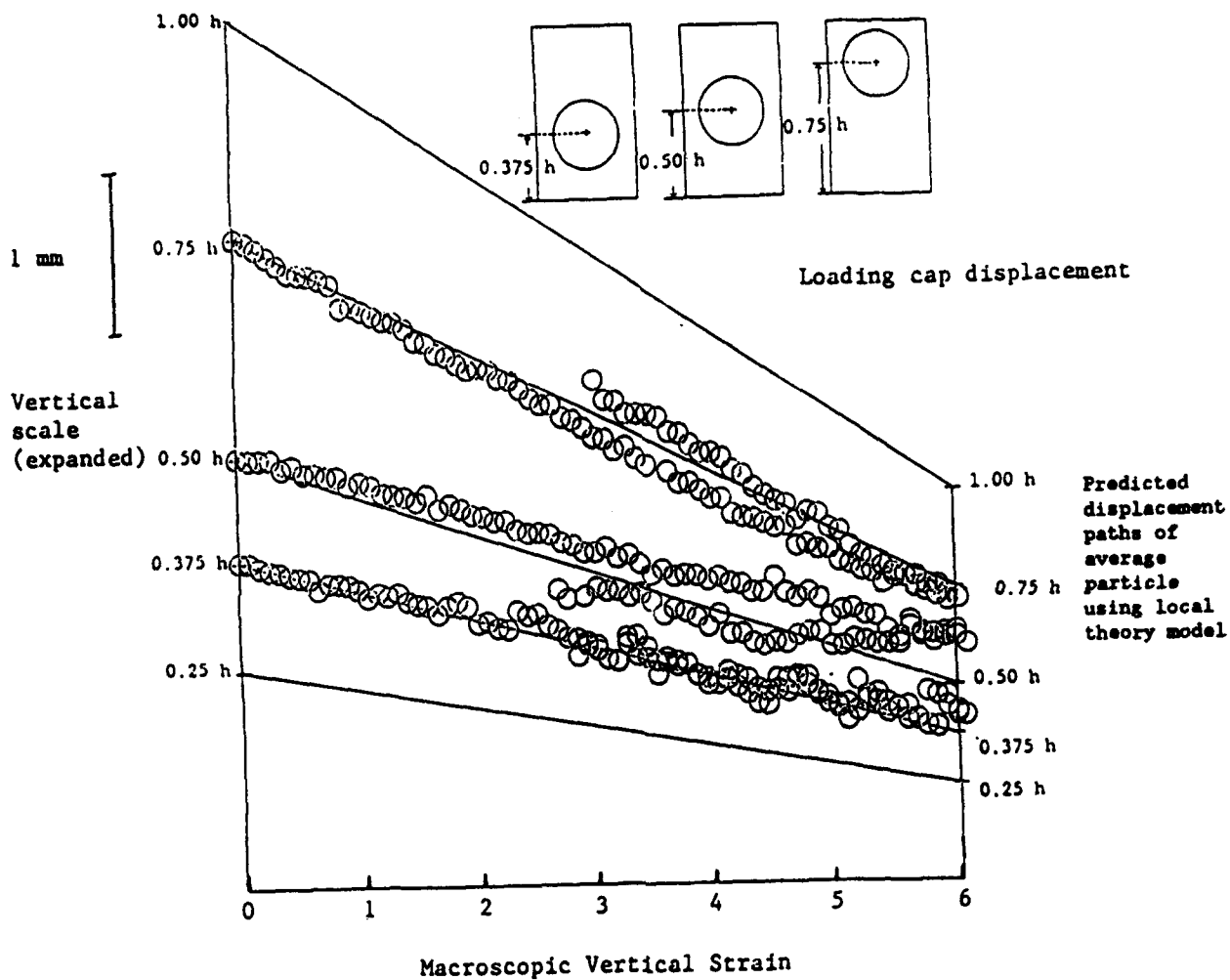
Figure 36. Displacement of average particle for observations made at 0.375, 0.50, and 0.75 h; monotonic loading to 6.0-percent macroscopic strain, monotonic unloading; and 0.75-mm-diam. particles.

76
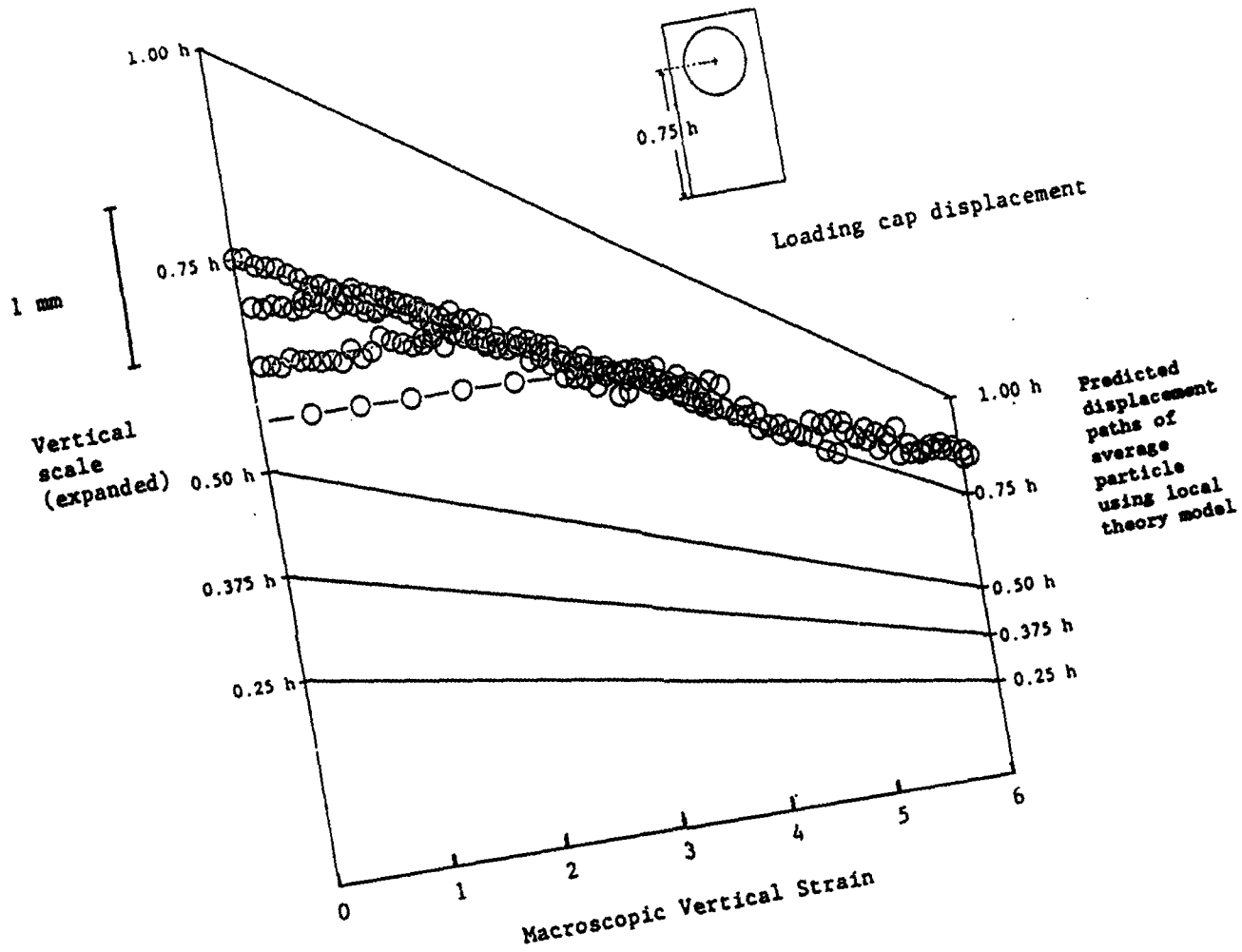
Figure 37. Displacement of average particle for observations made at 0.75 h; cyclic loading to 2.0-, 4.0-, and 6.0-percent macroscopic strain, monotonic unloading between cycles; and 0.75-mm-diam. particles.

gradient throughout the specimen. Indeed, displacement at some windows exceeded those predicted by a local displacement theory. One can conclude that the sidewall friction does influence the micromotion of grains adjacent to the wall; however, the influence is not so great that the natural mobility of the grains is destroyed. It is apparent that the microstructural responses may provide variation around the "theme" presented by observing the macrostructural response. This variation manifests itself in regions of relatively low and high displacement, strain, grain rotation and damage, etc. All of these responses occur in various measures during the loading process and contribute to the macrostructural response. The evolution of and interplay between these responses are obviously complex and are most likely the basis for variations in the results of tests using macroscopically similar specimens.

Some measure of the variation in the vertical of grains in a specimen subjected to uniaxial strain is given in Figure 38. This figure shows a summary of the vertical displacements of some 650 grains as observed through a window at 0.56 h with the 0.75-mm-diam. grain specimen while subjected to 3.0-percent macroscopic strain. The expected vertical displacement of the grains (if a linear displacement gradient is assumed) is shown by the vertical line designated local theory prediction. However, some of the grains are immobile and some have displaced approximately three times the expected distance. It is important to note that the average measured displacement (each grain having an equal "Weight") is equal to the displacement predicted by the assumption of a linear displacement gradient. This variation in the mobility of grains within a grouping or "neighborhood" provides insight into the dissipation of energy spread by the specimen as macroscopic strain is applied. Additionally, this variation serves as the basis for the development of a theory which uses the diffusion equation for the prediction of micromotions within a specimen subjected to uniaxial strain. This theory is presented in Reference 40.

The relationship between vertical and horizontal grain displacements as a function of macroscopic strain is shown in Figure 39. The micromotions were viewed through a window at 0.56 h. Data for this figure were produced by summing the vertical motions of all grains within a series of frames at predetermined increments of macroscopic strain. Likewise, the horizontal motions of all grains were summed over the same series of frames.
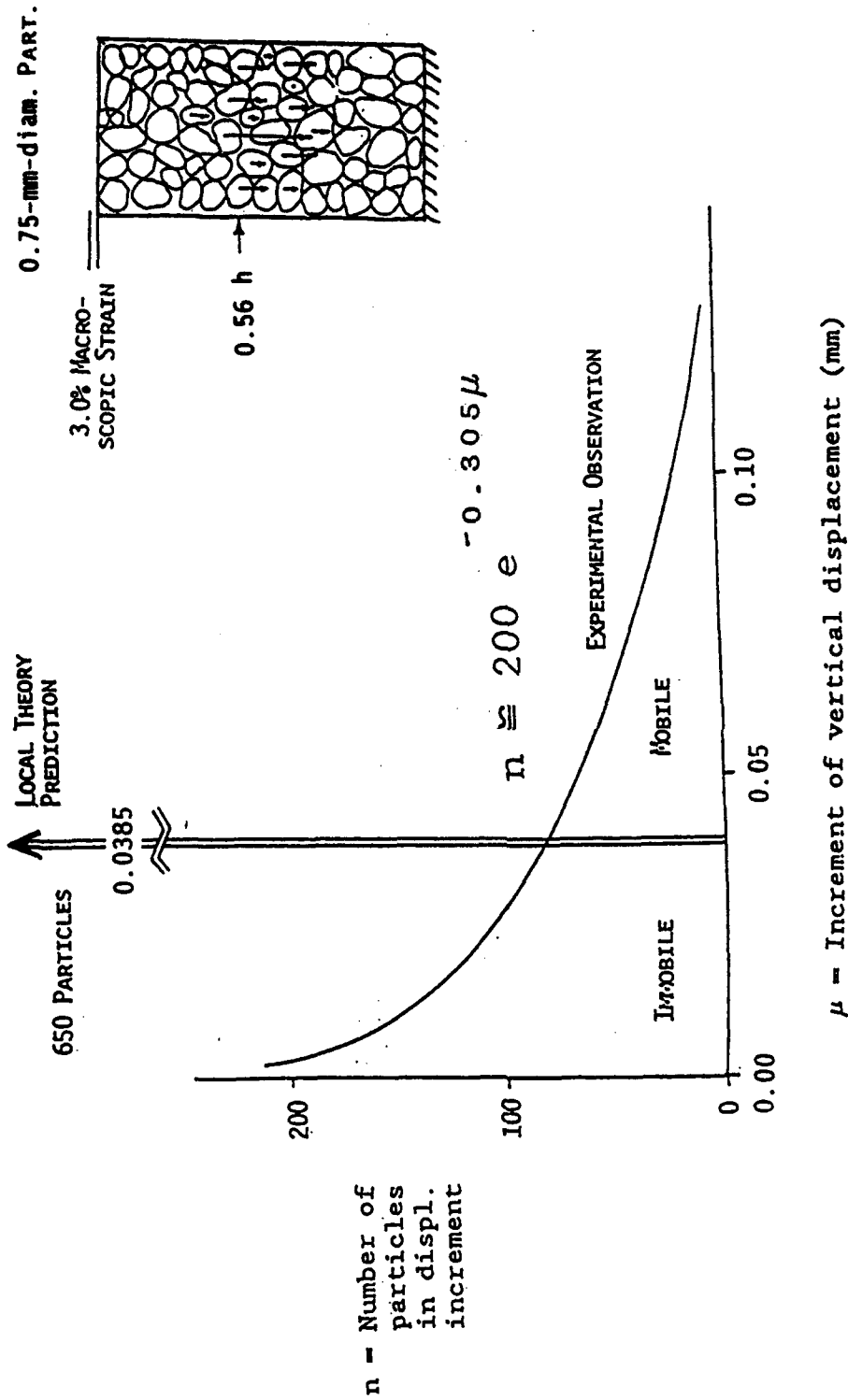
Figure 38.  Variation in the vertical displacement of sand grains under uniaxial strain (0.75-mm-diam. particles, window at 0.56 h, 3.0-percent macroscopic strain).
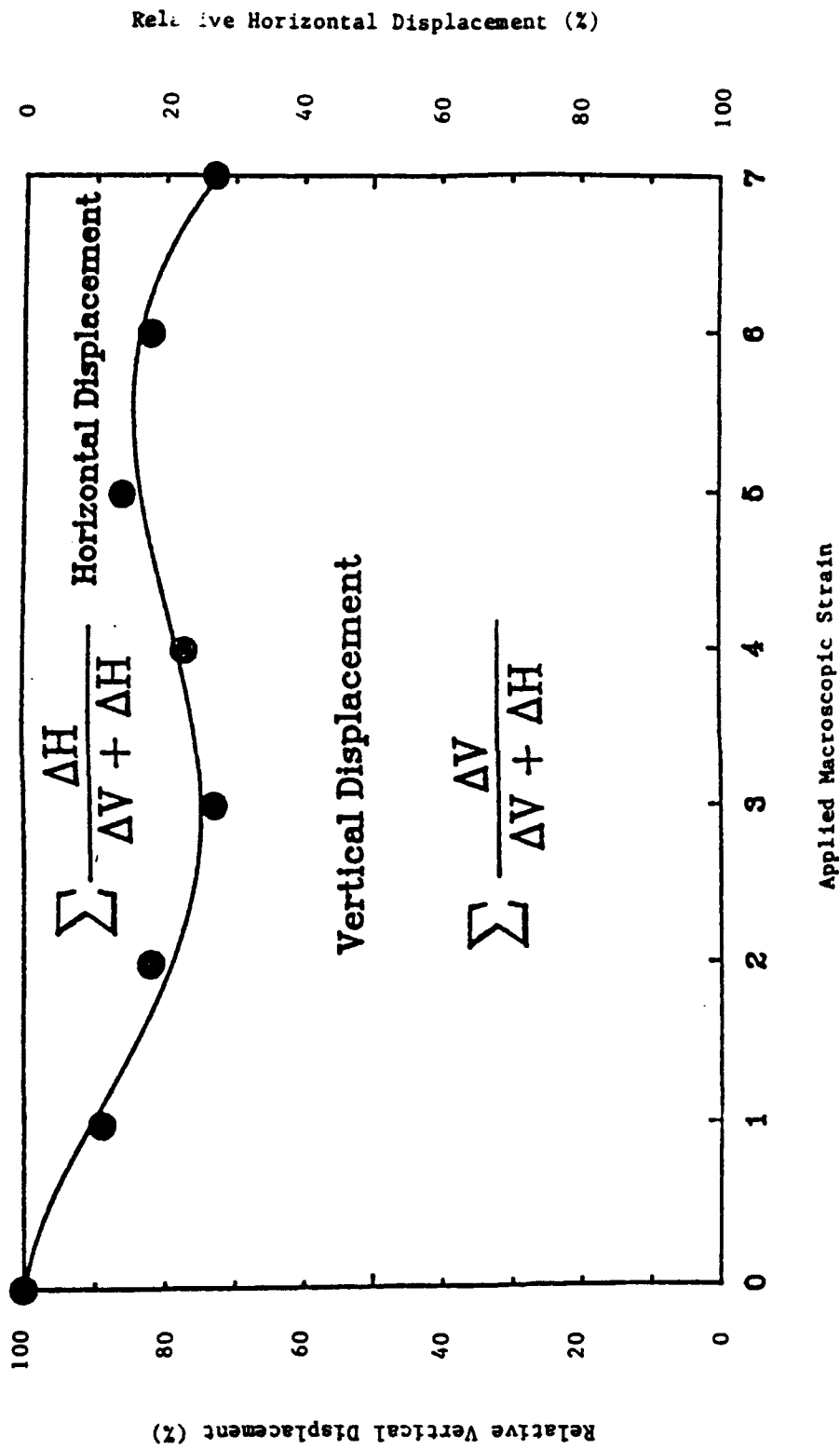
Figure 39. Percentage of vertical and horizontal displacement versus applied macroscopic strain.

The plot displayed in Figure 39 shows the relative amounts of average vertical and horizontal displacements with respect to the total observed displacement. A cyclical relationship between the magnitudes of the vertical and horizontal displacements appears to develop as uniaxial strain is applied. The grains move primarily vertically downward during the application of between 0- and 2-percent macroscopic strain. As strain application continues, the grains move laterally into a more compact arrangement. This lateral motion occurs between 2- and 4-percent macroscopic strain. At that point, grain fracture becomes significant. The cycle then repeats itself as the grains and remnants displace vertically and then shift horizontally into an even more compact arrangement before fracturing again.

Figure 40 shows the tracks made by grains which displace along the sidewalls of the confinement vessel. The photographs were taken following the application of 10-percent macroscopic strain. Grains and their remnants tend to move towards the nearest bottom corner of the specimen container. Lateral motion of the grains in the lower half of the specimen is most pronounced with grains only along the wall center line exhibiting generally vertical displacements.

The growth of clusters and development of damage are two responses which must be considered jointly as one examines the surficial microstructural response. As discussed previously, the grains displace vertically in response to the application of macroscopic uniaxial strain. This response predominates until the stress in individual grains becomes significant enough to result in fracture of the grain. The fracture of these grains appears to occur randomly during the onset of damage. However, as additional macroscopic strain is applied, chains of fractured grains appear to grow between the grains which fracture first. Such chains are highly evident if the specimen is subjected to >7.0-percent macroscopic strain. These damage chains are considered to be the boundaries of clusters within which there is relatively little damage. Clusters are three-dimensional structures which are formed within the specimen. Thus, only a portion or section of a cluster is visible through the sapphire window. Full definition of the cluster geometry and its evolution under uniaxial strain dictates the ability to "see" into the specimen as it is loaded. This is impossible using
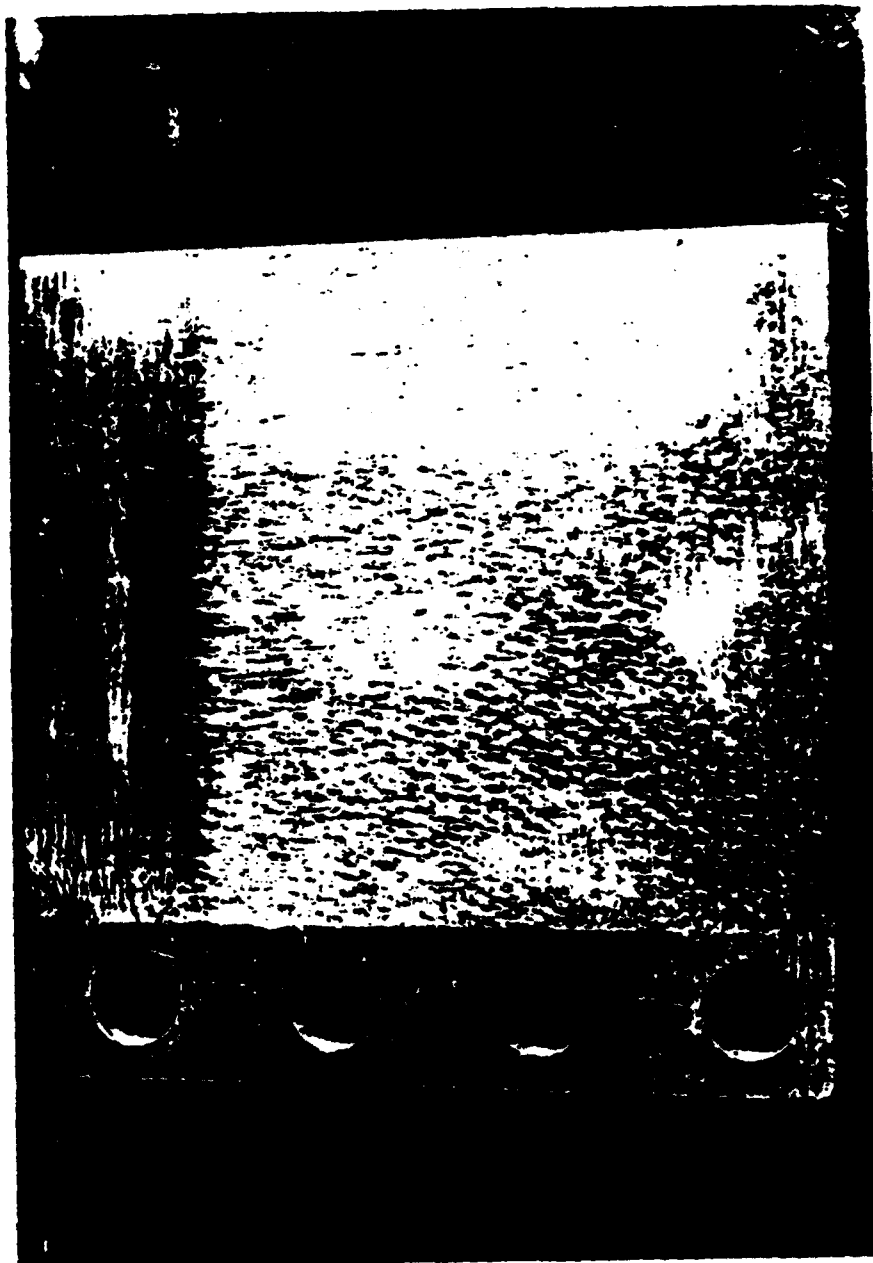
(a) Sidewall.

Figure 40. Grain displacement tracks on the inside of the confinement vessel walls.
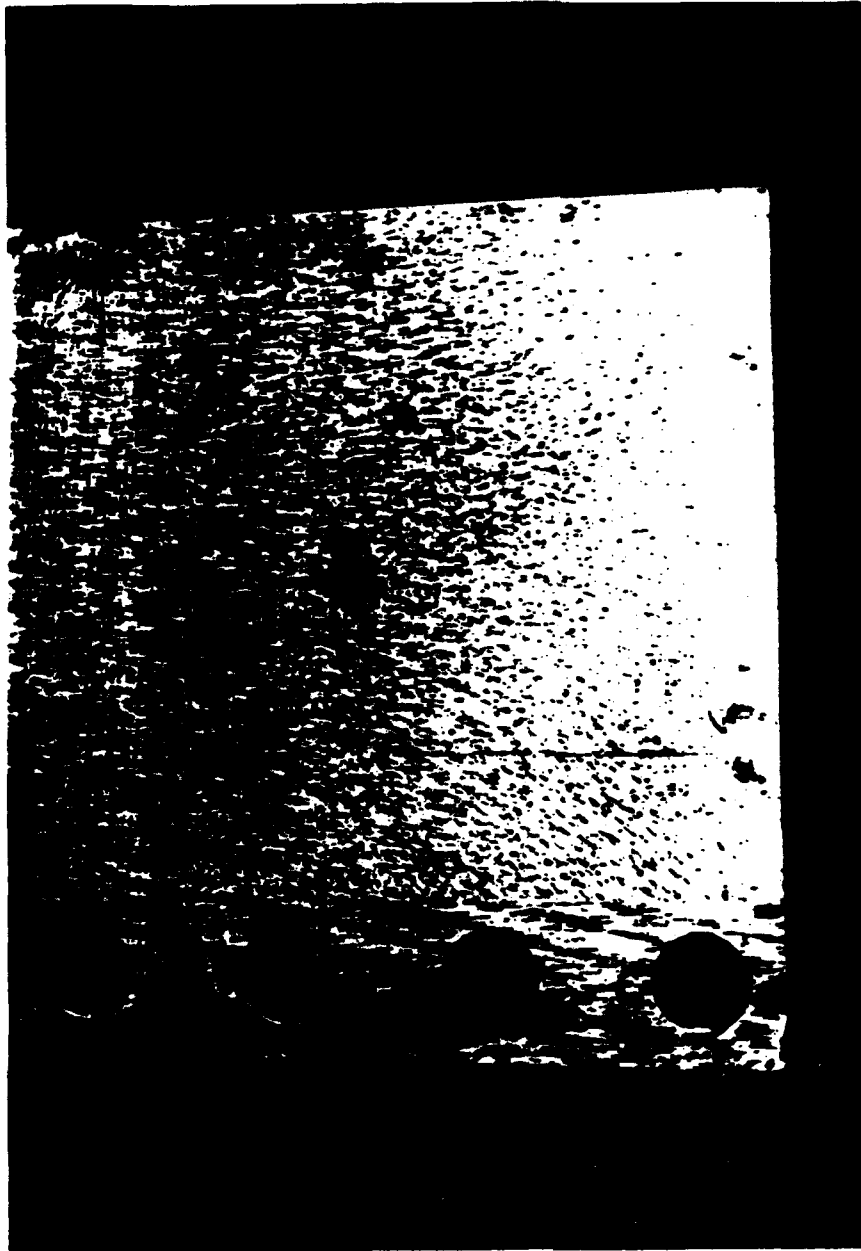
(b) Sidewall.

Figure 40. Continued.
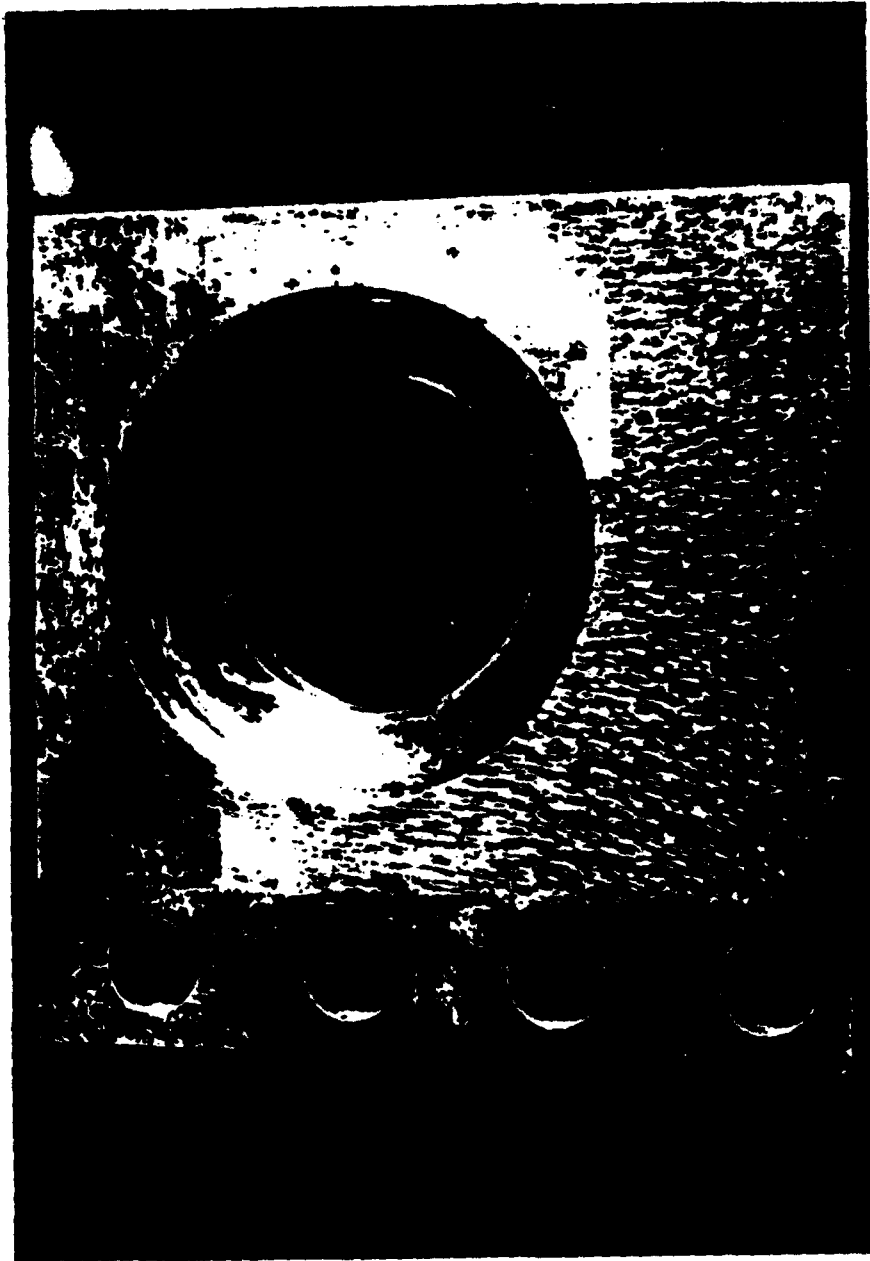
(c) Windowed sidewall, window at 0.75 h.

Figure 40. Continued.
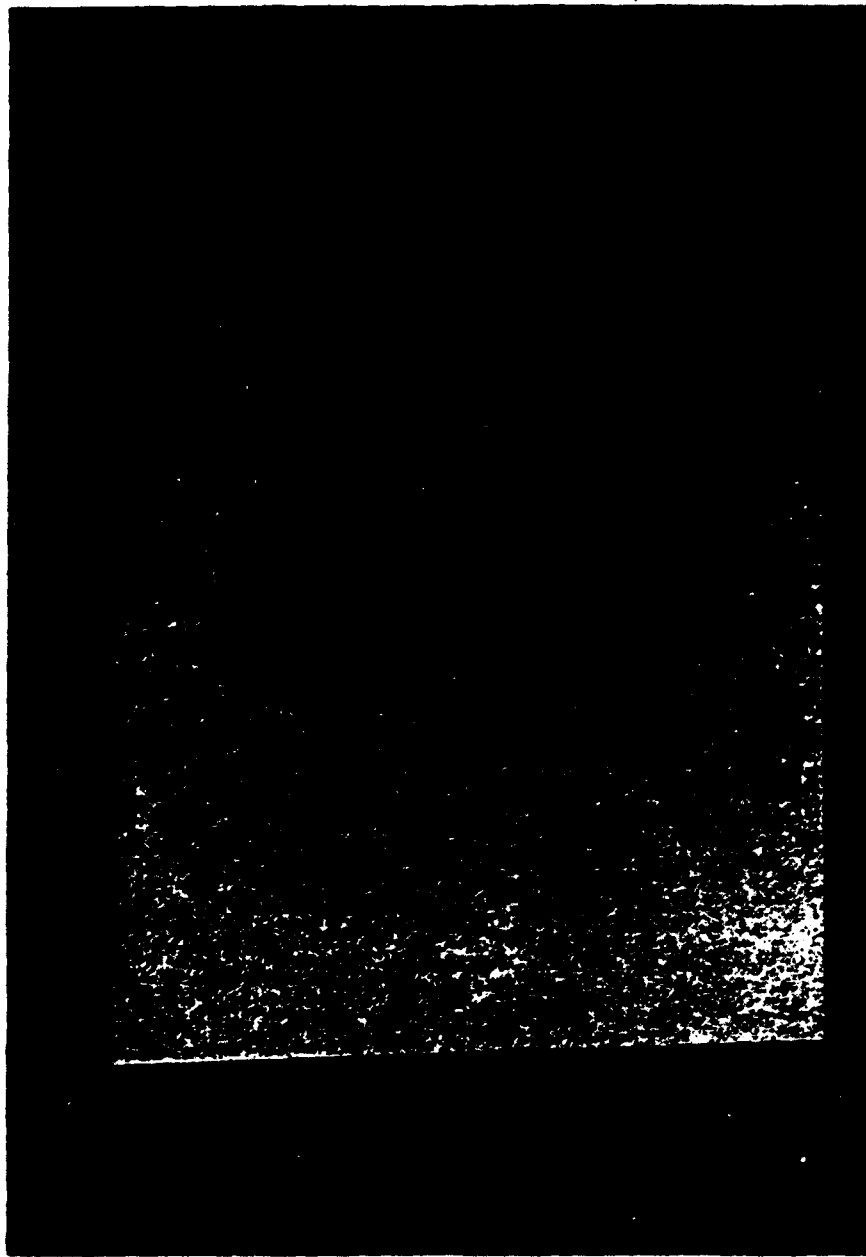
(d) Specimen side of loading plate.

Figure 40. Concluded.

the current experimental setup. Furthermore, the micromotion of a well-defined cluster is impossible to discern usi .g the current s ~p. It is thought that at macroscopic strain >5.0 percent, the micromotio and interactio.. of the clusters may influence the specimen macroscopic response more than interactions between individual grains. Additionally, the geometry of the clusters may be such that they efficiently mobilize the strength needed to resist the continued application of uniaxial strain. Subsequent rotation of the principal stress axes following the application of the initial increment of uniaxial strain will typically render a stress-strain response significantly different than the response of a virgin specimen. Again, investigation of this .esponse is not possible using the current device. This is because one is limited to actively viewing only the response of surficial grains, and the confinement vessel does not permit rotation of the principal stress axes.

The last point to be addressed is the late-time microstructural response of a specimen which has been subjected to some increment of uniaxial strain which was then held constant. The peak strength (Figs. 23-30) mobilized by the specimen immediately decreases upon attainment of the peak strain level. The peak mobilized strength decreases because microstructural activity continues after the peak macroscopic strain level has been attained. It is surmised that at the instant that the final increment of macroscopic strain is applied, there is some finite number of grains which are on the verge of fracture. Some do fracture and some may not. Adjacent grains receiving the load may or may not fracture. This process continues until the relatively high energy concentrated within several "key" grains ends up being more evenly distributed throughout the specimen. There is some level of distribution at which the grains and their remnants can withstand the applied strain with no additional fracture. This is a point of equilibrium. This premise was explored by analysis of micromotions following attainment of the peak macroscopic strain; however, little late time activity was recorded. It is further surmised that either very few key grains fracture during the process of distributing stored energy or the grains which fracture reside inside the specimen. The rate at which the specimen can distribute this energy may be an important consideration in the rate effects demonstrated by the mechanical response of some soils.

The micromotion of the surficial grains is closely tied to the internal microstructural response. Proper interpretation of the surficial response requires additional information with regard to the internal microstructural response of the grain assemblage. The required information is provided by x-ray tracking of lead particle displacement and epoxy impregnation and sectioning of the specimen.

## 6.4 INTERNAL MICROSTRUCTURAL RESULTS

The two techniques used to explore the internal microstructural response of the specimens were x-ray tracking of lead particles and epoxy impregnation and sectioning. The x-ray tracking technique is used during the application of macroscopic strain and provides the basis for comparison of surficial and internal micromotions. The epoxy impregnation technique permits the direct observation of microstructure after the load has been removed from the specimen.

The displacements of embedded lead particles were compared to those of the surficial grain displacements in Figure 41. (The diameter of the embedded lead particles was 1.3 mm whereas the nominal sand grain diameter was 0.50 mm). The given displacement history shows the average displacement of 20 embedded particles. As observed through a window at 0.56 h, posttest, the lead particles had indentations at each of the contacts with the silica grains. Each lead particle had 10-12 indentations whereas the average coordination number of the silica grains appeared to be between 3 and 5. As a result, the lead particles were more rigidly confined than the silica grains. Additionally, the lead particles did not fracture. The lead particles were constrained from displacing in discrete "jumps" whereas the silica grains were not. Thus, their displacement paths appeared more continuous. The average displacement path of the embedded lead particles indicates the same nonlinear displacement path during both loading and unloading as shown by the average grains at the specimen surface.
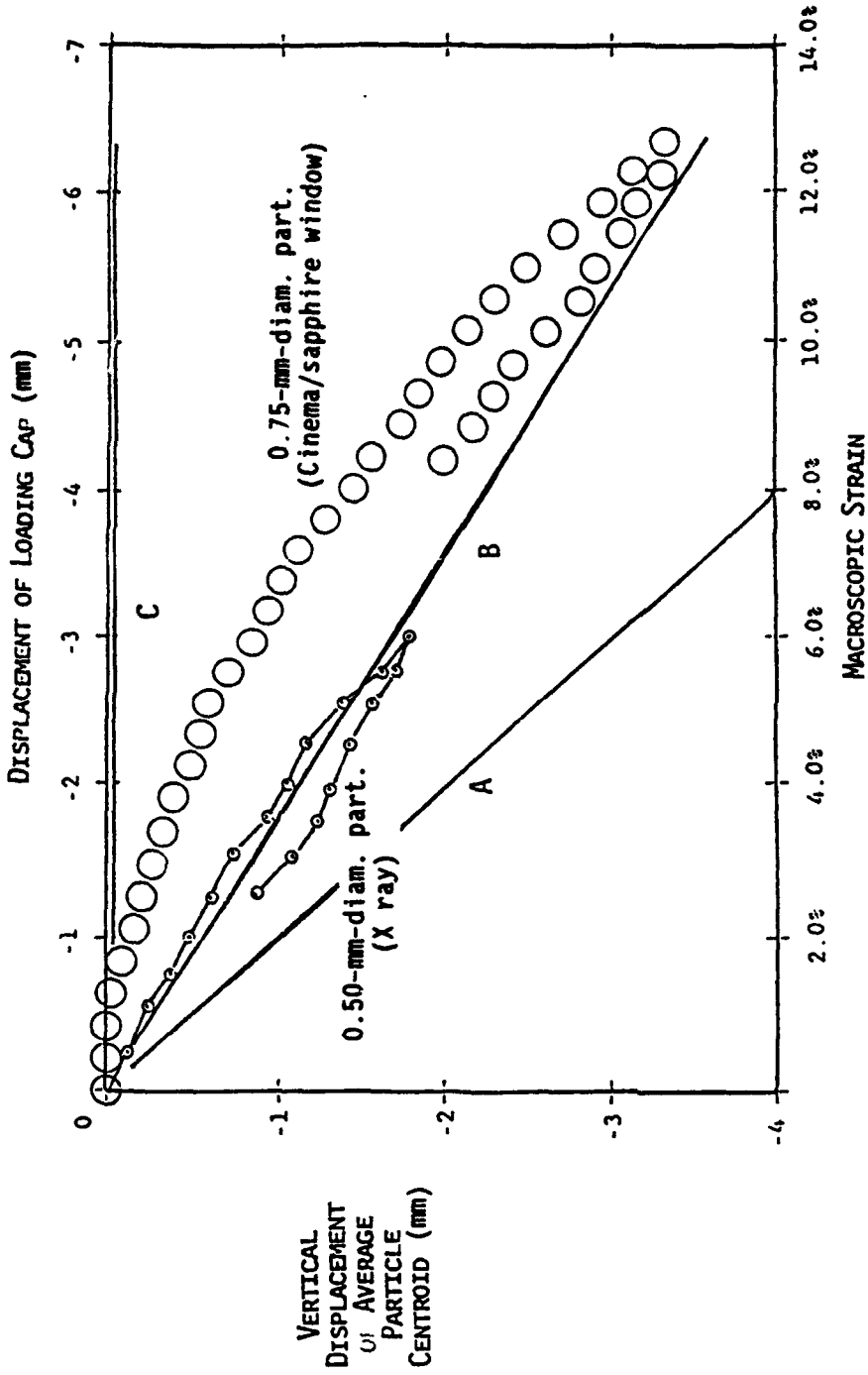
Figure 41. Vertical displacement of average particle centroid in response to applied macroscopic strain.

However, departure of the displacement path from that predicted by local theory is much less pronounced for the embedded lead particles than for the grains on the specimen surface. Thus, there appears to be some variation between the displacement paths of particles in the center of the specimen as compared to those which are adjacent to the sapphire window. The variation is found mainly in the magnitude of displacements but not the trends. No information was obtained regarding the distribution of the micromotions due to the small number of embedded lead particles (20). It appears, though, that the motion of the embedded particles is more of a continuous nature than the motion of grains located at the boundary of the specimen. This apparent continuity of displacement for embedded particles may result from (1) the particles are free to displace in any direction whereas the surface grains are restrained by the presence of the confinement vessel walls, and (2) the embedded particles are made of lead and are larger than the sand grains. The embedded particles, having the freedom to displace laterally in any direction, have inherently greater mobility than the grains restrained by the container walls. It is the restraint which leads to grain fracture and disintegration seen through the sapphire windows. The embedded particles displace and rotate more subtly than the wall-restrained grains.

While grain fracture and disintegration may be readily apparent on the specimen boundary, interior grains may remain relatively intact and yet retain the freedom of motion to orient themselves into a denser arrangement (prior to inevitable fracture and disintegration). The fact that the embedded particles are made of lead and are larger than the sand grains also makes their average motion differ from that of the sand grains. Being made of a malleable material, the lead particles simply deform in response to the forces applied by adjacent grains. Thus, they will not exhibit the discontinuous motion of the sand grain seen when asperities on the grains break. Furthermore, because of their size, the lead particles are more uniformly constrained than the sand grains. In summary, the embedded lead particles provide insight into the internal microstructural response of the specimen during loading. Limitations imposed by the use of the particles tend to make their response align itself more closely with displacements as predicted by the use of a local theorem. The lead particles may be incapable of experiencing the variation in mobility as is shown by direct observation of the sand grains.

Regarding the information gained from the epoxy impregnation and sectioning of the tested specimen, general insight is gained into the distribution of damage (individual grain fracture and disintegration) throughout the specimen. A qualitative observation will be presented prior to discussing the types and distribution of internal damage. Damage is readily apparent in the exposed specimen cross sections due to a change in the opacity of individual grains. The grains become opaque if they fracture. Consider the specimens subjected to the application of 10.0-percent macroscopic strain. Damage is concentrated at the corners of the specimen almost to the exclusion of damage at the specimen interior. If a sphere of some unit diameter encased within a cube having sides of the same unit length is pictured, the portion of the specimen contained within the sphere would be relatively undamaged, and the portion outside the sphere boundary would be relatively highly damaged. Specimens which had been subjected to various levels of macroscopic uniaxial strain were impregnated and sectioned. The damage appears to commence at the corners and propagate inward as the magnitude of macroscopic strain increases.

These observations are corroborated by conclusions drawn on the displacement of embedded particles (Fig. 41) as well as the grain tracks scored on the walls of the confinement vessel (Fig. 40). It has already been shown that grains which reside adjacent to the vessel wall are relatively immobile. The immobility causes stress concentration on individual grains resulting in fracture and disintegration. This tendency appears to be more pronounced in the grains which reside in the specimen corners (outside the boundary of the included sphere). Furthermore, the mobility of a given grain is more highly restricted if the grain is located relatively deeply within a given corner. As the highly immobile grains located at the corners are crushed during the initial stages of loading, the grain remnants are shifted into a more compact arrangement and, thus, permit inner grains (those away from the corners) to move outward in the direction of the corners. This activity occurs throughout the loading phase and, therefore, grains along the outer walls of the confinement vessel migrate toward the corners.

Grains located adjacent to the base of the confinement vessel, as well as those in contact with the loading cap, show no tendency to displace horizontally during loading. This is

readily explained by the stress state in the specimen. In the case of uniaxial strain, a vertical force is exerted on the specimen which forces the grains to primarily displace vertically. There is no external macroscopic force on the grains causing them to displace horizontally. Grains in contact with either the base plate or loading cap will generally not displace horizontally. Grains residing against the sidewalls are forced to displace vertically and only exert a macroscopic stress on the sidewall ≈ 30 to 40 percent of the vertical stress. Thus, the grains are relatively free to move laterally during the application of vertical uniaxial strain. This freedom is manifested as grain tracks which tend toward the corners of the specimen.

Figure 42 shows the types of damage which were apparent following epoxy impregnation and sectioning. The figure includes the binary (two-tone) images of two viewed sections. Figure 42 also shows other images of damaged grains. The damage was generally limited to fracture of grains with two possible outcomes. Either the remnants remained in direct contact with one another and the grain appeared to still be intact or the remnants broke apart leaving a slight void where the grain originally existed. Damage aside, very few of the grains appear to be in contact with one another. This single observation highlights the three-dimensional nature of the connectivity which exists between discrete grains. The contacts exist either above or below the level at which the section was taken. Likewise, damage has a three-dimensional nature which one can only hope to catch a glimpse of by employing the technique of impregnation and sectioning. It is possible to come up with some measure of the distribution of damage on some arbitrarily chosen plane in the specimen. Likewise, one can even quantify the type(s) of damage. However, such information can be misleading if one is trying to quantify the structure and distribution of the damage in three dimensions. The limitation of being able to view the specimen (or section) in only two dimensions is again imposed.

A significant amount of damage became evident only upon unloading. Consider the specimens subjected to the monotonic application of 10.0-percent macroscopic strain (Figs. 43 and 44). As mentioned previously, individual grain fracture and disintegration were

91
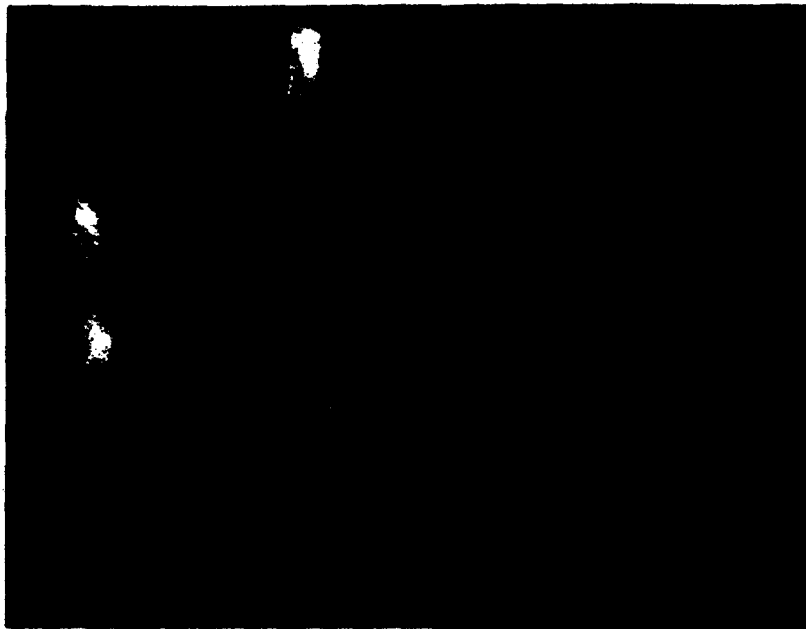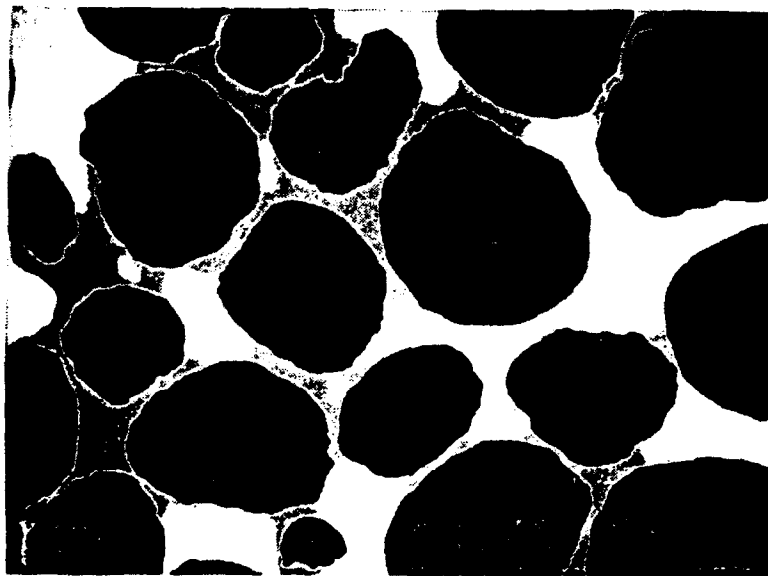
(a) Photomicrograph.



(b) The OASYS-enhanced image. Bonding agent shown in grey.

Figure 42. Virgin specimen (unstrained) (x 25).

(a) Photomicrograph.



(b) The OASYS-enhanced image. Bonding agent not shown.

Figure 43. Specimen after 10-percent applied strain (x 25).
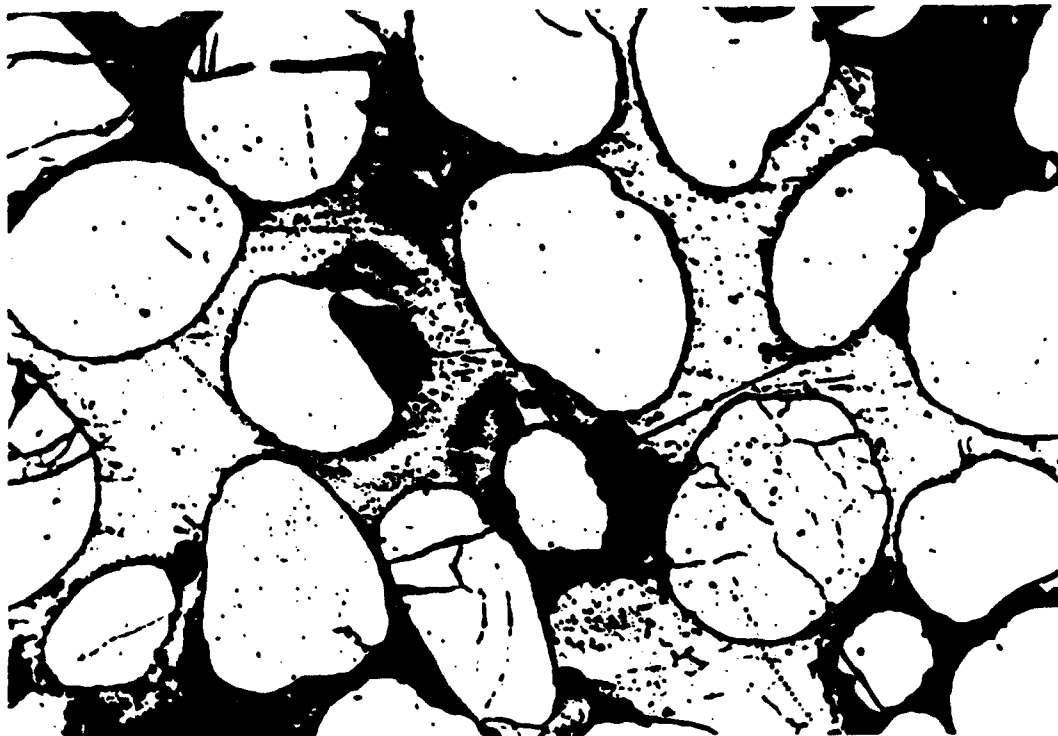
(a) Vertical cut, 10-percent macroscopic strain (x 25).
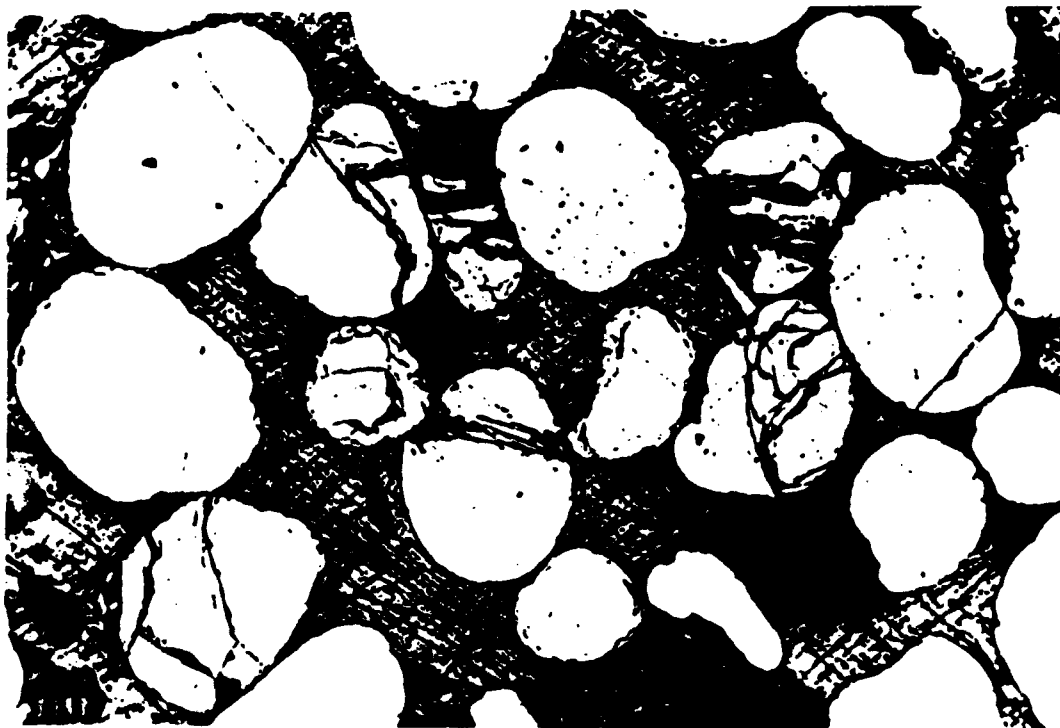


(b) Horizontal cut, 10-percent macroscopic strain (x 25).

Figure 44. Typical images of microstructural damage (10 percent macroscopic strain).

(c) Vertical cut, 10-percent macroscopic strain (x 50).



(d) Horizontal cut, 10-percent macroscopic strain (x 50).

Figure 44. Concluded.

highly evident in the cinema records as well as damage chains and grain clusters. However, it appeared (at least quantitatively) that an equal number of grains disintegrated during unloading as were destroyed during initial loading. Thus, fracture was much more prevalent in the grains than was apparent during loading. It was only during the unloading phase that these fractured grains made their presence known by disintegrating. This observation has significant importance when one considers the strength mobilized by specimens subjected to cyclic loading. Grain fracture occurring during the loading phase(s) may manifest itself in grain disintegration during unloading. The remnants then reorient themselves into more compact arrangements during subsequent loading. This usually leads to the specimens subjected to cyclic loading exhibiting lower mobilized peak strength at peak strain, as was observed.

## 7.0 CONCLUSIONS AND RECOMMENDATIONS

### 7.1 CONCLUSIONS

The micromotions of individual grains in a specimen under uniaxial macroscopic strain are discontinuous and stochastic. The magnitudes of individual grain displacements are broadly distributed about some mean value which is the displacement of the "average grain." This distribution of motions is exponential with relatively few grains being immobile within a moving neighborhood. Some grains displace three times as far as the "average grain" for a given increment of applied macroscopic strain. Although the underlying physics of this micromotion are still under investigation, the nature of the displacement calls for the use of nonlocal theories to accurately describe the constitutive response of granular media.

The observed differential motions and evolution of damage may provide insight regarding the mechanism of energy dissipation within granular material. Further insight will be provided by data obtained using an automated optical analysis system which is capable of providing highly consistent analysis of grain fracture and crushing. The influence of the confinement vessel walls (and sapphire windows) on damage evolution requires further investigation to correlate observed surficial damage with the interior damage. This is because the microstructural response at the specimen-container interface is quantitatively and qualitatively different from that of the specimen interior.

Regarding the motion history of the "average grain" which represents a neighborhood, nonlinear displacement fields have been observed through direct observation of micromotions via sapphire windows and through the use of x rays. The displacement fields are not directly proportional to applied macroscopic strain as predicted by local theories. Rather, strain in the immediate vicinity of the loading cap is greater than the applied macroscopic strain with other regions of the specimen generally experiencing strain levels less than the applied macroscopic strain. Three "zones" existing within the specimen under uniaxial strain are (1) a zone in which relatively high local displacements and strain occur, (2) a zone behind this "front" wherein the grains move directly in relation to the advance of

the loading cap, and (3) a zone which has not yet felt the influence of the advancing loading cap. Sidewall friction, although not negligible, appears not to play an overriding role in the grain micromotions.

A qualitative review of the micromotions reveals that the grains appear to only shift position and rearrange themselves into a more compact arrangement during the application of up to 4.0-percent macroscopic strain. Grain fracture and crushing become more apparent at higher macroscopic strain. This process repeats itself with the remnants of the fractured grains arranging themselves into a compact orientation prior to their being fractured also. These effects do not randomly occur. Each response is observed in localized zones which grow in recognizable patterns. Fracture may or may not occur before an individual grain is crushed. Once fracture and crushing have begun, clusters of intact grains are perceived with localized crushing zones and fracture "chains" are evident.

A theory has been proposed which is based on the diffusion equation. This theory evolved from the finding that displacement within a neighborhood of grains is nonuniform and obeys an exponential distribution. The mean of the distribution is centered about the motion of the "average grain" which represents the neighborhood. The thermodynamic foundation of the theory permits the later incorporation of two properties of granular media, configurational temperature and configurational entropy. Both of these properties are thought to play a central role in the explanation of localization during the deformation of granular media. The material constants in this theory can, for the most part, be determined by phenomenological experiments. However, microscopic (microstructural) observations in three dimensions are still needed to shed light on the underlying physics of the macroscopic mechanical behavior of the media.

A brief description of several classes of constitutive models for granular materials was presented in this report. The models can generally be grouped under two headings, macroscopic (phenomenological) and microstructural (particulate). Both types of models have been used extensively to understand and predict the mechanical response of soil. But each type is limited in its ability to predict the mechanical behavior of most naturally occurring soils. The macroscopic models are usually limited to predicting the response of

soils subjected to well-defined loading regimes within which the general response of the soil is already known. These models typically relate the soil response to macroscopic material properties and do not incorporate the underlying physics associated with the interaction of individual sand grains. Microstructural models have been developed to incorporate the underlying physics; however, these models appear to be limited by the current inability to model a sufficient number of irregularly shaped grains of soil. This limitation is driven by the need to conduct "experiments" using disks (2D) and spheres (3D) for computational efficiency. Experimental programs have been undertaken to explore the microstructural attributes of granular media and understand how these attributes manifest themselves in the material macroscopic response. These programs usually rely on viewing sections of soil which have been subjected to load and subsequently frozen or impregnated with epoxy. These studies have provided insight into what physical changes typically occur in stressed soils, but they provide little insight into the evolution of such changes. A unifying technique is needed, therefore, wherein one can quantify and even view the evolution of microstructural changes which occur in granular media under arbitrary loading. A technique is proposed next which shows reasonable promise for relating mechanical response to experimentally observed microstructural changes.

It is proposed that assemblages of irregularly shaped particles be subjected to arbitrary loading using distinct element computer programs. Rather than using large numbers of spherical or ovoid particles, the "specimen" would be created from the volumes rendered by suitable manipulation of images obtained from computed tomography (CT) scanning. The significant obstacle would be the creation of object-oriented volumes from the two-dimensional images provided by the CT scans. Determination of the basic descriptors of fabric and its evolution under loading would be trivial. Furthermore, advanced visualization techniques would permit one to highlight and view only those particles which undergo micromotions exceeding preset thresholds. Thus, one could isolate and study only those particles which participate in the development of a localization and which undergo excessive displacement, rotation, or damage, etc. The specimen could also be examined at any stage during the loading process without altering the structure of the assemblage. A preliminary step in this direction has been taken by integrating the use of machine vision and artificial intelligence in quantifying the micromotion and rotation of surficial particles of granular

specimens under uniaxial strain. The experimentally determined microstructural response(s) of the surficial particles will serve as a benchmark against which the microstructural response(s) of the surficial particles in the distinct element computation can be compared. If the response(s) match, it is thought that the microstructural changes occurring in the granular specimen will be mimicked by the changes occurring in the distinct element specimen. Thus, experimental and computational observations can be linked to provide a sound basis for the development of a microstructure-based continuum model for granular media.

## 7.2 RECOMMENDATIONS

The difficulty of obtaining consistent results using manual methods during observation of grain rotations, fracture, and disintegration dictates the need to automate the data collection process. This is true in light of the attempt to measure microstructural effects from the two-dimensional cinema images and became more apparent as three-dimensional microstructural effects were considered. Suitable off-the-shelf image analysis programs are now available which can be user-modified to suit specific needs (filters, shape functions, etc.). Automated optical techniques should be aggressively explored (mainly in the area of software development) if three-dimensional visualization and discrete element modeling of assemblies of irregularly shaped grains are to become a reality.

This three-dimensional visualization and discrete element modeling should also be intensively investigated as the coupling of these techniques (automated imaging and three-dimensional visualization) will aid in studying the evolution of fabric during specimen loading. The specimen in this example will be an assemblage of irregularly shaped particles which are in a suitable format for manipulation by a discrete element program. The primary activity in this pursuit will be to investigate the existence of anisotropy in the initial fabric and the evolution of both (anisotropy and fabric) during loading. An equally important goal will be to develop a deeper understanding regarding the relationship between these factors and the occurrence of localizations. These aspects are critically important if one is to develop a three-dimensional continuum model for granular materials founded upon microstructural effects.

# REFERENCES

1. Prevost, J.H., "Plasticity Theory for Soil Stress-Strain Behavior," Journal of the Engineering Mechanics Division, ASCE, Vol. 104, No. EM5, pp. 1177-1194, 1978.

2. Terzaghi, K. and Peck, R.B., Soil Mechanics in Engineering Practice, John Wiley & Sons, Inc., New York, New York, 1948.

3. Baladi, G.Y. and Rohani, B., Soil Plasticity, Report No. 79-0109, U.S. Army Engineer Waterways Experimental Station, Vicksburg, Mississippi, 1979.

4. Deman, F., Achsensymetrische Spannungs-und Verformunsfelder in Trockenem Sand, Dissertation, University of Karlsruhe, Germany, 1972.

5. Lambe, T.W. and Whitman, R.V., Soil Mechanics, Massachusetts Institute of Technology, John Wiley & Sons, Inc., New York, New York, 1969.

6. Saada, A.S. and Townsend, F.C., "State of the Art: Laboratory Strength Testing of Soils," Laboratory Shear Strength of Soil, ASTM STP 740, R.N. Yong and F.C. Townsend, Eds., American Society for Testing and Materials, pp. 7-77, 1981.

7. Ko, H. and Sture, S., Data Reduction and Applications for Analytical Modeling, University of Colorado, Boulder, Colorado, 1982.

8. Valanis, K.C. and Read, H.E., Endochronic Plasticity, Report No. 87-06, Endochronics, Inc., Vancouver, Washington, and S-Cubed, La Jolla, California, December 1987.

9. Duncan, J.M. and Chang, C.Y., "Nonlinear Analysis of Stress and Strain in Soils," J. of Soil Mech. and Found. Div., ASCE, Vol. 96, No. SM5, pp. 1629-1653, September 1970.

10. Chang, K.S. and Duncan, J.M., "Hyperbolic Stress-Strain Parameters for Nonlinear Finite Element Analyses of Stresses and Movements in Soil Masses," Report No. TE-74-3, Department of Civil Engineering, Institute of Transportation and Traffic Engineering, University of Colorado, Boulder, Colorado, July 1974.

11. Petrakis, E. and Dobry, R., Micromechanical Behavior and Modelling of Granular Soil, Department of Civil Engineering, Rensselaer Polytechnic Institute, Troy, New York, July 1989.

12. Drucker, D.C., "Some Implications of Work Hardening and Ideal Plasticity," Q. Appl. Math., Vol. 27, No. 4, pp. 411-418, 1950.

## REFERENCES (Continued)

13. Lade, P.V. and Nelson, R.B., "Nonassociated Flow and Stability of Granular Materials," _Journal of Engineering Mechanics_, Vol. 113, No. 9, pp. 1197-1217, September 1987.

14. Lade, P.V., Nelson, R.B., and Ito, Y.M., "Instability of Granular Materials with Nonassociated Flow," _Journal of Engineering Mechanics_, Vol. 114, No. 12, pp. 2019-2037, December 1988.

15. Lade, P.V. and Pradel, D., "Instability and Plastic Flow of Soils I: Experimental Observations," _Journal of Engineering Mechanics_, Vol. 116, No. 11, pp. 1987-2013, November 1990.

16. DiMaggio, F.L. and Sandler, I.S., "Material Models for Granular Soils," _Journal of the Engineering Mechanics Division_, ASCE, Vol. 97, No. EM3, pp. 935-950, 1975.

17. Sandler, I.S. and Baron, M.L., "Recent Developments in the Constitutive Modeling of Geological Materials," _Third International Conference on Numerical Methods in Geomechanics, Aachen, West Germany_, Vol. I, pp. 363-376, 1979.

18. Vardoulakis, I. and Graf, B., "Calibration of Constitutive Models for Granular Materials Using Data from Biaxial Experiment," _Geotechnique_, Vol. 35, No. 3, pp. 288-317, 1985.

19. Chen, Z. and Schreyer, H.L., "Simulation of Soil-Concrete Interfaces with Nonlocal Constitutive Models," _Journal of Engineering Mechanics_, ASCE, Vol. 113, No. 11, pp. 1665-1677, 1987.

20. Chang, C.S. et al., "Micromechanical Modelling of Cemented Sands under Low Amplitude Oscillations," _Geotechnique_, Vol. 40, No. 2, pp. 251-263, 1990.

21. Cundall, P.A. and Strack, O.D., "A Discrete Numerical Model for Granular Assemblies," _Geotechnique_, Vol. 29, No. 1, pp. 47-65, 1979.

22. Cundall, P.A. and Strack, O.D., _Mechanics of Granular Materials: New Models and Constitutive Relations_, University of Minnesota, Minneapolis, Minnesota, 1983.

23. Trent, B.C., "Microstructural Effects in Static and Dynamic Numerical Experiments," _Proceedings of the 29th U.S. Symposium on Rock Mechanics_, University of Minnesota, Minneapolis, Minnesota, 1978.

24. Trent, B.C. and Margolin, L.C., _The Micromechanics of Cemented Granular Material_, Elsevier Science Publishing Co., New York, New York, 1987.

## REFERENCES (Continued)

25. Trent, B.C., "Numerical Simulation of Wave Propagation Through Cemented Granular Material," Wave Propagation in Granular Media, Karamanlidis, D. and Stout, R.B., Eds., AMD-Vol. 101, Book No. H00538, pp. 72-88, 1989.

26. Chang, C.S. and Misra, A., "Packing Structure and Mechanical Properties of Granulates," Journal of Engineering Mechanics, Vol. 116, No. 5, pp. 713-732, May 1990.

27. Cundall, P.A. and Strack, O.D.L., The Distinct Element Method as a Tool for Research in Granular Media. Part I, Department of Civil and Mineral Engineering Institute of Technology, University of Minnesota, Minneapolis, Minnesota, November 1978.

28. Cundall, P.A. and Strack, O.D.L., The Distinct Element Method as a Tool for Research in Granular Media. Part II, Department of Civil and Mineral Engineering Institute of Technology, University of Minnesota, Minneapolis, Minnesota, October 1979.

29. Hertz, H., "Uber die Behrungsfester Elastischer Korper," J. Reine Angew. Math., Vol. 92, No. 7, pp. 156-171, 1882.

30. Mindlin, R.D., "Compliance of Elastic Bodies in Contact," Journal of Applied Mechanics, Vol. 103, No. 4, pp. 259-268, 1949.

31. Mindlin, R.D. and Deresiewicz, H., "Elastic Spheres in Contact Under Varying Oblique Forces," J. of Appl. Mech., Trans. ASME, Vol. 107, No. 9, pp. 327-344, September 1953.

32. Deresiewicz, H., Advances in Applied Mechanics, Academic Press Inc., New York, New York, 1958.

33. Deresiewicz, H., "Stress-Strain Relations for a Simple Model of a Granular Medium," J. of Appl. Mech., Trans. ASME, Vol. 112, No. 9, pp. 402-406, September 1958.

34. Seridi, A. and Dobry, R., An Incremental Elastic-Plastic Model for the Force-Displacement Relation at the Contact Between Two Spheres, Report No. 84-037, Department of Civil Engineering, Rensselaer Polytechnic Institute, Troy, New York, 1984.

35. Oda, M., "Significance of Fabric in Granular Mechanics," Continuum Mechanical and Statistical Approaches in the Mechanics of Granular Materials, U.S. National Science Foundation, Japanese Society for the Promotion of Science, Sendai, Japan, June 5-9, 1978, pp. 157-163.

## REFERENCES (Concluded)

36. Chen, Z. et al., <u>Experimental, Theoretical, and Computational Investigations of Failure of Quasi-Brittle Structures</u>, Report No. PL-TN--91-1030, Phillips Laboratory, Kirtland AFB, New Mexico, July 1991.

37. Kishino, Y., "Statistical Consideration on Deformation Characteristics of Granular Materials," <u>Continuum Mechanical and Statistical Approaches in the Mechanics of Granular Materials</u>, U.S. National Science Foundation, Japanese Society for the Promotion of Science, Sendai, Japan, June 5-9, 1978, pp. 69-75, 112, 127.

38. <u>Theoretical Foundation for Large-Scale Computations of Nonlinear Material Behavior</u>, Eds., Nemat-Nasser, S., Asaro, R., Hegemier, G.A., Martinus Nijhoff Publishers, Boston, Massachusetts, 1984.

39. Skukla, A. and Sadd, M.H., <u>Wave Propagation and Dynamic Load Transfer Due to Explosive Loading in Heterogenous Granular Media With Microstructure</u>, Report No. 90-86, U.S. Air Force Office of Scientific Research, Bolling Air Force Base, Washington, D.C., August 1990.

40. Valanis, K.C., <u>A Micromechanical Foundation of Plastic Non-Local Behavior of Grandular Media</u>, University of New Mexico Research Institute, Albuquerque, New Mexico, June 1990.